Study of the aggregation process of the amyloid beta-protein associated to Alzheimer's disease. Examination of pharmaceutically important small molecules.

Bernat Serra Vidal

Programa de Doctorat en Química Orgànica

Study of the aggregation process of the amyloid beta-protein associated to Alzheimer's disease. Examination of pharmaceutically important small molecules.

Bernat Serra Vidal

Tesi dirigida per:

Ernest Giralt Lledó

Natàlia Carulla Casanovas

Al papà i la mamà, a la Maria del Mar (i el Sergi), al Gerard i la Neus.
A aquella que deu ser allà i m'espera.

Impossible is not a word, it's just a reason for someone not to try.

—Kutless, *What faith can do*

Agraïments

> Il a prononcé alors distinctement, bien qu'avec une extrême lenteur, ces mots que je suis sûr de rapporter très exactement: ≪Qu'est-ce que cela fait? Tout est grâce.≫
> Je crois qu'il est mort presque aussitôt.
>
> —George Bernanos, *Journal d'un curé de campagne*

Com diu Bernanos en la seva obra mestra, "tot és gràcia", tot és do. I certament és així. La meva tesi no deixa de ser un altre exemple on es posa de relleu aquesta afirmació: jo en sóc l'autor, però aquesta feina no hauria estat possible sense la inestimable col·laboració de tantes i tantes persones, a tots els nivells. Tractaré, doncs d'enumerar-les, segur que no podré fer justícia en quant a la contribució específica de cadascuna.

Vull agrair en primer lloc als meus codirectors, l'Ernest i la Natàlia, el seu suport i la seva confiança en mi. Tots dos han tractat de comunicar-me la seva passió i entusiasme per la ciència i, sobre tot, m'han ensenyat a treballar amb perfeccionisme des de la humilitat. A la Natàlia li he d'agrair especialment la seva paciència i disponibilitat, així com el seu suport constant, especialment en els moments inicials i quan les coses no sortien o se'm feien difícils. A l'Ernest li agraeixo aquesta visió de conjunt, integral, serena, que té i tracta de transmetre amb senzillesa.

Gràcies també a tots els membres passats i presents del lab 300. M'he sentit molt a gust durant tots aquests anys i tots i cadascun m'heu deixat un record profund i personal. Un agraïment especial a l'*Amyloid team*: l'afabilitat de la Rosa, el *positive thinking* de la Montserrat, l'alegria de la Sílvia, i agrair la presència i acompanyament de l'Aurelio, el Martí i la Roberta. També molt satisfet d'haver compartit gran part d'aquests anys amb "l'altre" Bernat (ja doctor), i crec tenir en ell un molt bon amic. Gràcies als membres del

POP team, als del BBB team, als de la VGEF, als sintètics... I gràcies també als del grup del Fernando i a l'Eva, que fa tant fàcil el difícil món de la burocràcia.

Estic molt agraït a totes les persones amb qui he col·laborat durants aquests anys: les tres Mars d'Espectrometria de Masses (la Marta, la Marina i la Mar), el Lluís i la Daniela del grup de l'Eduardo, la Carmen, l'Elisenda i la Gemma a Microscopia, la Marga a RMN, el Sergio Madurga al departament de QF amb els ajustos gaussians i el Nick i la Raquel en la part d'expressió d'Aβ (ongoing work).

També vull mencionar els membres de la comissió de seguiment, el meu TAC: el Xavier Salvatella, la Marga Gairí, el Francesc Rabanal. Gràcies per les estones que m'heu dedicat i pels comentaris constructius i crítics que heu fet.

I'd like to mention as well the opportunity of a predoctoral stay in Zürich. I'd like to thank all the Riek group, especially Roland for accepting me in his lab (and teaching me to ski), Stefan for facilitating a place to live, Marielle for her dedication and Kristina for being such an efficient and wonderful secretary. Danke vielmals! Ich hatte viel Spaß in der Schweiz! Ich will zurück kommen!

Hi ha un col·lectiu amb poca aportació científica a la tesi, però que la seva contribució és igual o més important. M'agradaria recordar aquí tants amics i amigues que m'han donat suport, directe o indirecte, durant aquests anys. Són tants i ens coneixem des de fa tant de temps... Nombrar-los un a un seria allargar segurament massa aquest paràgraf, i ells saben que els estic agraït i que també compten amb la meva amistat. Menció especial als meus companys de Pis, els que han anat passant per Passeig de Sant Joan. Al Josep, que m'ha ajudat en el disseny de les tapes i també als grans amics, sincers i diàfans amb mi, que han estat sempre al meu costat: gràcies per la vostra amistat i pel vostre suport.

I finalment m'agradaria dedicar unes paraules a la meva família, a qui tant dec i sense la qual no hauria pogut dur a terme aquest treball. El papà i la mamà sempre han confiat en mi i m'han brindat un suport inestimable. És impressionant i colpidor adonar-se que han posat la seva vida al servei i en funció dels seus fills. Crec que no podré pagar mai el que han fet i fan per mi. La Maria del Mar, la dolça germana gran, també ha estat un bon suport, posant les coses al seu lloc, mirant endavant amb confiança i amb il·lusió, especialment ara que ja és una amb el Sergi. Al Gerard també li agraeixo la seva passió per la ciència, la seva capacitat crítica i de treball, i li auguro un futur prometedor en el camp de la recerca. Només cal que s'hi posi amb la intensitat i rapidesa amb què funciona el seu cervell. I amb la Neus també hem passat unes estones formidables de bon humor. Crec que no revel·lo cap secret si confesso que tinc una debilitat especial per la meva germana petita. Molts ànims amb la carrera, que també les carreres, com les tesis, s'acaben!

Deo gratias.

Contents

1 Introduction

1.1 Alzheimer's disease

Alzheimer's disease (AD) is a progressive, neurodegenerative brain disorder and the most common form of dementia, accounting for 50 % of the cases. The disease involves progressive cognitive and functional impairment, starting with inability to remember recently learned facts and eventually the inability to carry out the simplest tasks [1]. The main risk factor for AD is age, with its incidence doubling every 5 years after the age of 65. It is at this age when most people is diagnosed with AD, however early-onset, familial AD can occur much earlier, although it represents 5% of the cases [2]. More than 35 million people suffer from AD worldwide, and it is predicted to affect 1 in 85 people by 2050 [3]. The economic and social cost of AD is very high. Therefore, as our world population ages, the cure for AD has become one of the challenges of this century.

AD is named after Dr. Alois Alzheimer, a German psychiatrist that identified the first case in 1901. A woman patient had an unusual behavior with her symptoms including memory loss, language problems and unpredictable behavior. Her conditioned worsened and in 1906 she died. Dr. Alzheimer examined her brain and noticed great neuronal loss together with abnormal extracellular protein clumps (now referred as amyloid plaques) and intracellular tangled bungles of protein fibrils (currently denoted neurofibrillary tangles) [4]. Neuronal loss, amyloid plaques and neurofibrillary tangles are currently considered the three main hallmarks of AD.

It was not until the 80s that a significant effort towards the understanding of the molecular mechanisms of AD was made. Analysis of the extracellular amyloid deposits revealed that its major component was a short peptide named amyloid-β (Aβ) [5]. Intracellular neurofibrillary tangles were also found to be mainly composed of the protein tau, a microtubule-stabilizing protein, abnormally hyperphosphorylated [6]. These two findings prompted two approaches into studying the causative effect of Alzheimer's disease: the amyloid hypothesis [7] and

the tau hypothesis [8], postulating Aβ or tau as the fundamental causative agent in AD. After several years of research, it is currently accepted that the neurotoxic effect of tau is downstream to the effect of Aβ [9]. However, it is also known that tau is necessary for neuronal loss to take place [10, 11].

1.2 Aβ production

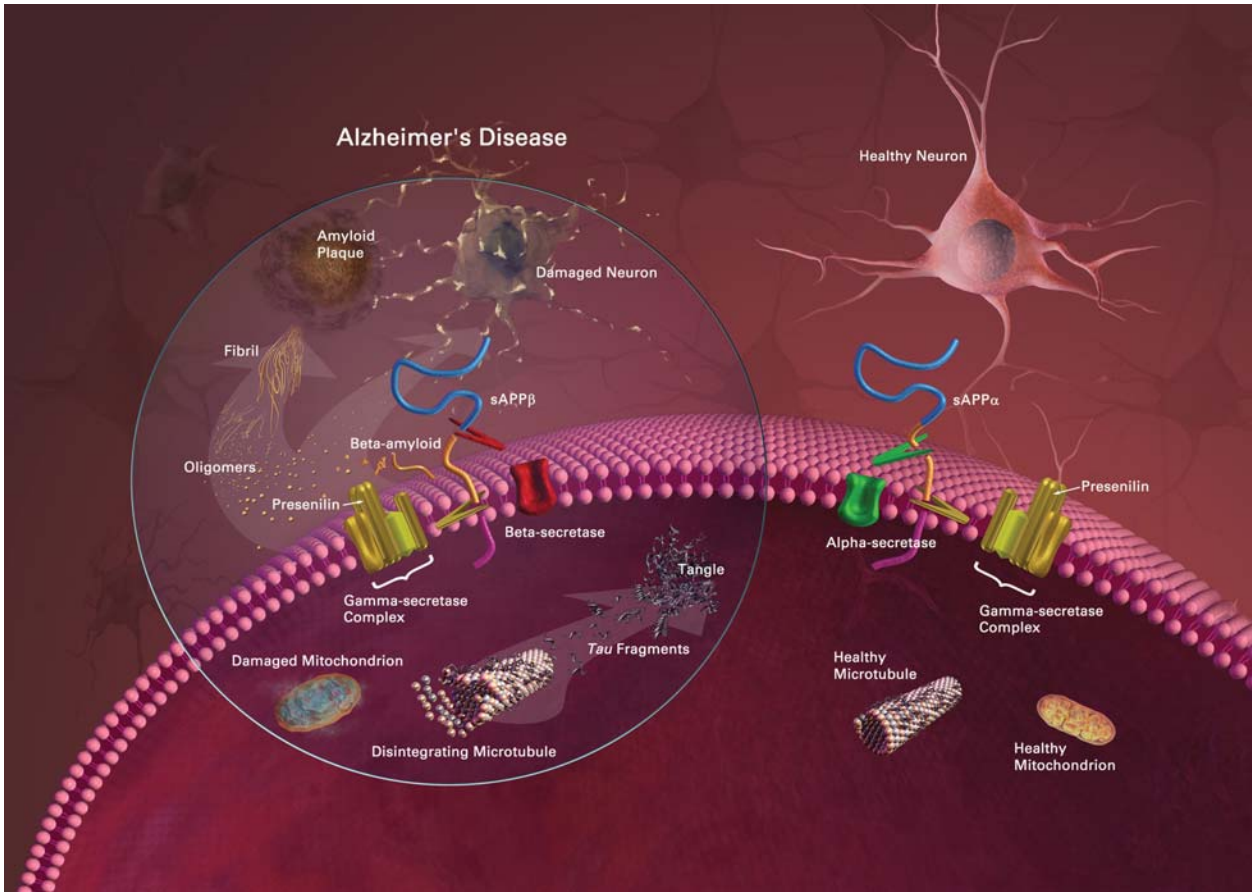

Figure 1.1: Schematic represenation of the formation and aggregation of the Aβ peptide together with the two other hallmarks of Alzheimer's disease: neuronal death and neurofibrillary tangles of hyperphosphorylated tau (left side of the figure). The picture shows as well the non-amyloidogenic processing of APP (right side of the figure). The image is a courtesy from the National Institute of Health (http://www.nia.nih.gov/alzheimers/scientific-images).

Aβ is a peptide obtained from a membrane protein, the amyloid precursor protein (APP) (Figure 1.1). Although the function of APP is not clearly defined, it has been proposed to be involved in neuronal development [12] or in a disputed iron-transport function [13, 14]. APP can be cleaved by two different pathways. The non-amyloidogenic pathway involves α- and γ-secretases, yielding the Amyloid precursor protein Intracellular Cytoplasmatic/C-terminal Domain (AICD) peptide. In the amyloidogenic pathway APP is sequentially cleaved by β- and γ-secretases, resulting in the production of the Aβ peptide. γ-secretase cleavage is not

specific, and a variety of Aβ peptides are formed, ranging from 38 up to 43 amino acids. The most abundantly produced Aβ variant is the one with 40 amino acids, Aβ40, while the most related to neurotoxicity and cognitive defects associated to AD is the one with 42 amino acids, Aβ42 [15, 16]. The ratio between Aβ40 and Aβ42 is a biomarker used in AD [17]. Moreover, Aβ42 is the most abundant variant found in amyloid plaques [18]. Both AICD and Aβ are produced throughout our lives. However, in AD Aβ accumulates either because of an excessive production or a defective clearance. Aβ self-assembles into intermediate oligomeric species that evolve into protofibrils, that finally self-assemble into amyloid fibrils, the main component of amyloid plaques (Figure 1.2). Amyloid fibrils present three main hallmarks [19, 20]: 1) they have a characteristic appearance under analysis in an electron microscope, 2) they are identified by apple-green birefringence when stained with the dye Congo Red and seen under polarized light and 3) they present a typical diffraction pattern, accounting for a beta pleated sheet conformation, with the direction of the polypeptide backbone perpendicular to the fibril axis, what is called a cross-β structure.

Researchers in Japan discovered a glutamate deletion in Aβ E22Δ-Aβ [21]. This peptide variant was reported to form Aβ oligomers but not fibrils, a significant fact that appealed the scientific community to further investigate this peptide. However, later reports showed that E22Δ-Aβ42 aggregated into fibrils as well [22, 23, 24].

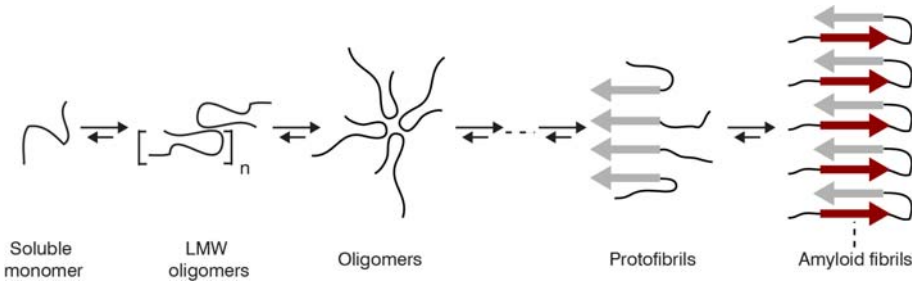

Figure 1.2: Schematic representation of Aβ aggregation. Aβ monomers self-assemble to form low-molecular weight (LMW) oligomers that further aggregate into protofibrils that finally evolve to amyloid fibrils.

1.3 The amyloid hypothesis

Since amyloid fibrils are the main component of amyloid plaques and Aβ is a natural product present in the brains and cerebrospinal fluid (CSF) of humans throughout life, amyloid fibrils were first proposed to be the main causative agents in AD [25]. However, subsequent studies found a lack of correlation between amyloid plaque load and severity of the disease [26], while the soluble pool of Aβ correlated much better with neurotoxicity [27]. For this reason, there was a shift in the amyloid hypothesis: the main causative agents were thought to be the intermediate soluble species in the aggregation of Aβ the so-called Aβ oligomers [28].

A lot of experimental evidence, coming from *in vitro* studies, genetic analysis and the use of mice models, supports the amyloid-β oligomer hypothesis (see review [29] and references therein). Evidence include:

1. APP gene is located in chromosome 21 and AD-like pathology is invariably observed in Down syndrome.
2. Synthetic Aβ peptides are toxic to hippocampal neurons both *in vitro* and *in vivo*.
3. Mutations in the APP gene flanking or inserted in the Aβ region alter the amount of Aβ produced and/or the Aβ aggregation properties. These mutations are involved in the development of early-onset AD.
4. Inherited mutations in the presenilin genes (encoding the β- and γ-secretases) increase the Aβ42:Aβ40 ratio causing early and aggressive forms of AD.
5. In humans, the ApoE ϵ4 allele is a major genetic risk factor to develop late-onset AD and when human ApoE is expressed in mice lacking endogenous ApoE, fibrillar deposits are observed.
6. Transgenic mice with human APP show a time-dependent increase in Aβ and develop behavioral and neuropathological changes equivalent to those observed in AD.
7. Injection of synthetic Aβ into the brains of tau transgenic mice or co-expression of mutant APP with mutant tau accelerates tau hyperphosphorylation and leads to the formation of neurofibrillary tangles similar to those characterizing AD in humans.

1.4 Aβ oligomers: isolation and characterization

In order to tackle AD, important efforts have been made to isolate the species responsible for neurotoxicity. Relevant work comes from the isolation of *in vivo*-derived oligomers. Naturally secreted oligomers of Aβ from cultured cells were found to inhibit hippocampal long-term potentiation (LTP), which is an electrophyisiological parameter related to memory [30]. Another contribution came from the group of Karen Ashe [31]. They were able to isolate an Aβ oligomer (a dodecamer, named Aβ*56) from the brain of transgenic mice modeling to AD-type pathology. Isolated Aβ*56 disrupted memory when administered to young rats. Work from Dennis Selkoe's laboratory showed that Aβ dimers extracted from cerebral cortexes of AD patients impaired synaptic plasticity and LTP in hippocampal neurons [32].

Although the work on *in vivo*-derived oligomers has been significant, these are not well characterized due to sample limitations. Most of the studies characterize the order of natives oligomers using sodium dodecyl sulfate-polyacrylamide gel electrophoresis (SDS-PAGE), with the limitations and artifacts this technique might have [33]. The fact that oligomers

survive the extraction protocol has lead some authors to postulate that these oligomers are covalently cross-linked [34]. However, recentwork from these same authors have suggested that they are an SDS artifact [35]. Besides, toxicity might not rely on just one defined oligomeric species, but on a group of them or on the process of aggregation itself [36, 37].

In order to obtain further structural information on soluble Aβ intermediates, there has been a great effort devoted to the preparation of Aβ oligomers *in vitro*. Protofibrils were isolated using size-exclusion chromatography. They are short, curvilinear species of around 200 nm length and shown to be toxic against cultured cells [38]. A combination of synthetic Aβ42 and cell culture media yields an oligomeric preparation called Amyloid-Derived Diffusible Ligands (ADDLs) [39]. They are a mixture of Aβ aggregates, mainly composed of spherical species of 5-6 nm size. ADDLs were found to be toxic against hippocampal culture cells, and they have been extensively used to model Aβ oligomers both *in vitro* and *in vivo*. Other Aβ oligomers preparations were obtained by stabilizing oligomers using detergents. In this context, Preglobulomers and Globulomers are oligomers derived from the incubation of Aβ42 aggregates with SDS [40, 41]. Preglobulomers are spherical aggregates of 1-2 nm size and a molecular weight of 16/20 kDa. Globulomers are larger, having a molecular weight of 38/42 kDa and 4-5 nm size. Globulomers were found to block LTP *in vitro*.

1.5 The quest for structural characterization of Aβ aggregation

In spite of the efforts to stabilize Aβ oligomers *in vitro*, characterizing them with the available biophysical techniques have proven difficult due to their heterogeneous and dynamic nature.

A wide variety of techniques have been used to characterize Aβ aggregates (Figure 1.3). The Thioflavin T (ThT) binding assay [42] is widely used to quantify the amount of amyloid fibrils in solution. ThT is the chloride salt of a cation (ThT^+) that consists of an N-methylated benzothiazole fragment linked to a dimethylaniline ring. ThT^+ binds to amyloid fibrils *via* two main stabilizing mechanisms [43]: a π–π interaction between the dimethylaniline moiety and the peptide backbone and the CH–π interaction between a Gly residue and the benzothiazole moiety. This second interaction influences ThT fluorescence properties and depends on the amino acid residues of the peptide chain. Although its use is limited to the end product of Aβ aggregation, the knowledge of the interaction of Aβ and ThT has enabled the development of powerful imaging agents in AD [44]. X-ray diffraction yields accurate inter- and intramolecular distance in fibrils and can be used as well to confirm its cross-β structure [45]. Transmission Electron Microscopy (TEM) or Atomic Force Microscopy (AFM) enable characterizing the morphology of aggregates. However, its usefulness is limited by the size of the aggregates (they must be large enough) and by the ability of these aggre-

gates to deposit on the surface analyzed. In combination with solid-state Nuclear Magnetic Resonance (ssNMR), extremely detailed structural information of amyloid fibrils has been obtained [46]. Furthermore, Robert Tycko's laboratory have shown polymorphic structures of Aβ fibrils [47] and recently they have been able to obtain 3D structures of Aβ fibrils derived from brains of actual AD patients [48]. Hydrogen/Deuterium Exchange (HDX) experiments have also been used to map the regions of the Aβ peptide in amyloid fibrils present in the core of the fibril or being part of a flexible and/or exposed region. It is notable the pioneering work by the Ronald Wetzel group in fibrils [49] and protofibrils [50, 51] of Aβ40. The group of Roland Riek made a major contribution by deriving a 3D structure of Aβ42 fibrils [52] when studying a series of Aβ42 mutants using HDX experiments analyzed by NMR.

Important efforts have also been devoted to the characterization of earlier stages of aggregation. An oligomer was isolated and their structure proposed in an AFM study [53]. When combining several techniques, high-resolution structures of oligomers have been obtained: Using EM and X-ray crystallization, David Eisenberg and coworkers were able to characterize a defined type of oligomer of a peptide segment of αB-crystallin, what they called cylindrins [54]. Based on this structure, they proposed a model for Aβ. The group of Yoshitaka Ishii, using EM and ssNMR, derived the structure of a β-sheet rich Aβ intermediate [55]. Solution NMR is a high-resolution technique yielding extremely detailed structural information on proteins and their kinetics. In fact, it has been used to determine the exchange kinetics of Aβ aggregation between monomer and oligomer [56] and monomer to protofibril [57]. Up to date, no Aβ oligomer has been characterized using solution NMR though. However, this technique is not applicable to the study of high-order aggregates as their relaxation properties hamper their detection. Another common technique used to study soluble Aβ aggregates, Dynamic Light Scattering (DLS), determines the hydrodynamic radius (the size) of the different species in solution and allows quantification of aggregates according to their size. However, large fibrillar aggregates cannot be detected quantitatively [58]. Other state-of-the-art techniques have given very valuable information on oligomer structure: Ion mobility coupled to mass spectrometry (IM-MS) gives detailed information on the size and number of subunits of an oligomer present in solution [59], having the ability to preserve the solution structure in the gas phase. This technique facilitates detection of defined Aβ oligomers: Michael Bowers' work stressed the relevance of tetramers and dodecamers in Aβ aggregation [60] as well as the possibility to monitor the influence that Aβ40 has in Aβ42 aggregation and vice-versa [61]. Aβ aggregates such as amyloid fibrils have not been successfully characterized by MS most likely due to difficulties in ionizing them and/or their non-homogeneous nature. Single molecule fluorescence techniques also allow to obtain information with regards to the order of an aggregate but its applicability is limited to low-molecular weight aggregates. Using this technique, it was possible to

characterize the order of different Aβ soluble intermediates in solution together with their interactions with non-covalent complexes of Aβ with another protein, clusterin [62]. Other techniques, such as circular dichroism (CD) or Fourier Transformed Infrared Spectroscopy (FT-IR) [63] can be confidently used throughout the full process of aggregation and they give information about secondary structure. In fact, application of an improvement of traditional FT-IR, Attenuated Total Reflection FT-IR, enabled the distinction of different types of oligomers [64]. However, both CD and FT-IR are not able to distinguis between different species coexisting in solution, since they are averaging techniques. Moreover, in the case of FT-IR the concentration of protein needs to be very high and the use of buffers is restricted.

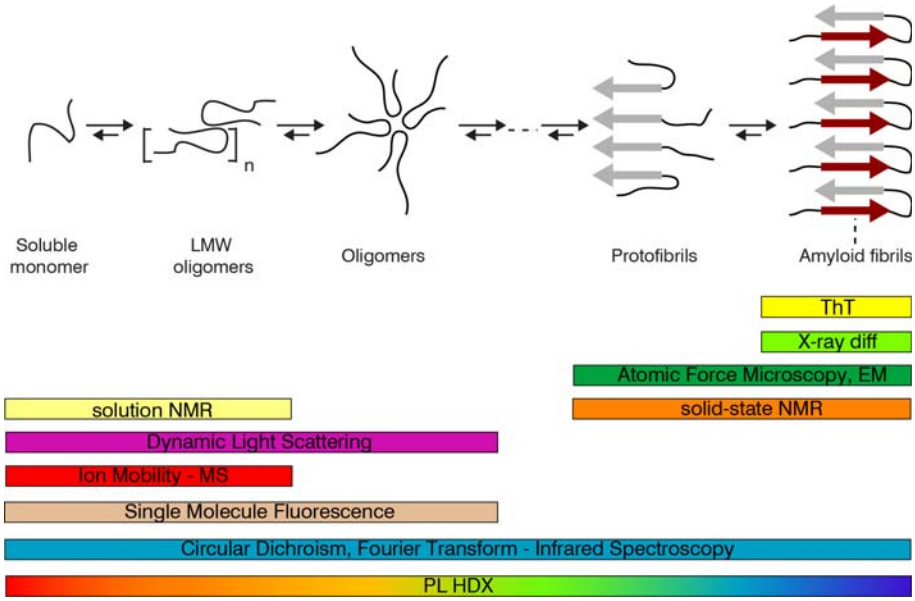

Figure 1.3: Several techniques can be used to characterize Aβ aggregates. To detect, characterize and quantify the different species populating Aβ aggregation we have used PL-HDX experiments.

In order to detect, quantify and characterize the different species formed during Aβ aggregation, we used a pulse-labeling hydrogen/deuterium exchange (PL-HDX) strategy [65]. This part of my work is described in Chapter 3 of this thesis.

1.6 Therapeutics for AD

Even though the mechanism of action of Aβ and even the causative agent of AD is still a matter of debate, much work has been done to pursue the cure of this devastating disease. Currently there are only four drugs marketed against AD, and all of them only provide symptomatic alleviation: Donepezil, Rivastigmine and Galantamine are three cholinesterase inhibitors. The mechanism of action of these drugs consists on enhancing the cholinergic transmission in neurons thus yielding moderate improvement on cognition, behaviour, and

functional and global clinical state in AD patients [66]. Memantine has also beneficial effects on AD patients, and it acts by antagonizing N-Methyl-D-Aspartate (NMDA) receptor [67]. However, none of these drugs are disease-modifying, so the need for a cure for AD is today necessary and urgent.

In order to treat AD several approaches have been taken, and several cellular mechanisms have been targeted [68]. To modulate Aβ production inhibitors of β- and γ-secretases as well as γ-secretase modulators (GSAM) have been developed. Rosiglitazone, a β-secretase inhibitor was discontinued at phase III in 2010 and tarenflurbil and semagacestat, two GSAMs, were discontinued at phase III in 2009. Currently, CHF-507, a small molecule, a GSAM, is in Phase II from 2011 [69]. To target Aβ aggregates, a great effort has been devoted to immunotherapy: antibodies with the ability to disrupt amyloid plaques or capture Aβ such as solaneuzumab and bapineuzumab, reached Phase III clinical trials, but were eventually discontinued. The scientific community met the failure of these two antibodies with disappointment, since they were entirely designed to target the disease according to the amyloid hypothesis. Even though some criticism on the hypothesis raised, it still holds valid to the community [70]. The immunotherapeutic approach to AD still holds an affitope, AD-2, in Phase II clinical trials [71]. Moreover, some small molecules exhibiting anti-aggregation activity have reached advanced clinical trials. The most notorious case was tramiprosate, that reached phase III clinical trials but failed to show a real effect and was discontinued in 2007. Currently, epigallocatechin gallate, a polyphenol isolated from the leaves of the green tea, is in phase III against AD and exhibits anti-aggregation as well as antioxidant activity. Exebryl-1 is a small molecule reducing amyloid load, currently in phase I [72], and PBT-2 is a molecule inhibiting Aβ aggregation together with a chelating activity in Phase II [73]. Most of the compounds described in this paragraph are reviewed in a work from Mangialashce et al. [74] and references therein.

In order to further understand the mechanism of action of the compounds showing anti-aggregation activity, there has been plenty of *in vitro* studies in which the effect of several small molecules have been tested in Aβ aggregation. The use of conformation-specific antibodies, such as A11, an antibody targeting oligomeric but not fibrillar amyloid [75], or OC, an antibody targeting fibrillar and protofibrillar assemblies [76], allowed to identify and classify small molecule mechanism of action in Aβ aggregation: Diallyltartardiamide, orange G, chicago sky blue 6B, direct red 80 and apigenin were found to inhibit Aβ fibrillization by stabilizing oligomers [77], while 2,2'-dihydroxybenzophenone, juglone [77] and methylene blue [78] were found to inhibit oligomer formation but not fibrillization. Studies using a combination of biophysical techniques, such as the ThT binding assay, TEM and MTT assays, showed that entacapone, currently marketed against Parkinson's disease, inhibited Aβ fibrillization and rescued toxicity in PC12 cells [79]. Similarly, salvianolic acid B was found to inhibit Aβ aggregation together with a neuroprotective effect on SH-SY5Y cells [80] and

tramiprosate, formerly in clinical trials, showed as well promising anti-aggregation activity *in vitro* [81]. Tetracycline, a widely used antibiotic, also inhibited Aβ aggregation and rescued neurotoxicity in N2a cells and the mechanism of action proposed consisted on the stabilization of a defined oligomeric species [82]. Stabilizing non-toxic oligomers was also found to be the mechanism of action of riluzole [83], scyllo-inositol, formerly in clinical trials [84, 85, 86] and epigallocatechin gallate [87, 88], currently in clinical trials. Other small molecules act on AD toxicity by chelating metals, such as Cu^{2+}, Zn^{2+} or Fe^{2+}, but have also been shown to inhibit Aβ aggreationon. This is the case of clioquinol [89] and ammonium tetrathiomolybdate [90]. Other compounds showing potential in inhibiting Aβ aggregation are peptides. They offer the possibility of fine-tuning the inhibitory activity due to their affinity for Aβ. Several works have shown *in vitro* the potential of these molecules, although their *in vivo* application is still limited [91]. Of special interest are a group of peptides derived from the same sequence as Aβ found to inhibit Aβ aggregation and exhibiting neuroprotective effects on cell cultures, such as the C-terminal fragments (CTFs) [92] or inrD, a peptide developed in our laboratory [93].

In spite of all the efforts in finding molecules that modulate Aβ aggregation, there is still a significant lack of information in defining the type of Aβ aggregate they stabilize. By applying the PL-HDX strategy we aim at contributing to a better understanding of the mechanism of action of molecules that interfere with Aβ aggregation.

2 Objectives

The objectives we posed for my thesis were the following:

1. Detect, characterize and quantify the different aggregates formed during Aβ aggregation for three Aβ variants with different roles in Alzheimer's disease: Aβ40, Aβ42 and E22Δ-Aβ42.
2. Determine the neurotoxicity associated to each of the detected Aβ aggregates.
3. Monitor the effect of small molecules and a peptide on the different aggregates detected during Aβ42 aggregation.

3

Aβ aggregation

3.1 Results

3.1.1 Characterization of Aβ aggregation by conventional methods

As stated in the objectives of this thesis (Chapter 2), we worked with three different Aβ variants: Aβ40, Aβ42 and E22Δ-Aβ42. The reason for this choice is due to Aβ40 being the Aβ variant most abundantly produced, Aβ42 the most associated with AD and E22Δ-Aβ42 was described, at the beginning of our work, to form oligomers but not amyloid fibrils (see Introduction, section 1.2).

In order to study the aggregation of Aβ using the PL-HDX experiment analyzed by Electrospray Ionization-Mass Spectrometry (ESI-MS), Aβ variants were aggregated at 25°C in MS compatible buffer conditions, such as 50 mM NH_4OAc, 1 mM Tris $\cdot$ HCl and 0.01% NaN_3, pH 7.4. We first monitored the process by using conventional methods. We monitored the aggregation by the ThT binding assay [42], an assay that quantifies amyloid fibrils (Figure 3.1).

Aβ40 showed a lag phase of 13 days and a plateau of maximum fluorescence at 19 days of aggregation, indicating that after 19 days most of the peptide was in fibrillar form. The behavior for Aβ42 was different, showing a lag phase of 6 days and the plateau of maximum fluorescence was reached after 9 days. The behavior of E22Δ-Aβ42 did not follow the typical sigmoidal curve: there was no lag phase and the fluorescence increased throughout the aggregation experiment.

Next, we monitored the aggregation of the Aβ variants by Transmission Electron Microscopy (TEM). Negative-stain TEM allowed us to study the different morphologies of Aβ aggregates at different times during aggregation (Figure 3.2). In agreement with ThT results, Aβ40

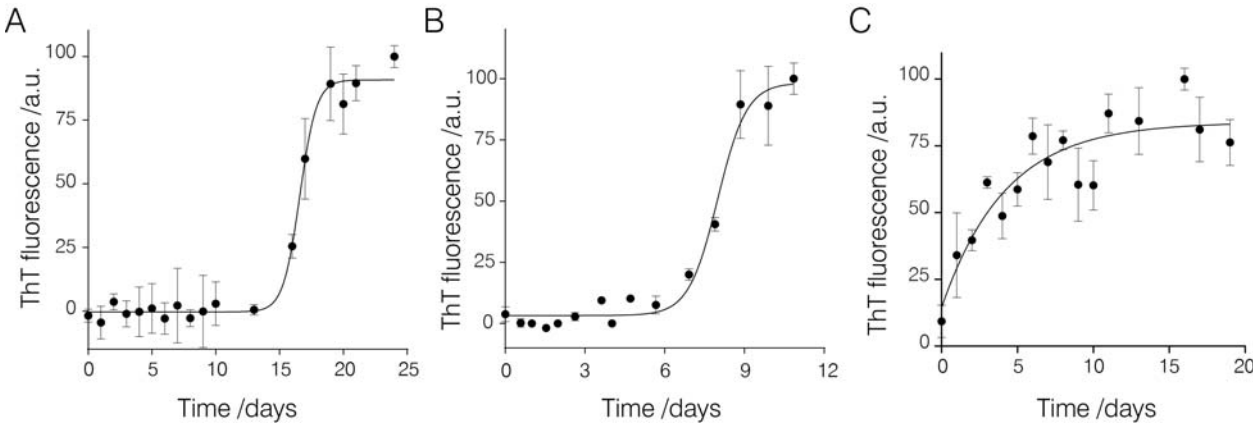

Figure 3.1: The ThT binding assay monitors Aβ fibril content. (A) Aβ40 showed a lag phase of 13 days and after 19 days Aβ40 was aggregated into amyloid fibrils. (B) Aβ42 exhibited 6 days of lag phase and reached the plateau of fluorescence at 9 days. (C) E22Δ-Aβ42 showed a non-conventional behavior, without lag phase and constant increase in ThT fluorescence.

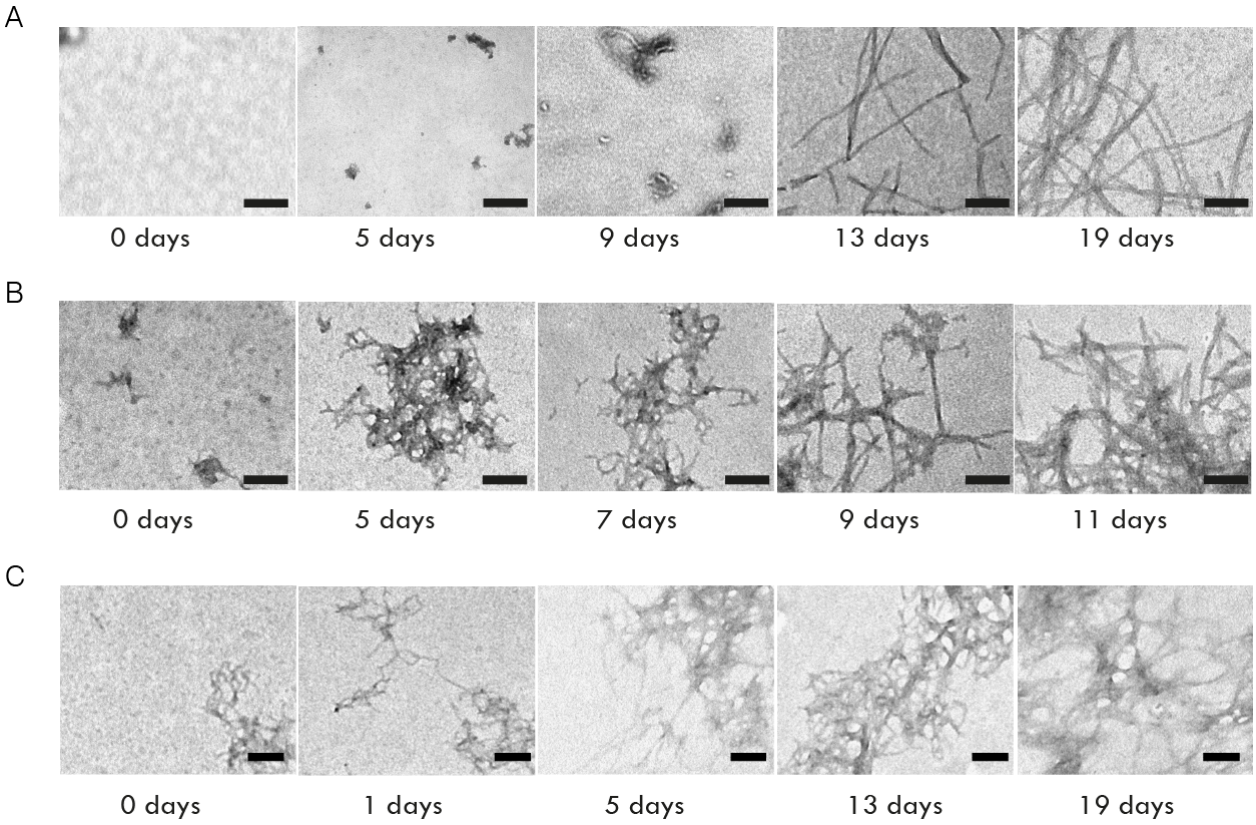

Figure 3.2: Aβ aggregation monitored using negative-stain TEM. A) Aβ40 showed protofibrillar aggregates at early stages, while it formed fibrils after 13 days. B) In Aβ42, protofibrils were observed at intermediate aggregation time points(5-7 days), significantly different from the fibrils observed at later stages (9-11 days). C) E22Δ-Aβ42 aggregated very fast and showed fibrillar material from the initial stages of aggregation (scale bar: 100 nm).

fibrils were observed later than those of Aβ42. Aβ40 required 17 days to form well-defined fibrils, whereas Aβ42 required 9 days of aggregation. It is also significant to notice that both Aβ40 and Aβ42 aggregation showed protofibrillar intermediates (short, curvilinear, small

filaments of around 200 nm) at 9 and 5-7 days, respectively. In the case of E22Δ-Aβ42, we observed protofibrils as well as fibrils from the earliest aggregation time points; after 2 days of aggregation, most of the peptide was in fibrillar form.

Fibrils formed by each of the different Aβ variants were further characterized using X-ray fiber diffraction. Although we experienced difficulties in preparing aligned fibrils, we could obtain diffraction patterns for the intramolecular distance between β-strands as well as the intermolecular distance between consecutive strands by plotting the azimuthal plots (Figure 3.3). In the case of Aβ40 and Aβ42 we obtained identical values: 10.4 and 4.7 Å, respectively, while for E22Δ-Aβ42 the intramolecular distance differed: it was found to be shorter: 10.1 Å. Although there are no reported values in the literature for E22Δ-Aβ42, E22Δ-Aβ40 intermolecular distances were found to be significantly shorter: 9.4 Å [22].

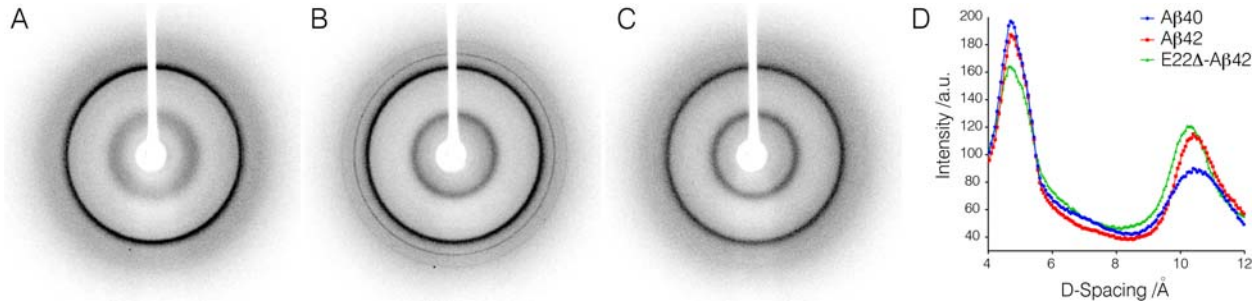

Figure 3.3: Characterization of Aβ fibrils. The fibrils were not aligned, but they showed their reflections in (A) Aβ40, (B) Aβ42 and (C) E22Δ-Aβ42. (D) One-dimensional azimuthal plots, showing intensity as a function of D spacing for Aβ40 (blue), Aβ42 (red) and E22Δ-Aβ42 (green).

3.1.2 Optimization of MS experiments to analyze PL-HDX samples

Both ThT binding assay or TEM studies gave us relevant information with regards to Aβ aggregation. However, the ThT binding assay is not able to distinguish between different species populating Aβ aggregation, as it is only able to interact with amyloid fibrils. Electron microscopy distinguishes between morphologies, being most useful in characterizing high-molecular weight aggregates fibrils, but does not give detailed information on different low-molecular weight aggregates. Moreover, its applicability is determined by the ability of a determined species to deposit on the copper grid. X-ray fiber diffraction, as its names implies, gives structural information on the end-products of the aggregation –the fibrils. For this reason we moved to a technique that might give relevant structural information with regards to the different species populating Aβ aggregation.

The PL-HDX-ESI-MS experiment is based on the solvent accessibility of amide hydrogens. Aβ aggregation is started in a protonated buffer and at a given time of aggregation Δt_{agg},

the solution is exchanged to a deuterated buffer for a short, fixed, labeling time Δt_{label}. This *pulse* of exchange is chosen so that amide protons located in unprotected (unstructured) regions of the aggregates undergo isotope exchange, while amide protons located in protected (structured) regions are retained. To quench the exchange, the sample is freeze-dried. To analyze the deuterium incorporation in the aggregates, these will be dissociated into monomers by transfer to a dimethyl sulfoxide (DMSO) solution, able to preserve the deuteration content [94], and analyzed by ESI-MS (Figure 3.4). MS has the unique ability to detect and characterize populations of molecules with different degrees of exchange, thus enabling the detection of the different species present at a given aggregation time. Therefore, this methodology has the potential to detect and characterize the transient and dynamic intermediate species populating Aβ aggregation.

Desalting methodology

Previous work in our laboratory involving HDX-MS was performed directly infusing the DMSO solution into the mass spectrometer, using disposable needles as a source of nano-ESI and providing an inert atmosphere in the infusion chamber [95]. This methodology was used to study molecular recycling in amyloid fibrils [96] and involved a previous step of ultracentrifugation, so that all the buffer was removed and only the pellet containing the proteic material was analyzed by MS. The ultracentrifugation step, apart from allowing the separation of amyloid fibrils from soluble Aβ species involved as well the virtually complete elimination of salts that may interfere with ESI.

In our case, HDX was quenched by lyophilization, thus the salts were not eliminated. Although NH_4OAc is a volatile salt, $Tris \cdot HCl$ and NaN_3 are not, and they may interfere with ESI-MS spectra giving undesirable adduct peaks. For this reason we decided to include a desalting step prior to the infusion of our sample into the mass spectrometer (see Materials and Methods). This step consisted of the transport of the peptide sample with aqueous buffer to a C8 column, where desalting took place for 1 min at 50 μL/min. Following the product specifications, 10 column volumes were needed for a complete desalting, and 1 minute at 50 μL/min was enought to ensure a complete desalting. The sample was then eluted with acetonitrile (ACN)-based solution into the mass spectrometer for detection. Since the sample to be injected was dissolved in DMSO, we substituted all the PEEK® material by the more resistant Teflon®, including tubing, fittings and the two valves needed for the desalting step. Moreover, in order to minimize the back exchange in the desalting step, the system was kept at low temperature using ice to cool the solvents and the valve system.

Once we had the experimental design for the ESI-MS analysis, we optimized the working conditions. We performed the optimization experiments with the Aβ40 peptide dissolved at 50 μM in the DMSO-based buffer (composition described in the Materials and Methods

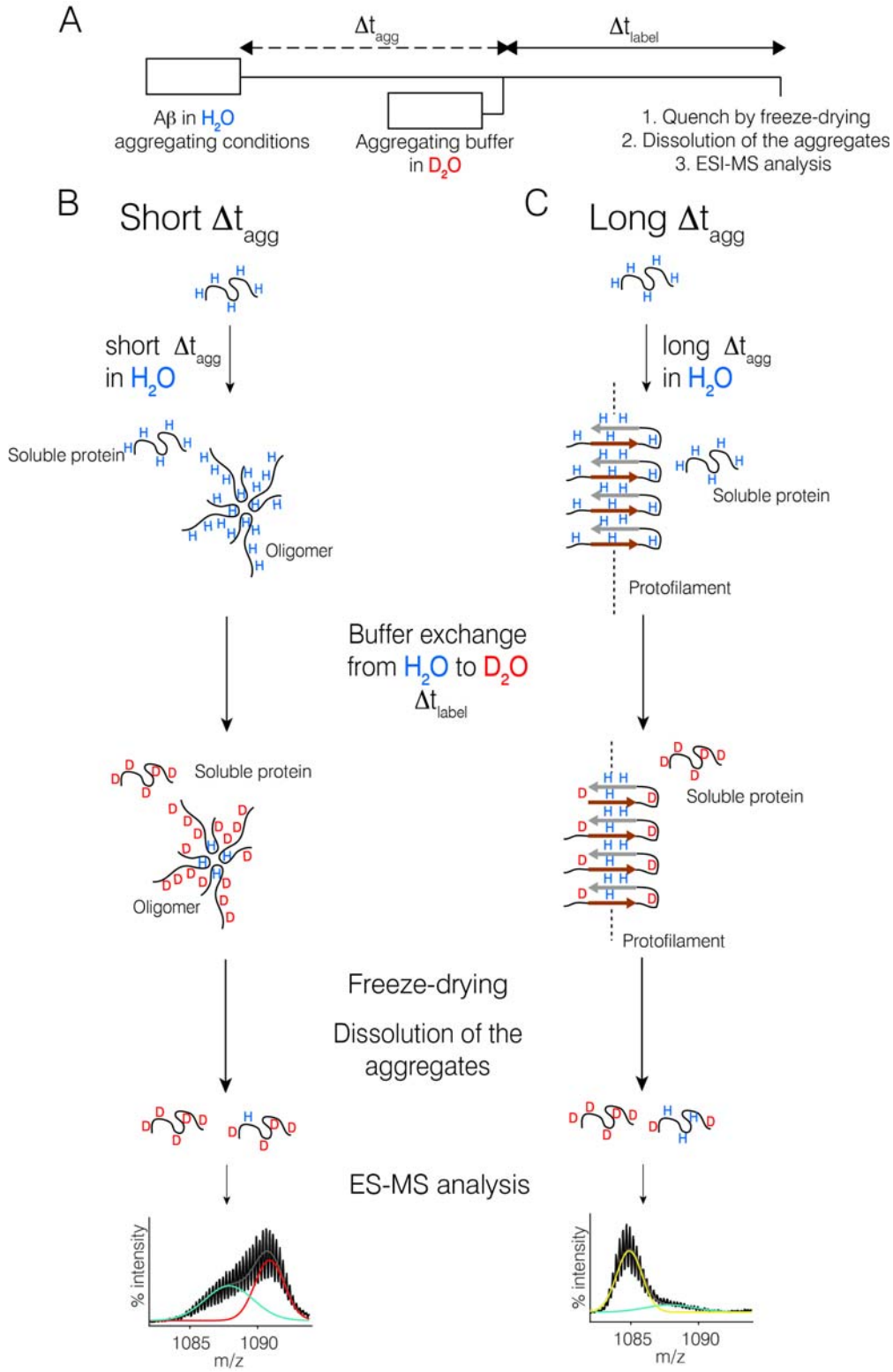

Figure 3.4: Schematic representation of the PL-HDX-ESI-MS exchange experiment. (A) The experiment starts by incubating soluble protein under aggregation conditions in a protonated buffer. After a variable aggregation time, Δt_{agg}, labeling takes place for a fixed period, Δt_{label}, using deuterated buffer. The magnitude of Δt_{label} is chosen so that only unprotected amide protons will significantly exchange with the solvent. After the labeling pulse, freeze-drying is used to quench exchange. Different samples are prepared at defined Δt_{agg} values, which are later solubilized into monomers by transfer to a DMSO solution and analyzed by ESI-MS. The figures depict hypothetical scenarios in which Aβ is left to aggregate for a short Δt_{agg} (B) or a long Δt_{agg} (C).

section of this chapter). We found out that increasing from 2 to 4 kV the capillary voltage and keeping the standard 100 V of sample cone, highly reduced the amount of DMSO and dichloroacetic adducts on Aβ40 peaks (Figure 3.5).

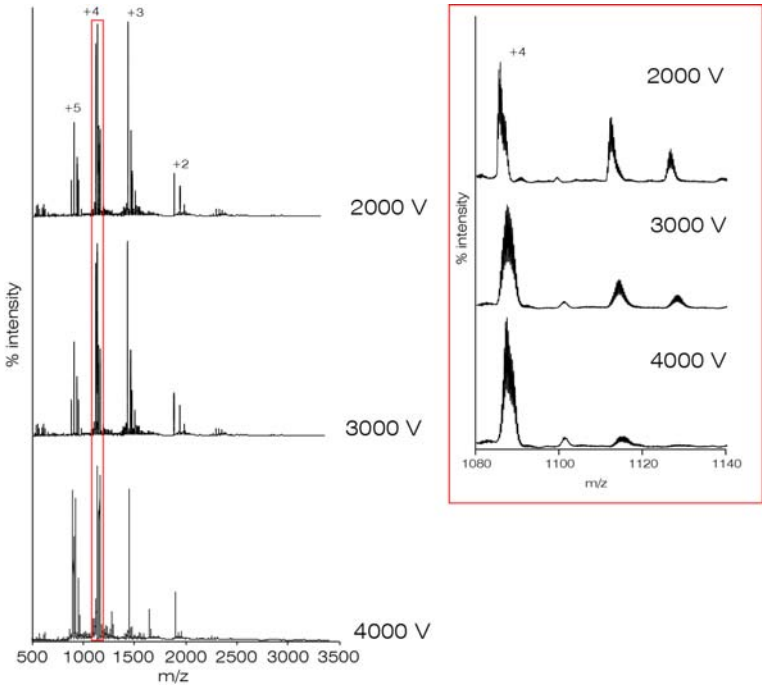

Figure 3.5: Complete MS spectra for Aβ40 are shown at 2000 V, 3000 V and 4000 V of capillary voltage at constant 100 V of sample cone. An inset of the +4 charge state is shown in which adduct content is decreased as capillary voltage is increased.

Preserving HDX information during PL-HDX experiments

An important feature when performing HDX experiments is minimizing exchange during experimental manipulation. There is the possibility to incorporate additional deuterium atoms due to exchange with the solubilizing agent (Forward Exchange) and the possibility of losing incorporated deuterium due to exchange with hydrogens of atmospheric water or the hygroscopic nature of the solvent (Back Exchange). Controls for forward and back exchange were prepared and analyzed as described in the Materials and Methods section.

Additional controls were carried out to establish that HDX information was preserved during PL-HDX sample preparation. We dissolved monomeric Aβ40 at 30 μMin protonated buffer (50 mM NH_4OAc, 1 mM Tris $\cdot$ HCl and 0.01% NaN_3, pH 7.4) and we diluted the sample 1/10 with D_2O. After 10 seconds of exchange, we froze the sample in liquid N_2 and lyophilized it. Afterwards, we dissolved it in the DMSO-based buffer and analyzed it by ESI-MS. We expected that all backbone amides of monomeric Aβ40 had exchanged to deuterons during the labeling pulse and therefore obtained m/z values comparable to those for back exchange controls. However, we obtained a m/z value lower than that for the back exchange control

(see Materials and Methods in this chapter for the control preparation), which meant that throughout the PL-HDX experiment, the deuterium content in Aβ was not preserved (Figure 3.6B). When we analyzed by MS Aβ40 after exchange but without the lyophilization step we obtained m/z values identical to those for back exchange; this meant that in the lyophilization step a high amount of back exchange was occurring (Figure 3.6C). For this reason we did not lyophilize the sample but used a centrifugal evaporator, and this contributed to minimizing back exchange (Figure 3.6D). However, when we performed the PL-HDX experiment and we lyophilized the exchanged Aβ40 peptide "alone", that is, being the only sample in the lyophilizer, we were able to obtain an m/z value comparable to the back exchange control. This meant that inside the lyophilizer there is HDX occurring from the different samples being processed. From then on, we performed our experiments lyophilizing in our own lyophilizer, thus avoiding any water interference coming from other samples.

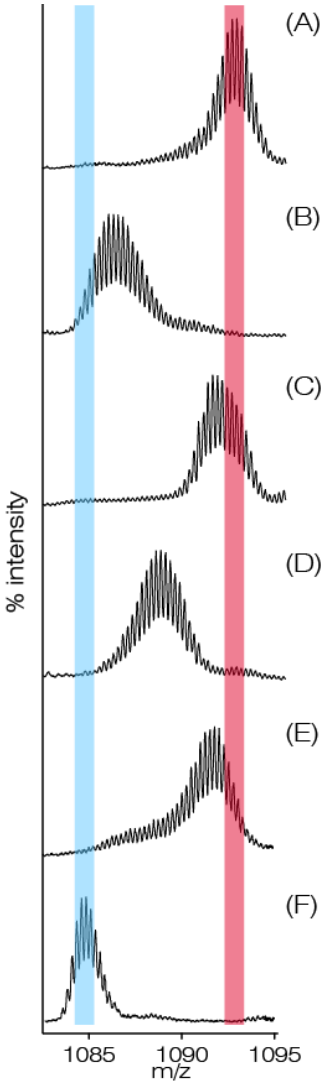

Figure 3.6: Keeping deuterium content in Aβ samples: (A) Aβ40 back exchange control (B) Deuterated Aβ40 after lyophilization dissolved in the DMSO-based buffer. (C) Aβ40 after HDX. (D) Deuterated Aβ40 analyzed after centrifugal evaporation dissolved in the DMSO-based buffer. (E) Deuterated Aβ40 after isolated lyophilization dissolved in the DMSO-based buffer. (F) Aβ40 forward exchange control. The blue and red bars indicate the m/z corresponding to the forward and back control respectively.

3.1.3 Characterization of Aβ aggregation by PL-HDX-ESI-MS overcomes the heterogeneity of the process

We applied the PL-HDX-ESI-MS methodology to characterize the different species populating Aβ aggregation for Aβ40 (Figure 3.7), Aβ42 (Figure 3.8) and E22Δ-Aβ42 (Figure 3.9). In the three cases the MS spectra follow a similar pattern: at the earlier time points, Aβ has higher mass while at the end of the aggregation, the spectra correspond to peptide with lower mass. This is consistent with the fact that Aβ is at first in a low aggregated form, having more exposed amide protons available to exchange to deuterons, while after several days of aggregation Aβ forms higher order aggregates, those adopting more compact structures and thus having less exposed amides available to HDX.

In order to obtain more information from the PL-HDX experiment, we globally adjusted the mass spectra obtained for each Aβ variant to a combination of gaussian curves in collaboration with Dr. Sergio Madurga, from the University of Barcelona (for a detailed explanation of the fitting see Materials and Methods). Each gaussian curve represents a different species present during Aβ aggregation. For each Aβ variant, all the MS spectra (triplicates for each timepoint) were adjusted to a specific number number of gaussians: 3 in the case of Aβ40 and Aβ42, and 2 for E22Δ-Aβ42.

Aβ40

When the PL-HDX-ESI-MS experiment was used to study the aggregation of Aβ40, three different species were detected by ESI-MS (Figure 3.7). The first species detected corresponded in mass to the protein with all backbone amides exposed (37.4 ± 0.5, in red), suggesting that it might include monomer and/or aggregates giving no protection against HDX.Besides, the relative population of this species gradually decreased from 0 days to 17 days. This species was named early aggregates ($EA_{A\beta40}$). The second species detected corresponded to average masses indicative of 25.1 ± 1.0 amides (in cyan). Based on the peak width, this was the most heterogeneous species formed during aggregation when compared to the other two detected (Figure 3.7C), and its presence was constant being maximal at 13 days of aggregation. Combining this information with the TEM results (Figure 3.2), this species was assigned to protofibrils of Aβ40 ($PF_{A\beta40}$). The last species detected corresponded to average masses that indicated the presence of 13.5 ± 0.6 exposed amides (in ochre). Because these species appeared toward the end of the aggregation and its population significantly correlated with the ThT signal and the observations of well-defined fibrils by TEM, we attributed these species to fibrils, $F_{A\beta40}$ [49].

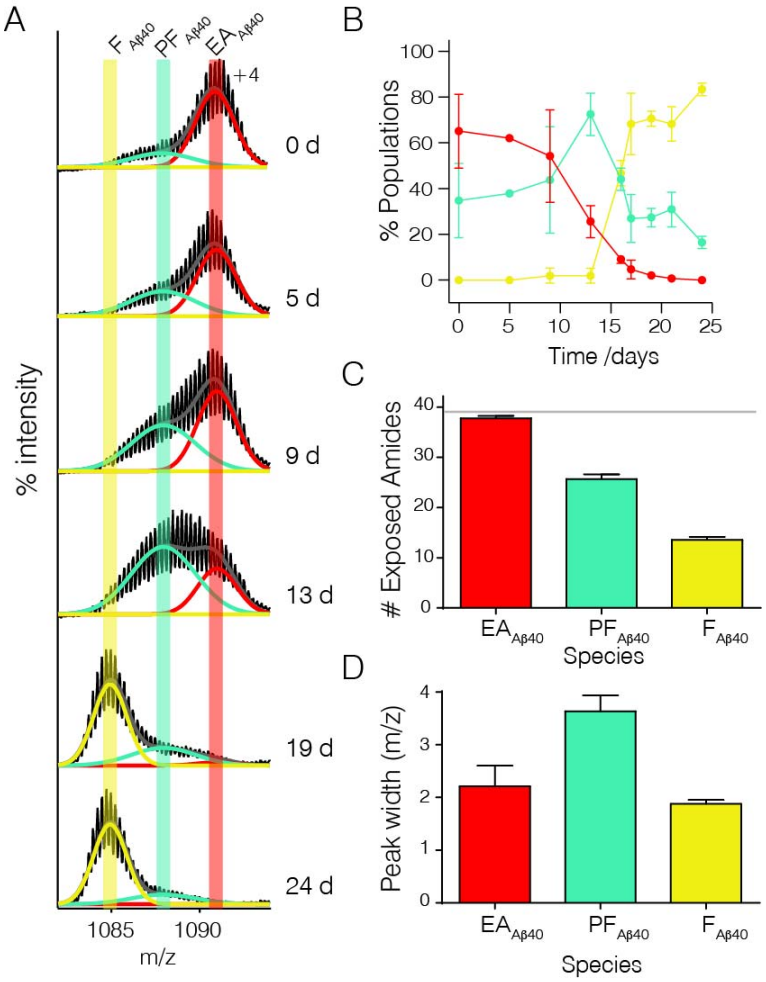

Figure 3.7: PL-HDX results analyzed by ESI-MS for Aβ40. (A) The MS spectra show the relative populations of the species detected: $EA_{A\beta40}$ (red), $PF_{A\beta40}$ (cyan) and $F_{A\beta40}$ (ochre). (B) Population percentage of each detected species as a function of Δt_{agg}. (C) Number of exposed amides for each detected species. (D) Peak width for each detected species.

Aβ42

The aggregation of Aβ42 was also studied by means of the PL-HDX-ESI-MS strategy (Figure 3.8). Three species were detected for Aβ42 aggregation, the same as for Aβ40. However, our experiments showed that the nature of some of the species detected were different for both peptides. The number of exposed amides detected for the first species detected (32.8 $\pm$ 0.8, in green) was significantly lower than what we would expect if all the amide protons of monomeric Aβ42 were exposed to the solvent (41). We named them $EA_{A\beta42}$. These results are consistent with the higher tendency of Aβ42 to aggregate. Similarly to Aβ40, the majoritary species at intermediate Δt_{agg}, with 23.6 $\pm$ 1.8 exposed amides, was the most heterogeneous species detected (in blue) (Figure 3.8C) and its presence was constant throughout the aggregation being maximal at 7 days. This species were less aggregated than fibrils. Electron microscopy images clearly show abundant protofibrils (short, curvilinear

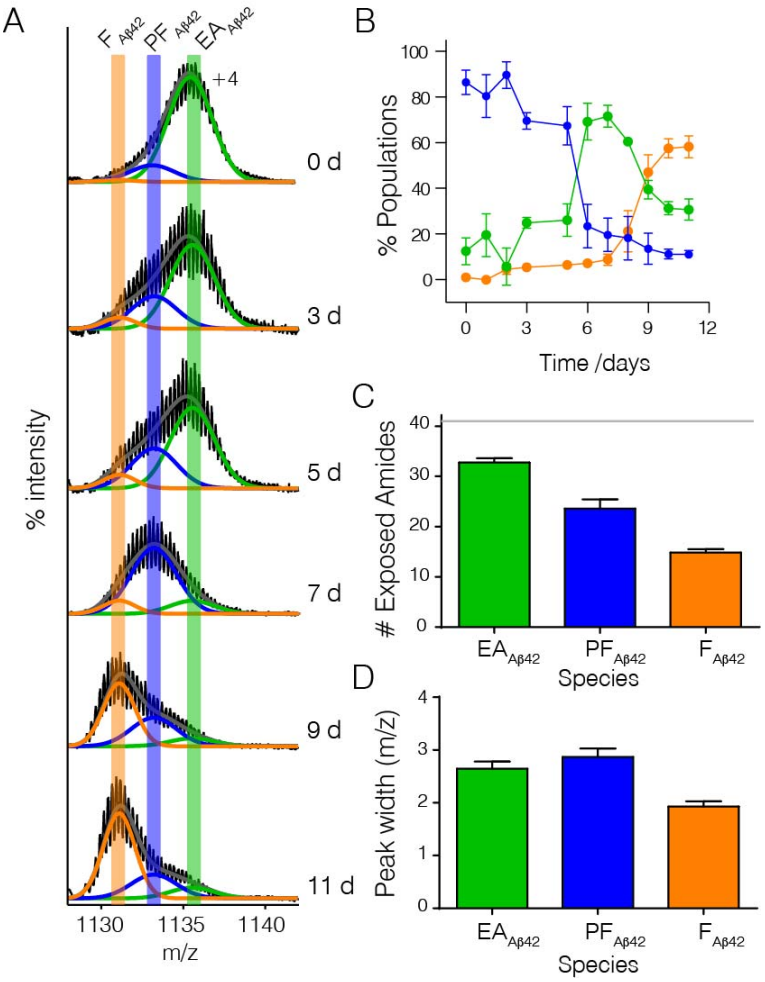

Figure 3.8: PL-HDX-ESI-MS results for Aβ42. (A) The MS spectra show the relative populations of the three species detected: $EA_{A\beta42}$ (green), $PF_{A\beta42}$ (blue) and $F_{A\beta42}$ (orange). (B) Population percentage of each detected species as a function of Δt_{agg}. (C) Number of exposed amides for each detected species. (D) Peak width for each detected species.

aggregates of 200 nm) when the amount of this species is maximal (at 7 days). These observations pointed to this species as being protofibrils, $PF_{A\beta42}$. This assumption can be corroborated taking into account other work in the bibliography: in 2006, it was found that the HDX protection of isolated protofibrils [51] was 26 ± 2 (for Aβ40), which closely resembles the values obtained in our experiments. The last detected species corresponded in mass to species presenting 14.8 ± 0.7 exposed amides (in orange). This species were assigned to fibrils, $F_{A\beta42}$ [52], and its relative population significantly correlated with the ThT signal.

E22Δ-Aβ42

The PL-HDX-ESI-MS experiment was applied as well to the study of E22Δ-Aβ42 (Figure 3.9). Two different species were detected. The most abundant species at early aggregation times corresponded to an aggregate showing higher protection than monomeric E22Δ-Aβ42

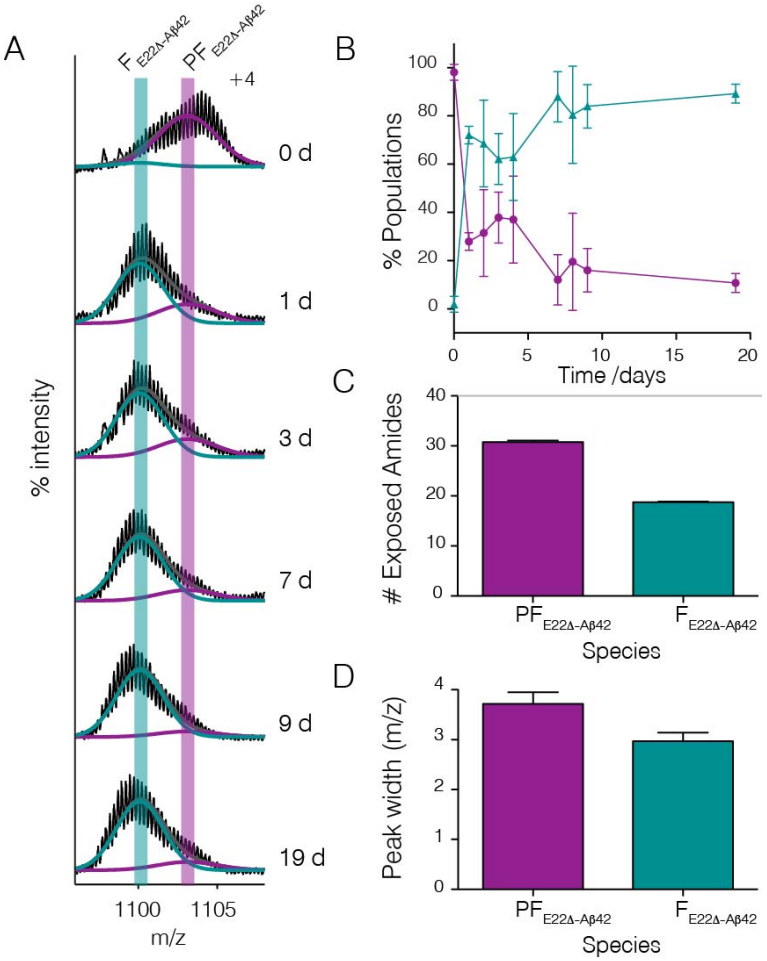

Figure 3.9: PL-HDX-ESI-MS results for E22Δ-Aβ42. (A) The MS spectra show the relative populations of the two species detected: $PF_{E22\Delta\text{-}A\beta42}$ (violet) and $F_{E22\Delta\text{-}A\beta42}$ (turquoise). (B) Population percentage of each detected species as a function of Δt_{agg}. (C) Number of exposed amides for each detected species. (D) Peak width for each detected species.

(30.8 $\pm$ 0.3). EM results described before(Figure 3.2C) showed the presence of abundant protofibrils and we named it $PF_{E22\Delta\text{-}A\beta42}$. The relative amount of $PF_{E22\Delta\text{-}A\beta42}$ immediately decreases after the initial stages of aggregation, while the later aggregates, E22Δ-Aβ42 fibrillar ($F_{E22\Delta\text{-}A\beta42}$) population concomitantly increases. All together, these experiments provide further evidence of the extremely higher tendency of this peptide to aggregate.

3.1.4 Setup of a primary neuronal viability assay to study Aβ neurotoxicity

The previous section showed the ability of the PL-HDX-ESI-MS strategy to "dissect" the different species populating Aβ aggregation. Once we were able to detect these aggregates, we aimed at assigning the contribution of any species to a given variable. Since Aβ is related to the neurotoxicity observed in AD, we decided to test the neurotoxicity of Aβ aggregates (for

experimental details, see Materials and Methods) in collaboration with Dr. Lluís Pujadas, Dr. Daniela Rossi and Prof. Eduardo Soriano from the University of Barcelona.

In order to measure the toxicity of the Aβ preparations, we decided to work with primary neuronal cultures from mice hippocampus. The assay we used to monitor neurotoxicity was the well-established, rapid, convenient, economical and widely used 3-(4,5-dimethylthiazol-2-yl)-2,5-diphenyltetrazolium bromide (MTT) assay [97]. This assay is based on the cleavage of MTT, a yellow tetrazolium salt, to form a soluble blue/violet formazan product by mitochondrial enzymes. The amount of formazan produced is directly proportional to the number of living, not dead cells, present during MTT exposure and can be quantified by an absorbance plate reader.

To optimize the MTT conditions such as Aβ concentration and incubation time, we worked with ADDLs. ADDLs are synthetically derived Aβ42 oligomers that have been widely used to study Aβ oligomer neurotoxicity (see Introduction, section 1.4). We treated primary neural cultures with ADDLs and its corresponding vehicles at an Aβ42 concentration of 3, 5 and 10 μM. Sampls were left incubating different time before performing the MTT reaction: 4, 15 and 24 hours (Figure 3.10). ADDLs showed a dose-response effect and the vehicle some toxicity, a result consistent with previous reports [98]. Only after 24 h incubation the toxicity of ADDLs was significantly different from the vehicle. As an additional control, we tested the toxicity of our aggregating buffer. Since the buffer contains 0.01% NaN_3 and NH_4OAc we wanted to ensure that the putative buffer toxicity would not be so high as to hamper our measurements. We determined a good compromise between ability to observe toxicity in ADDLs and low toxicity of its vehicle and our aggregating buffer when working at a 5 μM Aβ concentration and incubating for 24 h.

3.1.5 PFs are the main responsible for neurotoxicity in primary hippocampal neurons

Having established a protocol to assay the effect of Aβ aggregates in neural cultures, we tested the contribution of the different Aβ species detected during aggregation to toxicity. To establish the effect of all the samples obtained at different Δt_{agg} in the same primary neuronal culture, we first determined the effect of sample freezing and thawing on the structure of the aggregates. We found that aggregates formed during fibril formation retained their structure after a freezing/thawing cicle (Figure 3.11).

We next treated primary hippocampal neuronal cultures with frozen and thawed aliquots of the same samples that had been studied in the PL-HDX-ESI-MS experiment and measured the percentage of neuronal survival by the MTT assay.

In the case of Aβ40, neuronal survival steadily decreased from 90% to a maximum toxicity of

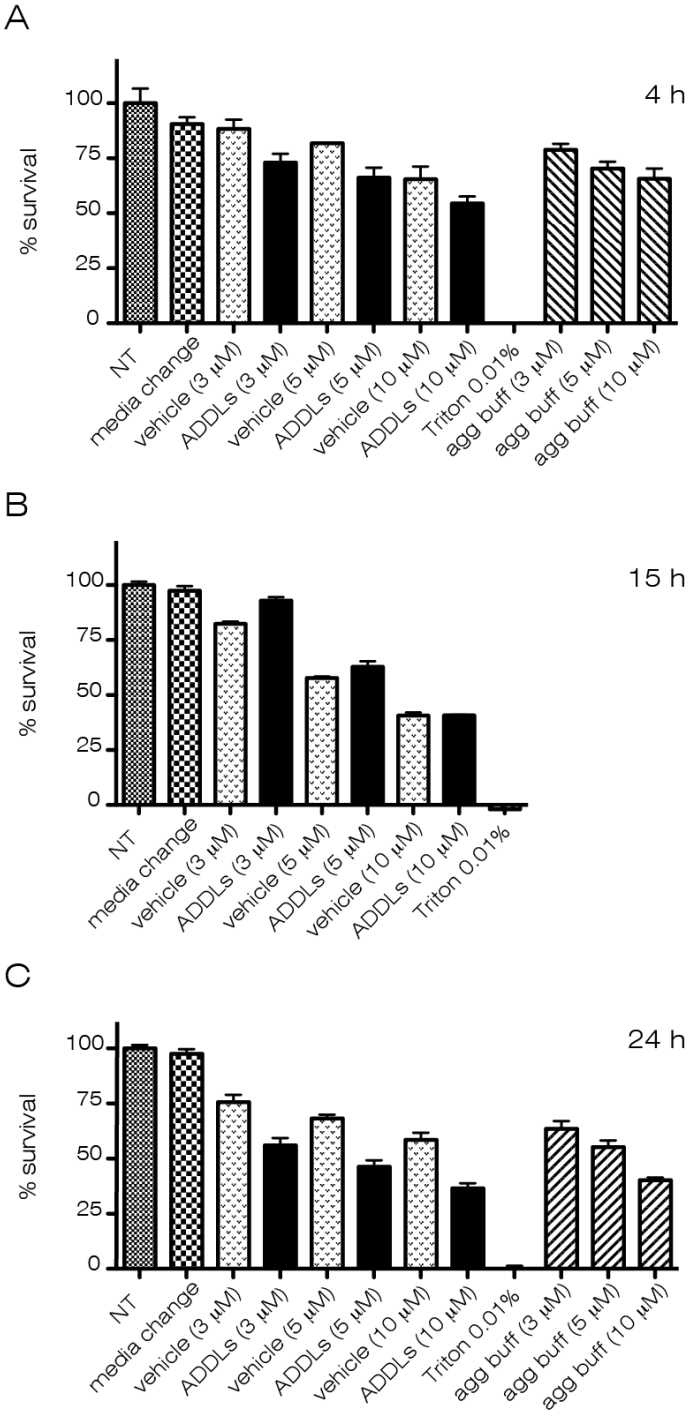

Figure 3.10: Optimization for the MTT assay using ADDLs. Viability in primary cultures incubated (A) 4 hours, (B) 15 hours and (C) 24 hours after sample treatment previous to the MTT reaction. 100 % viability is adjusted to NT (non-treated) cells. The aggregating buffer (agg buff) is composed of 50 mM NH_4OAc, 1 mM Tris $\cdot$ HCl and 0.01% NaN_3, pH 7.4.

65% at 17 days. Later aggregation time points showed less toxicity thus survival gradually increased to 80% of viability at 24 days (Figure 3.12A). For a given Δt_{agg}, we combined the populations obtained by ESI-MS with the MTT results and then used a multi-linear regression analysis to obtain the toxicity adscribed to each detected species ($EA_{A\beta 40}$: 101 $\pm$

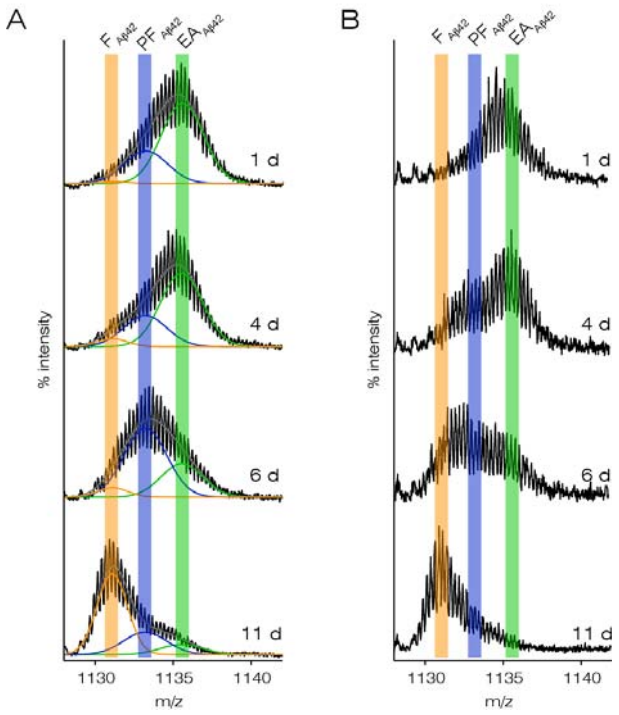

Figure 3.11: Freezing and thawing samples obtained at different times of Aβ aggregation retains the structure of the aggregates. ESI-MS mass spectra (+4 charge state) showing the relative populations of species detected during Aβ42 aggregation at the indicated Δt_{agg} times for (A) samples that have not undergone freezing and thawing and (B) samples that have undergone freezing and thawing previous to PL-HDX-ESI-MS experiments. Peaks representing EA, PF and F are shown as green, blue and orange bands, respectively. Peak intensities are normalized to the overall species population.

12, $PF_{A\beta40}$: 56 ± 13, $F_{A\beta40}$: 78 ± 7). $PF_{A\beta40}$ was the population most strongly associated to neurotoxicity.

When the same experiment was carried out with the Aβ42 preparations, a similar pattern to that of Aβ40 was observed although the relationship between $PF_{A\beta42}$ and neurotoxicity was even more noticeable (Figure 3.12B). Earlier aggregation time points displayed higher toxicity than for Aβ40 (exhibiting 80% viability at day 0) and the viability gradually decreased to 38% at 7 days (maximum toxicity). Then viability increased until reaching the same value as at the beginning, 80% at 11 days. When combining the ESI-MS data with the MTT results in a multi-linear regression analysis, the toxicity of each detected species was found to be the following: $EA_{A\beta42}$: 74 ± 7, $PF_{A\beta42}$: 17 ± 10, $F_{A\beta42}$: 106 ± 12. Although the relative ratios of PF during Aβ40 and Aβ42 aggregation are similar, $PF_{A\beta42}$ showed higher neurotoxicity and higher correlation to the global toxicity observed.

For E22Δ-Aβ42 almost no toxicity was observed (Figure 3.12C), so we did not determine the toxicity corresponding to the species populating the aggregation of E22Δ-Aβ42.

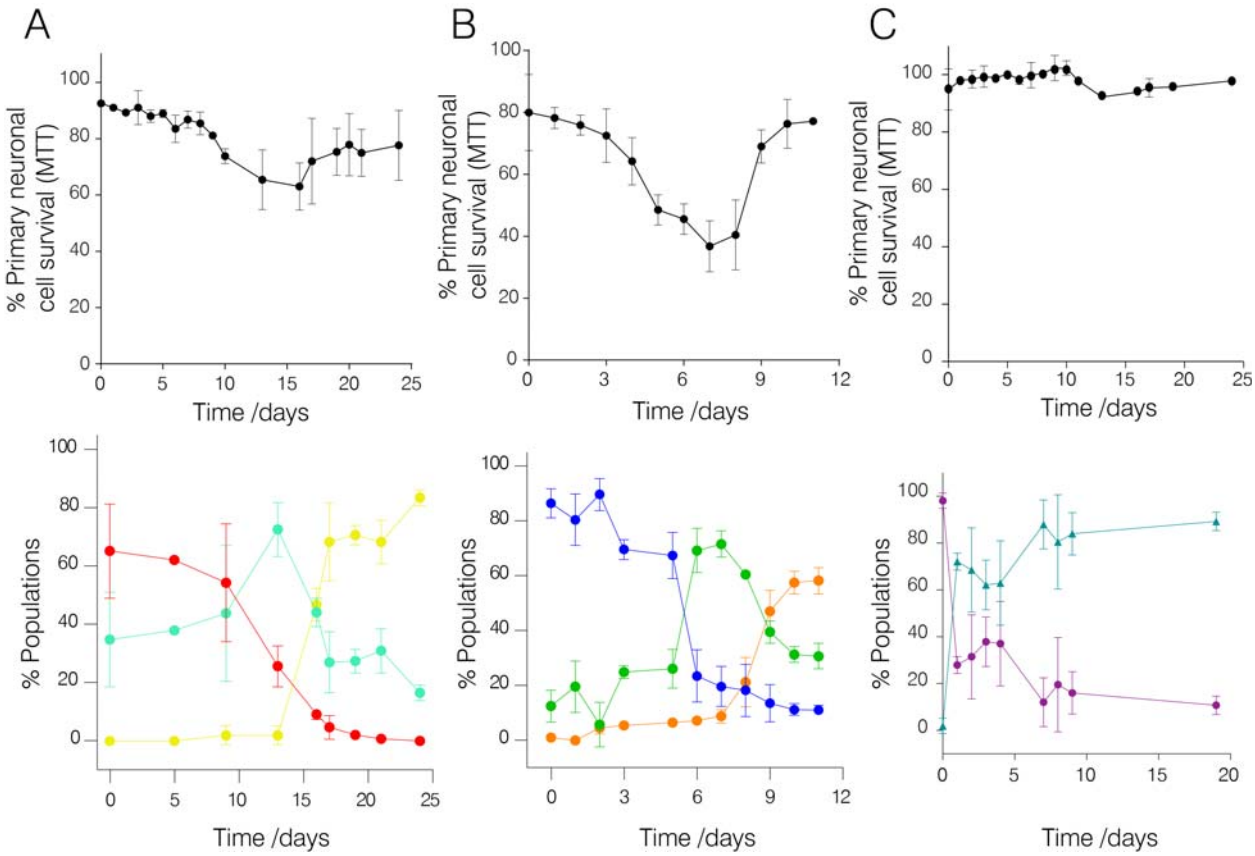

Figure 3.12: Toxicity of Aβ was evaluated by the MTT assay. (A) Aβ40 showed a profile in which the earlier and later aggregation times were less toxic than the intermediates. (B) The trend for Aβ42 was even clearer, pointing to PFs as the principal responsible for neurotoxicity. (C) In the case of E22Δ-Aβ42 almost no toxicity was observed. Aβ concentration was 5 μM. 100 % viability is adjusted to the vehicle (the ammonium acetate buffer).
Population percentages of Aβ species are included below to help visualize the significant correlation between cell viability and PF abundance.

3.2 Discussion

With the PL-HDX-ESI-MS experiment we have been able to overcome the heterogeneity of the process of Aβ aggregation. We have been able to detect, characterize and quantify the different species populating Aβ aggregation: three for Aβ40 and Aβ42, and two for E22Δ-Aβ42.

Although the same number of species were detected for both Aβ40 and Aβ42, our data indicates that there are structural differences. The differences in exposed amides in $EA_{A\beta40}$ and $EA_{A\beta42}$ is consistent with early aggregates of Aβ40 being soluble monomer and/or unstructured and/or highly dynamic aggregates while those of Aβ42 comprising more structured and/or less dynamic aggregates. Thus, the different structure and/or dynamic properties of the early aggregates formed by the two Aβ variants offer an explanation for the higher

tendency to aggregate of Aβ42 compared to Aβ40. Besides, there are differences between $PF_{A\beta40}$ and $PF_{A\beta42}$, although their protection against HDX is very similar and consistent with previously reported data [50]. In agreement with the general finding that Aβ42 is more toxic than Aβ40 [15, 16], the toxicity of $PF_{A\beta42}$ was shown to be significantly higher than $PF_{A\beta40}$. The two extra amino acids confer Aβ42 a higher tendency to aggregate and form different species [99]. One possibility to explain differences in toxicity between $PF_{A\beta40}$ and $PF_{A\beta42}$ could be that $PF_{A\beta42}$ have a higher fraction of hydrophobic side chains exposed to the solvent than $PF_{A\beta40}$.

We showed PFs as the most toxic species populating Aβ aggregation. If Aβ toxicity is exerted via cell membrane disruption by pore formation or any other mechanism [100], the ability of $PF_{A\beta42}$ to disrupt the cell membrane would be higher than for $PF_{A\beta40}$. One possible explanation could be due to the higher hydrophobicity of Aβ42 when compared to Aβ40 and the different aggregation behavior of the two peptides as explained above. However, there are two studies claiming that toxicity is not linked to specific prefibrillar aggregates but to the ability of these species to grow and undergo fibril formation [36, 37]. The toxicity of a defined species (be it oligomer/protofibril or fibril) was found to be lower than this same species in contact with monomeric Aβ or both species together. The relative population of protofibrils as a function of aggregation time, as determined in our PL-HDX-ESI-MS experiments, follows a gaussian distribution. During the first half of the distribution, protofibrils coexist with early aggregates so toxicity might be mediated by the process of protofibril-early aggregate interactions. However, during the second half of the distribution protofibrils coexist mainly with fibrils and toxicity is still observed. Thus, although our results are not consistent with specific protofibril-monomer/early aggregate interactions, they would be consistent with protofibrils exerting their neurotoxicity through maturation. It is also important to take into account that the toxicity of protofibrils is higher than monomer and fibrils [37] and these species have been proposed to be the main culprits of Alzheimer's disease [101].

The detection of three species with different structure as well as their evolution as a function of time is in agreement with the nucleated conformational conversion (NCC) mechanism of amyloid formation [102]. NCC proposes that monomers and/or low structured early aggregates, EA, progress to more structured protofibrilar aggregates, PF, not yet locked into rigid structure yet capable to evolve into rigid fibrillar forms, F. Our results are also in agreement with a recent work carried out using single molecule fluorescence to study the aggregation of α-synuclein [103]. The authors also identified structural rearrangements during α-synuclein aggregation from initially formed oligomers to stable, more compact proteinase-K-resistant oligomers that ultimately lead to fibril formation. In agreement with our results, the more compact oligomers were those found more damaging to cells.

An aspect that also must be taken into consideration is the behavior of E22Δ-Aβ42. Con-

sistently with previous reports, this peptide aggregated very fast [24, 23, 22]. However, we failed to reproduce the toxicity observed in previous reports. We attribute this to a different way to measure toxicity: in our MTT assays we show that Aβ fibrils (either 40, 42 or E22Δ) do not display much toxicity and In a similar experiment carried out by the Glockshuber group, the Lactate Dehydrogenase (LDH) assay, [23] they observed toxicity for Aβ42 but not for E22Δ-Aβ42. However, when determining E22Δ-Aβ42 toxicity with LTP measurements [21] or by neurite length measurements [23], E22Δ-Aβ42 as well as Aβ42 displayed significant neurotoxic behavior.

To summarize, we have detected different aggregates present during Aβ aggregation using the PL-HDX-ESI-MS. The fact that aggregates formed during the process of aggregation show different protection against HDX indicates that each of them adopts different structures and therefore that during the process of Aβ aggregation structural rearrangements occur. By carrying out parallel neurotoxicity experiments, we found that protofibrils, formed as a result of a structural rearrangement, were the most toxic species to neurons. Thus, our work points to the establishment of the structural determinants of Aβ protofibril neurotoxicity as a critical step to develop efficient therapeutic strategies against AD.

3.3 Materials and methods

All reagents were purchased in Sigma-Aldrich unless otherwise specified.

3.3.1 Preparation of Aβ samples for aggregation experiments

Aβ40, Aβ42 and E22Δ-Aβ42 peptides were synthesized and purified by Dr. James I. Elliott at Yale University (New Haven, CT, USA). To obtain Aβ in its lowest aggregation state we used Size Exclusion Chromatography (SEC) (Figure 3.13). Aβ was dissolved in 6.8 M Gdn $\cdot$ SCN, sonicated for 5 min, diluted to 4 M Gdn $\cdot$ SCN at a 5 mg/mL Aβ concentration, centrifuged at 10,000 g for 5 min, and passed through a 0.45-μm Millex filter. The resulting solution was injected into a HiLoad Superdex 75 HR 16/60 column (GE Healthcare) previously equilibrated with 50 mM NH_4OAc, 1 mM Tris $\cdot$ HCl and 0.01% NaN_3, pH 7.4, and eluted at a flow rate of 1 mL/min. The system was kept at 4°C.

The peak attributed to the lowest aggregation state of Aβ was collected, and its protein concentration was determined by HPLC (Waters, MA, US) in a Waters 2695 HPLC system. The column used was a C4 Symmetry column and the runs were performed at 60°C (Figure 3.14). HPLC quantification was carried out using a calibration curve generated from Aβ solutions previously quantified by amino acid analysis.

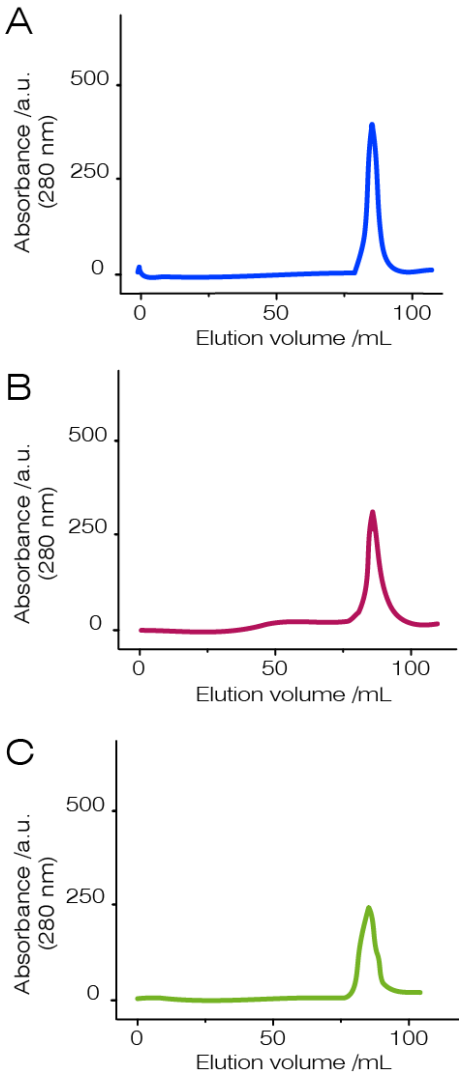

Figure 3.13: SEC chromatograms of (A) Aβ40 (in blue), (B) Aβ42 (in maroon) and (C) E22Δ-Aβ42 (in green). The peak attributed to the lowest aggregation state eluted at around 83 mL.

The Aβ solution was then diluted to 30 μM and left to aggregate at room temperature. Aliquots of the solutions were taken at Δt_{agg} ranging from 0 to 24 days for Aβ40, from 0 to 11 days for Aβ42 and from 0 to 19 days for E22Δ-Aβ42 to carry out the assays described below.

3.3.2 ThT binding assay

ThT analysis was performed by mixing 50 μL of the Aβ aggregating solutions withdrawn at specific Δt_{agg} times with 15 μL of 100 μL ThT and 35 μL of 142 mM Gly·OH at pH 8.3 in a Hard Shell® Thin Wall 96-well fluorescence plate (Costar, NY, US). The ThT fluorescence of each sample was measured using a fluorescence plate reader (FluoDia T70, Photal, Photon Technology International, Japan) at excitation and emission wavelengths of 450 and 485 nm,

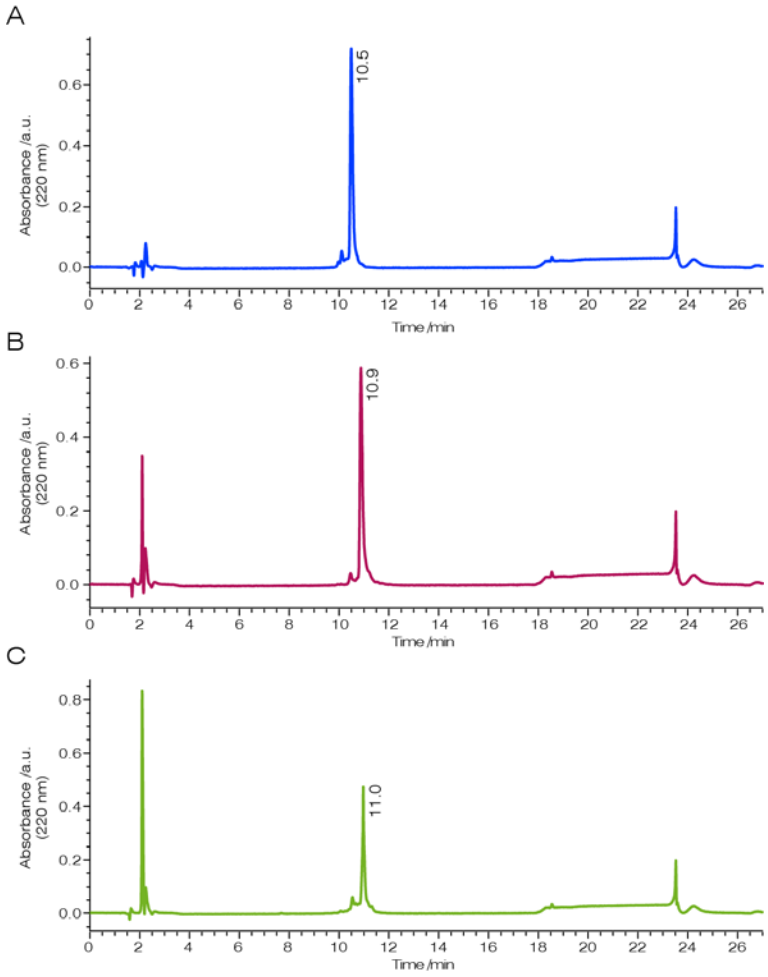

Figure 3.14: Representative HPLC chromatograms of (A) Aβ40 (in blue), (B) Aβ42 (in maroon) and (C) E22Δ-Aβ42 (in green). Notice that the retention time directly correlates with the hydrophobicity of the Aβ peptide. The gradient used was 0-60% B (ACN, 0.036% trifluoroacetic acid) in 20 minutes. Purity of the Aβ peptides was higher than 95%.

respectively. The samples were analyzed in triplicate and average fluorescence values and standard deviation plotted. The recorded kinetic traces were fitted to a sigmoidal function as described by the following equation:

$$F = F_0 + \frac{(F_{max} - F_0)}{1 + exp((t - t_{0.5})/b)} \tag{3.1}$$

F is the fluorescence intensity, t is time, $t_{0.5}$ is the time to reach 50 % of maximal fluorescence, b is the slope, and F_{max} and F_0 values correspond to the maximum and minimum fluorescence intensities. Estimated lag-time is $t_{0.5} - 2 \times b$.

3.3.3 Electron microscopy

TEM analysis was carried out with samples withdrawn from the aggregating solution at different Δt_{agg} times. A 10-μL aliquot of the samples was applied to a 200-mesh carbon-coated formvar copper grid (Electron Microscopy Sciences, US), previously glow-discharged for 5 minutes. After 1 min, the grid was washed with 30 μL of water and negatively stained by treatment with 30 μL of 2% uranyl acetate for 1 min. Samples were observed in a Tecnai Spirit electron microscope (FEI, The Netherlands) equipped with a LaB6 cathode. Images were acquired at 120 kV with a MegaView III CCD camera using Analysis software (Soft imaging System).

3.3.4 X-ray diffraction

After Δt_{agg} of 30 days for Aβ40, 17 days for Aβ42 and 24 days for E22Δ-Aβ42, 5-μL drop of the aggregating solution were suspended between two glass rods with beeswax tips approximately 1.5 mm apart. Before complete drying of the first drop, sequential addition of extra drops of 5 μL was performed twice. Finally, fibrils were allowed to dry completely. Fibril diffraction data were collected on a crystallography beam line at the Department of Biochemistry at the University of Cambridge. Azimuthal plots from diffractions were represented using ImageJ®.

3.3.5 PL-HDX experiments

Triplicate aliquots of 50 μL were withdrawn from the aggregating Aβ solution at different Δt_{agg}. The buffer was exchanged to D_2O (Euriso-top, France) by means of a 1/10 dilution with D_2O. Afterwards, the sample was left to exchange for a fixed labeling time, Δt_{label}. Under the aggregation conditions used, a Δt_{label} of 10 s was found to be the minimum, controllable time required to exchange all protons to deuterons in a monomeric Aβ40 sample. After the Δt_{label}, samples were freeze-dried to quench exchange in a Christ Alpha 1-2 LD Freeze Dryer (Martin Christ Gefriertrocknungsanlagen GmbH, Germany). The lyophilization was carried out for 14 hours and 0.10 mbar were reached.
The experiments of centrifugal evaporation were carried out in a SPD SpeedVac® (ThermoFisher Scientific Inc., NY, US).

3.3.6 HDX analyzed by ESI-MS

To analyze the deuterium content of the samples, lyophilized samples were transferred into a solution of 95% dimethylsulfoxide-d_6(DMSO-d_6, Euriso-top, France)/5% D_2O at pH* 4.6

(adjusted with Dichloroacetic acid-d_2) [104]. This buffer solubilizes the various aggregates into monomers and its pH* (pH read) is adjusted to the minimum exchange rate so that it preserves the deuterium content of the protein molecules [94].

The samples were dissolved at a 50 μM concentration in the DMSO-based buffer and immediately injected into a C8 desalting column (Micro Trap 1 mm ID x 8 mm, Michrom Bioresources Inc., Auburn, CA, US). To remove involatile salts and buffers from the sample solution, the C8 column was washed with aqueous acidic solution (H_2O, 0.1% formic acid(FA)) for 1 min at a flow of 50 μL/min. To elute the peptide from the C8 desalting column, a mixture of 80:20 ACN:H_2O, 0.1% FA was used. To pump solvent A (H_2O, 0.1% FA) a Reagent Manager pump (Waters) was used, and to pump solvent B (80:20 ACN:H_2O, 0.1% FA) a pump from an Acquity UPLC (Waters) was used. The sample was directly infused at 50 μL/min into a Waters LCT mass spectrometer (Premier XE, Micromass MS) with a modified ESI probe. A two-position/eight-port and a two-position/ten-port Teflon® valves (Valco Instruments Co. Inc. AG International, Switzerland) were used together with Teflon® tubing and fittings (Teknokroma, Spain). A schematic representation of the desalting system is depicted in Figure 3.15.

Data were collected in positive ion, with an applied capillary voltage of 4 kV, a cone voltage of 100 V, a capillary temperature of 20°C, a gas desolvation flow rate of 300 mL/min and a cone gas value of 50 mL/min. The same dead time (3 min) was used for sample preparation and parameter adjustment for all measurements. The spectra were analyzed using MassLynx V4.1 (Waters). All mass spectra presented were averages of 25 scans (1 s per scan), Aβ peaks (including +3, +4, and +5 charge states) were observed and the most abundant +4 charge state was selected for analysis.

3.3.7 Global multigaussian fitting of PL-HDX-ESI mass spectra

To establish the number of species detected during aggregation of Aβ40, Aβ42 and E22Δ-Aβ42, triplicate mass spectra for all Δt_{agg} studied were globally analyzed and fitted to Gaussian distributions.

To this end, a program with a predefined number of Gaussians/species N (from 1 to 4) was developed in C, a general purpose programming language, by Dr. Sergio Madurga at the University of Barcelona. The script for the program is shown at the end of this Materials and Methods section.

In this multigaussian fitting program, the objective function was the sum of chi squares corresponding to the functions of N Gaussians that fitted each experimental spectra: a total of 29 for Aβ40, 34 for Aβ42 and 33 for E22Δ-Aβ42. The fitting procedure minimize the objective function such that the position and width of the Gaussians was equivalent

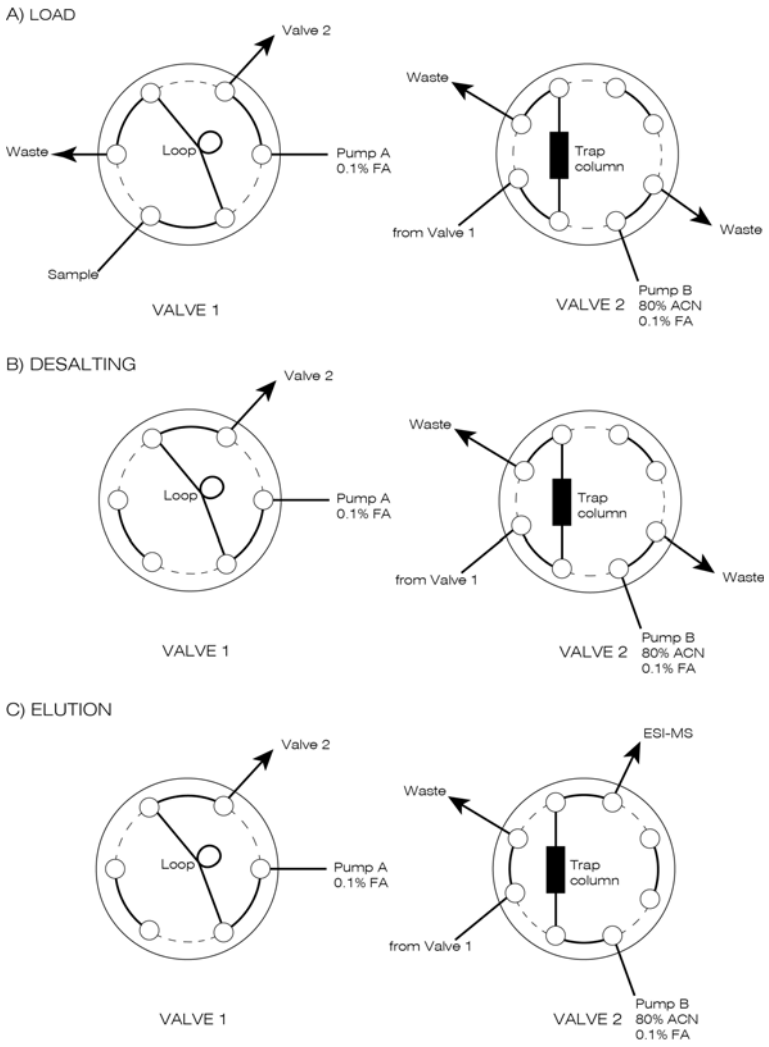

Figure 3.15: Schematic drawing of the desalting setup. The valves are depicted in (A) load, (B) desalting and (C) elution positions. After sample injection and desalting on the trap column, the protein sample is eluted directly into the ESI source of the mass spectrometer.

for all spectra while the weight of each Gaussian was optimized for each spectrum. This procedure was performed using a 2N-dimensional simplex on the position and width of the N Gaussians in combination with a non-linear least squares regression for each function of N Gaussians to obtain the weight of each Gaussian. The amoeba algorithm was used to carry out the simplex search while the *mrqmin* algorithm of Numerical Recipes [105] was used to implement the Levenberg-Marquardt method for the non-linear regression. To start the fitting procedure, approximate values for the unknowns were required. The optimization procedure was performed several times with different initial values to ensure that the global minimum was reached. The number of N Gaussians/species that best described a given aggregation process was taken to be n when the relative error associated to the fitting described by n+1 Gaussians was less than 20%. Following this criterion we found that three Gaussians/species were needed to characterize Aβ40 and Aβ42 aggregation, while E22Δ-Aβ42 required two (Table 3.1). To estimate the error of the parameters, the global set of

spectra was divided in three groups, taking in each group one of the replicates of each day. For those days in which only duplicate samples were available, one of the groups missed the information for that day. Three independent fittings were performed with the three subsets of spectra. The obtained dispersion of width and position of the Gaussian allowed estimating the standard error for the position and the width. The estimation of the standard error of the weight of each Gaussian was obtained from the global fitting using the dispersion of values among the replicates. From this fit, we derived several parameters for each of the species detected such as the homogeneous or heterogeneous nature, the number of exposed amides, and the relative population as a function of time.

Aβ40

# gaussian	error	relative error
1	1,21E+11	
2	5,76E+10	52,3
3	3,26E+10	43,4
4	2,77E+10	15,1

Aβ42

# gaussian	error	relative error
1	1,38E+10	
2	5,73E+09	58,5
3	3,79E+09	33,8
4	3,58E+09	5,6

E22Δ-Aβ42

# gaussian	error	relative error
1	3,08E+10	
2	1,90E+10	38,3
3	1,63E+10	14,2
4	1,56E+10	4,3

Table 3.1: The error comes from the calculation after adjusting all the spectra to a given number of gaussians. The relative error is defined as $relative\,error = \frac{error_{(i-1)} - error_i}{error_{(i-1)}} \times 100$ where $error_i$ corresponds to the error of and adjustment with "i" gaussians.

The homogeneous or heterogeneous nature of the species was determined through the peak widths, width of the peak at half height, which were taken directly from the adjustment. The number of exposed amides was obtained by applying the following equation:

$$number\,of\,exposed\,amides = m - MW - FE + BE \tag{3.2}$$

whereby m is the measured average mass corresponding to each detected species using the center of the gaussian peak determined from the fitting; MW is the measured average molecular weight of Aβ in H_2O (MW = 4329.8 Da for Aβ40, MW = 4514.1 Da for Aβ42 and MW = 4384.9 Da for E22Δ-Aβ42); and FE and BE refer, respectively, to the forward exchange and the back exchange controls. The FE refers to the additional incorporation of

deuterium atoms due to exchange with the solubilizing solvent (95% DMSO−d_6, 5% D_2O at pH* 4.6) and the BE refers to the loss of incorporated deuterium due to exchange with hydrogens of atmospheric water as a result of the hygroscopic nature of DMSO, during ionization itself, and the presence of H_2O in the desalting system. To account for FE and BE, we used the following correction method adapted from a previously reported one [106].

$$FE = m_{0\%} - MW \tag{3.3}$$

$$BE = MW + N - m_{100\%} \tag{3.4}$$

whereby $m_{0\%}$ is the measured mass of fully protonated Aβ disolved in the DMSO-based buffer at 50 μM and processed as with the HDX samples (injected to the MS after 3 minutes of dissolution); $m_{100\%}$ is the measured mass of fully deuterated Aβ prepared using the same sample used in the FE control after 6 hours in the DMSO-based buffer; and N is the number of labile amide groups (39, 41 and 40 for Aβ40, Aβ42 and E22Δ-Aβ42, respectively). Equation 3 gives a value of 3.2 for Aβ40, 2.8 for Aβ42 and 2.8 for E22Δ-Aβ42, meaning that roughly three backbone amide protons had undergone FE. Application of equation 4 gives a value of 11.8 for Aβ40, 11.5 for Aβ42 and 10.0 for E22Δ-Aβ42, meaning that approximately eleven deuterons (out of 39, 41 and 40 for Aβ40, Aβ42 and E22Δ-Aβ42, respectively) had undergone BE. These values were obtained by analyzing triplicate control samples for the BE and FE.

The relative population of a species at a given Δt_{agg} was obtained by dividing the area of the peak representing that species by the sum of the areas of each of the other species contributing at Δt_{agg}.

$$P_i = \frac{A_i}{A_i + A_j + A_k} \times 100 \tag{3.5}$$

3.3.8 Toxicity assays

ADDLs preparation

ADDLs were prepared as described [107]. Briefly, Aβ42 was dissolved in hexafluoro-2-propanol (HFIP) at 1 mg/mL concentration, aliquoted in low-binding Eppendorf tubes, and then HFIP was removed by freeze-drying. An aliquot of Aβ42 was dissolved in anhydrous DMSO to 5 mM and further diluted with ice-cold Ham's F-12 medium without phenol red (PromoCell GmbH, Germany) to 100 μM. This solution was incubated at 4°C for 24 h and then centrifuged at 14000 g for 10 min. The Aβ42 concentration in the supernatant was determined using Bradford assay and found to range between 60 and 100 mM. The peptide solution was diluted to the desired concentrations for MTT assays.

Primary neuronal cultures

Hippocampal neurons were obtained from E16 OF1 mouse embryos (Charles River Laboratories, MT, US). Briefly, brains were dissected in PBS containing 0.6% glucose, and hippocampi were dissected out. After trypsin (Gibco, CA, US) and DNAse (Roche Diagnostics, Switzerland) treatments, tissue pieces were dissociated by gentle sweeping. Cells were then counted and seeded onto poly-D-lysine-coated dishes in Neurobasal medium containing B27 supplement (Gibco).

Neuronal viability measurements

Primary hippocampal neurons were seeded at 3104 cells/well in 96-well plates (Costar, NY, US) maintained for 72-96 hours and then treated with Aβ samples frozen and thawn obtained at different Δt_{agg} (at final concentrations of 3 μM and 5 μM) or the corresponding volumes of vehicle (50 mM NH_4OAc, 1 mM Tris $\cdot$ HCl and 0.01% NaN_3, pH 7.4) as a control. After 24 hours at 37°C, the 3-(4,5-dimethylthiazol-2-yl)-2,5-diphenyltetrazolium bromide (MTT) neuronal viability was determined using the (3-(4,5-dimethylthiazol-2-yl)-2,5-diphenyltetrazolium bromide (MTT) assay from Roche (Cell Proliferation Kit I). Neuronal viability was expressed as percent of MTT absorbance in treated cells as compared to cognate vehicle-treated cells, which was taken as 100%. The assay was quantified at 595-690 nm on an absorbance plate reader.

3.3.9 Summary of statistical analysis

GraphPad Prism was used for all statistical analyses. The data are presented as mean $\pm$ s.d. The images shown are representative of those obtained in at least three independent experiments.

3.3.10 C-script for multigaussian fitting

```
/* Programa per Fitting simultani d'experiments  */
#include <stdio.h>
#include <math.h>
#define NRANSI
#include "nr.h"
#include "nrutil.h"
#include <string.h>

#define NPTMAX 1200
#define DIESMAX 40
#define NumGauss 4
#define MA 3*NumGauss
#define SPREAD 0.001
```

```
#define MP 9     /* nombre de punts  per amoeba MP=NP+1 */
#define NP 8     /* Nombre de dimensions per amoeba */
#define FTOL 1.0e-6
#define PI 3.14159265358979323846

float fit2gauss(float xcenters[6+1]);
float fit3gauss(float xcenters[6+1]);
float fit4gauss(float xcenters[8+1]);  /* fit4gauss amb format inicial */

void fgauss2(float x, float a[], float *y, float dyda[], int na);
void fgauss3(float x, float a[], float *y, float dyda[], int na);
void fgauss4(float x, float a[], float *y, float dyda[], int na);

float fitexperimentsMult(float xcenters[8+1]);  /* CANVI a versio ANTERIOR */
void proc1(void);

//float func(float x[])
//{
// return 0.6-exp(SQR(x[1]-0.5)+SQR(x[2]-0.6)+SQR(x[3]-0.7));
//}

float mz[NPTMAX+1],intensity[DIESMAX+1][NPTMAX+1];
float yb0_ini[DIESMAX+1],A1_ini[DIESMAX+1],xc1_ini[DIESMAX+1],w1_ini[DIESMAX+1];
float A2_ini[DIESMAX+1],xc2_ini[DIESMAX+1],w2_ini[DIESMAX+1];
float A3_ini[DIESMAX+1],xc3_ini[DIESMAX+1],w3_ini[DIESMAX+1];
float A4_ini[DIESMAX+1],xc4_ini[DIESMAX+1],w4_ini[DIESMAX+1];
float pa1_ini[DIESMAX+1],pa2_ini[DIESMAX+1],pa3_ini[DIESMAX+1],pa4_ini[DIESMAX+1];
float pw1_ini[DIESMAX+1],pw2_ini[DIESMAX+1],pw3_ini[DIESMAX+1],pw4_ini[DIESMAX+1];
float chiq_min,chiqdies_min[DIESMAX+1];
float xc1_min[DIESMAX+1],xc2_min[DIESMAX+1],xc3_min[DIESMAX+1],xc4_min[DIESMAX+1];
float pa1_min[DIESMAX+1],pa2_min[DIESMAX+1],pa3_min[DIESMAX+1],pa4_min[DIESMAX+1];
float pw1_min[DIESMAX+1],pw2_min[DIESMAX+1],pw3_min[DIESMAX+1],pw4_min[DIESMAX+1],
yb0_min[DIESMAX+1];
float yb0[DIESMAX+1],A1[DIESMAX+1],xc1[DIESMAX+1],w1[DIESMAX+1];
float A2[DIESMAX+1],xc2[DIESMAX+1],w2[DIESMAX+1];
float A3[DIESMAX+1],xc3[DIESMAX+1],w3[DIESMAX+1];
float A4[DIESMAX+1],xc4[DIESMAX+1],w4[DIESMAX+1];
float pa1[DIESMAX+1],pa2[DIESMAX+1],pa3[DIESMAX+1],pa4[DIESMAX+1];
float pw1[DIESMAX+1],pw2[DIESMAX+1],pw3[DIESMAX+1],pw4[DIESMAX+1];
float yres[NPTMAX+1];

int fit_g1,fit_g2,fit_g3,fit_g4;
int   fix[20];
int NCALC;
int NoNegs;
int NPT,DIES;
int main(void)
{
float xcenters[8+1];
long idum=(-917);
float chi_primerfit;
float fdelta;
FILE *fpdades;
char filexyzinicial[200];
char comentari[500];
int i,nfunc,j,ndim=NP;
float *y,**p;
float ygauss1,ygauss2,ygauss3,ygauss4;
int diestot,opt[DIESMAX],index[DIESMAX],jj;
```

```
int punt_xc1,punt_xc2,punt_xc3,punt_xc4;
char nom[100][100];
float valintensity;
    strcpy(filexyzinicial,"Ab.fit.input");
    fpdades = fopen(filexyzinicial,"r");
    if (fpdades == NULL)
    {    printf("Error al abrir el archivo %s\n",filexyzinicial);
         return (1);  }
    fgets(comentari,200,fpdades);
      fscanf(fpdades,"%d %d",&diestot,&NPT);
if(NPT>NPTMAX) { printf("ERROR NPT > NPTMAX\n"); exit(1); }
      printf("Total series: %d\n",diestot);
      printf("Noms: ");
      for(i=1;i<=diestot;i++)
      {
      fscanf(fpdades,"%s",nom[i]);
      printf("%s ",nom[i]);
      }
      printf("\n");

      DIES=0;
      for(i=1;i<=diestot;i++)
      {
      fscanf(fpdades,"%d",&opt[i]);
      printf("%d ",opt[i]);
      if(opt[i]==1)
        {
        DIES++;
        index[DIES]=i;
        }
      }
      printf("\nTotal Experiments a Analitzar: %d\n",DIES);
         fscanf(fpdades,"%f %f %d",&xc1_ini[1],&w1_ini[1],&fit_g1);
         fscanf(fpdades,"%f %f %d",&xc2_ini[1],&w2_ini[1],&fit_g2);
         fscanf(fpdades,"%f %f %d",&xc3_ini[1],&w3_ini[1],&fit_g3);
         fscanf(fpdades,"%f %f %d",&xc4_ini[1],&w4_ini[1],&fit_g4);
         printf("      xc   w \n");
         printf("Pic1: %f %f fit: %d\n",xc1_ini[1],w1_ini[1],fit_g1);
         printf("Pic2: %f %f fit: %d\n",xc2_ini[1],w2_ini[1],fit_g2);
         printf("Pic3: %f %f fit: %d\n",xc3_ini[1],w3_ini[1],fit_g3);
         printf("Pic4: %f %f fit: %d\n",xc4_ini[1],w4_ini[1],fit_g4);
      for(j=1;j<=DIES;j++)
       { xc1_ini[j]=xc1_ini[1];
 xc2_ini[j]=xc2_ini[1];
 xc3_ini[j]=xc3_ini[1];
 xc4_ini[j]=xc4_ini[1];
 w1_ini[j]=w1_ini[1];
 w2_ini[j]=w2_ini[1];
 w3_ini[j]=w3_ini[1];
 w4_ini[j]=w4_ini[1];
       }

/* Lectura de les dades */
    strcpy(filexyzinicial,"Ab.fit.data");
    fpdades = fopen(filexyzinicial,"r");
    if (fpdades == NULL)
    {    printf("Error al abrir el archivo %s\n",filexyzinicial);
         return (1);  }
    fgets(comentari,200,fpdades);
```

```
     for(i=1;i<=NPT;i++)
      {
      fscanf(fpdades,"%f",&mz[i]);
       jj=1;
      for(j=1;j<=diestot;j++)
        {
           fscanf(fpdades,"%f",&valintensity);
          if(opt[j]==1)
           {
            intensity[jj][i]=valintensity;
//    printf("%d %d %f\n",jj,i,intensity[jj][i]);
           jj++;
           }
        }
      }

      printf("Reading: Primer punt: %f ",mz[1]);
 for(j=1;j<=DIES;j++)
        { printf("%f ",intensity[j][1]); }
      printf("\n");
      printf("Reading: Ultim punt (%d): %f ",NPT, mz[NPT]);
 for(j=1;j<=DIES;j++)
        { printf("%f ",intensity[j][NPT]); }
      printf("\n");
      fclose(fpdades);

/* Lectura de les variables */

punt_xc1=1;
punt_xc2=1;
punt_xc3=1;
punt_xc4=1;
     for(i=1;i<=NPT;i++)
      {
if(fabs(mz[punt_xc1]-xc1_ini[1])>fabs(mz[i]-xc1_ini[1]))
          { punt_xc1=i; }
if(fabs(mz[punt_xc2]-xc2_ini[1])>fabs(mz[i]-xc2_ini[1]))
          { punt_xc2=i; }
if(fabs(mz[punt_xc3]-xc3_ini[1])>fabs(mz[i]-xc3_ini[1]))
          { punt_xc3=i; }
if(fabs(mz[punt_xc4]-xc4_ini[1])>fabs(mz[i]-xc4_ini[1]))
          { punt_xc4=i; }
      }
      for(j=1;j<=DIES;j++)
      {  yb0_ini[j]=intensity[j][1];
 pa1_ini[j]=intensity[j][punt_xc1];
 pa2_ini[j]=intensity[j][punt_xc2];
 pa3_ini[j]=intensity[j][punt_xc3];
 pa4_ini[j]=intensity[j][punt_xc4];
 pw1_ini[j]=w1_ini[j]/sqrt(2);
 pw2_ini[j]=w2_ini[j]/sqrt(2);
 pw3_ini[j]=w3_ini[j]/sqrt(2);
 pw4_ini[j]=w4_ini[j]/sqrt(2);
      }

printf("Initial Vabs values from esprectrum \n");
      printf("*yb0: ");
      for(j=1;j<=DIES;j++)
        { printf("%10.2f ",yb0_ini[j]); }  printf("\n");
```

```
      printf("*pa1:  ");
      for(j=1;j<=DIES;j++)
        {
        printf("%10.2f ",pa1_ini[j]);
        }   printf("\n");
      printf("*xc1:  ");
      for(j=1;j<=DIES;j++)
        { printf("%10.2f ",xc1_ini[j]); } printf("\n");
      printf("w1:   ");
      for(j=1;j<=DIES;j++)
        { printf("%10.2f ",w1_ini[j]); } printf("\n");
      printf("*pw1:  ");
      for(j=1;j<=DIES;j++)
        { printf("%10.2f ",pw1_ini[j]); } printf("\n");
      printf("*pa2:  ");
      for(j=1;j<=DIES;j++)
        {
        printf("%10.2f ",pa2_ini[j]);
        }   printf("\n");
      printf("*xc2:  ");
      for(j=1;j<=DIES;j++)
        { printf("%10.2f ",xc2_ini[j]); } printf("\n");
      printf("w2:   ");
      for(j=1;j<=DIES;j++)
        { printf("%10.2f ",w2_ini[j]); } printf("\n");
      printf("*pw2:  ");
      for(j=1;j<=DIES;j++)
        { printf("%10.2f ",pw2_ini[j]); } printf("\n");
      printf("*pa3:  ");
      for(j=1;j<=DIES;j++)
        {
        printf("%10.2f ",pa3_ini[j]);
        }   printf("\n");
      printf("*xc3:  ");
      for(j=1;j<=DIES;j++)
        { printf("%10.2f ",xc3_ini[j]); } printf("\n");
      printf("w3:   ");
      for(j=1;j<=DIES;j++)
        { printf("%10.2f ",w3_ini[j]); } printf("\n");
      printf("*pw3:  ");
      for(j=1;j<=DIES;j++)
        { printf("%10.2f ",pw3_ini[j]); } printf("\n");
      printf("*pa4:  ");
      for(j=1;j<=DIES;j++)
        {
        printf("%10.2f ",pa4_ini[j]);
        }   printf("\n");
      printf("*xc4:  ");
      for(j=1;j<=DIES;j++)
        { printf("%10.2f ",xc4_ini[j]); } printf("\n");
      printf("w4:   ");
      for(j=1;j<=DIES;j++)
        { printf("%10.2f ",w4_ini[j]); } printf("\n");
      printf("*pw4:  ");
      for(j=1;j<=DIES;j++)
        { printf("%10.2f ",pw4_ini[j]); } printf("\n");

// Inicialitzar vabs del fitting:
      for(j=1;j<=DIES;j++)
```

```
        { pa1[j]=pa1_ini[j];
          pa2[j]=pa2_ini[j];
          pa3[j]=pa3_ini[j];
          pa4[j]=pa4_ini[j];
          pw1[j]=pw1_ini[j];
          pw2[j]=pw2_ini[j];
          pw3[j]=pw3_ini[j];
          pw4[j]=pw4_ini[j];
          xc1[j]=xc1_ini[j];
          xc2[j]=xc2_ini[j];
          xc3[j]=xc3_ini[j];
          xc4[j]=xc4_ini[j]; }

y=vector(1,MP);
p=matrix(1,MP,1,NP);
NoNegs=1 ;   /* Keyword: Per no tenir coeficients negatius */

//////////////////

p[1][1]=xc1_ini[1];
p[1][2]=xc2_ini[1];
p[1][3]=xc3_ini[1];
p[1][4]=xc4_ini[1];
p[1][5]=pw1_ini[1];
p[1][6]=pw2_ini[2];
p[1][7]=pw3_ini[3];
p[1][8]=pw4_ini[4];
y[1]=fitexperimentsMult(p[1]);
chiq_min=y[1];
printf("*** RESULTAT y[1]= %f\n",y[1]);
fdelta=1;
p[2][1]=p[1][1]+(ran1(&idum)-0.5)*fdelta;
p[2][2]=p[1][2];
p[2][3]=p[1][3];
p[2][4]=p[1][4];
p[2][5]=p[1][5];
p[2][6]=p[1][6];
p[2][7]=p[1][7];
p[2][8]=p[1][8];
y[2]=fitexperimentsMult(p[2]);
printf("RESULTAT y[2]= %f\n",y[2]);
p[3][1]=p[1][1];
p[3][2]=p[1][2]+(ran1(&idum)-0.5)*fdelta;
p[3][3]=p[1][3];
p[3][4]=p[1][4];
p[3][5]=p[1][5];
p[3][6]=p[1][6];
p[3][7]=p[1][7];
p[3][8]=p[1][8];
y[3]=fitexperimentsMult(p[3]);
printf("RESULTAT y[3]= %f\n",y[3]);
p[4][1]=p[1][1];
p[4][2]=p[1][2];
p[4][3]=p[1][3]+(ran1(&idum)-0.5)*fdelta;
p[4][4]=p[1][4];
p[4][5]=p[1][5];
p[4][6]=p[1][6];
p[4][7]=p[1][7];
p[4][8]=p[1][8];
```

```
y[4]=fitexperimentsMult(p[4]);
printf("RESULTAT y[4]= %f\n",y[4]);
p[5][1]=p[1][1];
p[5][2]=p[1][2];
p[5][3]=p[1][3];
p[5][4]=p[1][4]+(ran1(&idum)-0.5)*fdelta;
p[5][5]=p[1][5];
p[5][6]=p[1][6];
p[5][7]=p[1][7];
p[5][8]=p[1][8];
y[5]=fitexperimentsMult(p[5]);
printf("RESULTAT y[5]= %f\n",y[5]);
p[6][1]=p[1][1];
p[6][2]=p[1][2];
p[6][3]=p[1][3];
p[6][4]=p[1][4];
p[6][5]=p[1][5]+0.1;
p[6][6]=p[1][6];
p[6][7]=p[1][7];
p[6][8]=p[1][8];
y[6]=fitexperimentsMult(p[6]);
printf("RESULTAT y[6]= %f\n",y[6]);
p[7][1]=p[1][1];
p[7][2]=p[1][2];
p[7][3]=p[1][3];
p[7][4]=p[1][4];
p[7][5]=p[1][5];
p[7][6]=p[1][6]+0.1;
p[7][7]=p[1][7];
p[7][8]=p[1][8];
y[7]=fitexperimentsMult(p[7]);
printf("RESULTAT y[7]= %f\n",y[7]);
p[8][1]=p[1][1];
p[8][2]=p[1][2];
p[8][3]=p[1][3];
p[8][4]=p[1][4];
p[8][5]=p[1][5];
p[8][6]=p[1][6];
p[8][7]=p[1][7]+0.1;
p[8][8]=p[1][8];
y[8]=fitexperimentsMult(p[8]);
printf("RESULTAT y[8]= %f\n",y[8]);
p[9][1]=p[1][1];
p[9][2]=p[1][2];
p[9][3]=p[1][3];
p[9][4]=p[1][4];
p[9][5]=p[1][5];
p[9][6]=p[1][6];
p[9][7]=p[1][7];
p[9][8]=p[1][8]+0.1;
y[9]=fitexperimentsMult(p[9]);
printf("RESULTAT y[9]= %f\n",y[9]);

amoeba(p,y,ndim,FTOL,fitexperimentsMult,&nfunc);
printf("\nNumber of function evaluations: %3d\n",nfunc);
printf("Vertices of final 3-d simplex and\n");
printf("function values at the vertices:\n\n");
printf("%3s %10s %12s %12s %14s\n\n",
"i","x[i]","y[i]","z[i]","function");
```

```
for (i=1;i<=MP;i++) {
printf("%3d ",i);
for (j=1;j<=NP;j++) printf("%12.6f ",p[i][j]);
printf("%12.6f\n",y[i]);
}
printf("\n\nRESULTAT FINAL\n\n");
      for(NCALC=1;NCALC<=DIES;NCALC++)
        {
 printf("+++++++++\n");
for(i=1;i<=NPT;i++)
         {
ygauss1 = pa1_min[NCALC]*exp(-SQR((mz[i]-xc1_min[NCALC])/pw1_min[NCALC]));
ygauss2 = pa2_min[NCALC]*exp(-SQR((mz[i]-xc2_min[NCALC])/pw2_min[NCALC]));
ygauss3 = pa3_min[NCALC]*exp(-SQR((mz[i]-xc3_min[NCALC])/pw3_min[NCALC]));
ygauss4 = pa4_min[NCALC]*exp(-SQR((mz[i]-xc4_min[NCALC])/pw4_min[NCALC]));
                yres[i] = yb0_min[NCALC] + ygauss1+ygauss2+ygauss3+ygauss4;
                printf("RES%d: %8.2f %8.2f  %8.2f  %8.2f %8.2f %8.2f %8.2f \n",
                NCALC,mz[i], intensity[NCALC][i], yres[i],ygauss1+yb0_min[NCALC],
                ygauss2+yb0_min[NCALC],
                ygauss3+yb0_min[NCALC], ygauss4+yb0_min[NCALC]);
         }
        }

printf("\nValors Finals, Unitats calcul:\n");
printf("## day  pa1 xc1  pw1   pa2 xc2 pw2   pa3 xc3 pw3   pa4 xc4 pw4  yb0\n");
 for(NCALC=1;NCALC<=DIES;NCALC++)
 {
 printf("## %d  %11.3f %11.3f %11.3f  %11.3f
 %11.3f %11.3f  %11.3f %11.3f %11.3f  %11.3f
 %11.3f %11.3f  %11.3f \n ",NCALC,
        pa1_min[NCALC],xc1_min[NCALC], pw1_min[NCALC],
        pa2_min[NCALC],xc2_min[NCALC], pw2_min[NCALC],
        pa3_min[NCALC],xc3_min[NCALC], pw3_min[NCALC],
        pa4_min[NCALC],xc4_min[NCALC], pw4_min[NCALC],
         yb0_min[NCALC]);
 }
printf("\nValors Finals, Unitats Dades:\n");
printf("## day   A1 xc1 w1          A2 xc2 w2 i       A3 xc3 w3    A4 xc4 w4  yb0\n");
 for(NCALC=1;NCALC<=DIES;NCALC++)
 {
 printf("## %d %s  %11.3f %11.3f %11.3f  %11.3f %11.3f %11.3f  %11.3f %11.3f %11.3f
 %11.3f %11.3f %11.3f  %11.3f \n ",NCALC,nom[index[NCALC]],
        pa1_min[NCALC]*sqrt(PI)*pw1_min[NCALC],xc1_min[NCALC], pw1_min[NCALC]*sqrt(2),
        pa2_min[NCALC]*sqrt(PI)*pw2_min[NCALC],xc2_min[NCALC], pw2_min[NCALC]*sqrt(2),
        pa3_min[NCALC]*sqrt(PI)*pw3_min[NCALC],xc3_min[NCALC], pw3_min[NCALC]*sqrt(2),
        pa4_min[NCALC]*sqrt(PI)*pw4_min[NCALC],xc4_min[NCALC], pw4_min[NCALC]*sqrt(2),
        yb0_min[NCALC]);
 }
printf("CHIQTOTAL: %f \n CHI_INDV:  \n",chiq_min);
  for(NCALC=1;NCALC<=DIES;NCALC++)
  { printf("%d %s  %f ",NCALC,nom[index[NCALC]],chiqdies_min[NCALC]); printf("\n");}
printf("En Per 100: \n ");
  for(NCALC=1;NCALC<=DIES;NCALC++)
  { printf("%d %s %f ",NCALC,nom[index[NCALC]],100*chiqdies_min[NCALC]/chiq_min);
  printf("\n"); }
free_matrix(p,1,MP,1,NP);
free_vector(y,1,MP);
return(0);
}
```

```
////////////////////////////

float fitexperimentsMult(float xcenters[8+1])
{
//float chi1,chi2,chi3,chi4,chi5,chi6,chi7,chi8,chitotal;
float chitotal;
float chiexp[DIES+1];
int canvi,i;

for(NCALC=1;NCALC<=DIES;NCALC++)
{
//NCALC=1;
canvi=0;

// FIXAR VALORS: 0
// pre-exp   xc       sig
fix[1]=fit_g1; fix[2]=0;  fix[3]=0;
fix[4]=fit_g2; fix[5]=0;  fix[6]=0;
fix[7]=fit_g3; fix[8]=0;  fix[9]=0;
fix[10]=fit_g4; fix[11]=0;  fix[12]=0;
fix[13]=1;
if(pa1[NCALC]<0) {  pa1[NCALC]=10000; }  /* Canvi de signe, per la seguent iteració */
if(pa2[NCALC]<0) {  pa2[NCALC]=10000; }  /* Canvi de signe, per la seguent iteració */
if(pa3[NCALC]<0) {  pa3[NCALC]=10000; }  /* Canvi de signe, per la seguent iteració */
if(pa4[NCALC]<0) {  pa4[NCALC]=10000; }  /* Canvi de signe, per la seguent iteració */
if(fix[1]==0)  {  pa1[NCALC]=0; }   /* Si no s'ajusta, la gaussiana es fa 0 */
if(fix[4]==0)  {  pa2[NCALC]=0; }   /* Si no s'ajusta, la gaussiana es fa 0 */
if(fix[7]==0)  {  pa3[NCALC]=0; }   /* Si no s'ajusta, la gaussiana es fa 0 */
if(fix[10]==0) {  pa4[NCALC]=0; }   /* Si no s'ajusta, la gaussiana es fa 0 */
chiexp[NCALC]=fit4gauss(xcenters);
printf("** RESULTAT Pel CAS %d CHI= %f\n",NCALC,chiexp[NCALC]);
printf("** Valors fixats: ");
  for(i=1;i<=13;i++)
   { printf("%d ",fix[i]); }
printf("\n");
printf("** %11.3f %11.3f %11.3f %11.3f %11.3f %11.3f %11.3f %11.3f %11.3f %11.3f %11.3f
%11.3f %11.3f %11.3f",
        pa1[NCALC],xc1[NCALC], pw1[NCALC],
        pa2[NCALC],xc2[NCALC],pw2[NCALC],
        pa3[NCALC],xc3[NCALC], pw3[NCALC],
        pa4[NCALC],xc4[NCALC], pw4[NCALC],yb0[NCALC]);
printf("\n");
if(NoNegs==1)
  {
if(pa1[NCALC]<0) {  pa1[NCALC]=0; fix[1]=0; canvi=1; }
/* Canvi de signe, per la seguent iteració */
if(pa2[NCALC]<0) {  pa2[NCALC]=0; fix[4]=0; canvi=1; }
/* Canvi de signe, per la seguent iteració */
if(pa3[NCALC]<0) {  pa3[NCALC]=0; fix[7]=0; canvi=1; }
/* Canvi de signe, per la seguent iteració */
if(pa4[NCALC]<0) {  pa4[NCALC]=0; fix[10]=0; canvi=1; }
/* Canvi de signe, per la seguent iteració */
        while(canvi==1) {
         canvi=0;
chiexp[NCALC]=fit4gauss(xcenters);
if(pa1[NCALC]<0) {  pa1[NCALC]=0; fix[1]=0; canvi=1; }
/* Canvi de signe, per la seguent iteració */
if(pa2[NCALC]<0) {  pa2[NCALC]=0; fix[4]=0; canvi=1; }
```

```
 /* Canvi de signe, per la seguent iteració */
if(pa3[NCALC]<0) {  pa3[NCALC]=0; fix[7]=0; canvi=1; }
 /* Canvi de signe, per la seguent iteració */
if(pa4[NCALC]<0) {  pa4[NCALC]=0; fix[10]=0; canvi=1; }
/* Canvi de signe, per la seguent iteració *
        }
printf("** Fixant1: RESULTAT Pel CAS %d CHI= %f\n",NCALC,chiexp[NCALC]);
printf("** Valors fixats: ");
  for(i=1;i<=13;i++)
   { printf("%d ",fix[i]); }
printf("\n");
printf("** %11.3f %11.3f %11.3f %11.3f %11.3f %11.3f %11.3f %11.3f %11.3f %11.3f
%11.3f %11.3f %11.3f",
pa1[NCALC],xc1[NCALC], pw1[NCALC],
pa2[NCALC],xc2[NCALC],pw2[NCALC],
pa3[NCALC],xc3[NCALC], pw3[NCALC],
pa4[NCALC],xc4[NCALC], pw4[NCALC],yb0[NCALC]);
printf("\n");
  }
}

/**************/
    chitotal=0;
  for(NCALC=1;NCALC<=DIES;NCALC++)
  { chitotal+=chiexp[NCALC]; }
printf("** CHI2 TOTAL %f\n",chitotal);
if(chitotal<chiq_min)
  {
        chiq_min=chitotal;
for(i=1;i<=DIES;i++)
        {
         pa1_min[i]=pa1[i];
         pa2_min[i]=pa2[i];
         pa3_min[i]=pa3[i];
         pa4_min[i]=pa4[i];
         pw1_min[i]=pw1[i];
         pw2_min[i]=pw2[i];
         pw3_min[i]=pw3[i];
         pw4_min[i]=pw4[i];
         xc1_min[i]=xc1[i];
         xc2_min[i]=xc2[i];
         xc3_min[i]=xc3[i];
         xc4_min[i]=xc4[i];
         yb0_min[i]=yb0[i];
         }
  }
  for(NCALC=1;NCALC<=DIES;NCALC++)
  { chiqdies_min[NCALC]=chiexp[NCALC]; }
return(chitotal);
}

////////////////////////////////7

float fit4gauss(float xcenters[8+1])
{
#define NumVabs 13
long idum=(-911);
int i,*ia,itst,j,k,mfit=NumVabs;
float alamda,chisq,ochisq,*x,*y,*sig,**covar,**alpha;
```

```
float *yres1;
float a[NumVabs+1];
float a1[NumVabs+1];
ia=ivector(1,NumVabs);
x=vector(1,NPT);
y=vector(1,NPT);
yres1=vector(1,NPT);
sig=vector(1,NPT);
covar=matrix(1,NumVabs,1,NumVabs);
alpha=matrix(1,NumVabs,1,NumVabs);
     for(i=1;i<=NPT;i++)
      {
       x[i]=mz[i];
       y[i]=intensity[NCALC][i];
       sig[i]=1.;
      }

//Entrada valors:
a[1]=pa1[NCALC];
a[2]=xcenters[1];
a[3]=xcenters[5];
    a[4]=pa2[NCALC];
a[5]=xcenters[2];
a[6]=xcenters[6];
a[7]=pa3[NCALC];
a[8]=xcenters[3];
a[9]=xcenters[7];
a[10]=pa4[NCALC];
a[11]=xcenters[4];
a[12]=xcenters[8];
    a[13]=yb0[NCALC];

// FIXAR VALORS: 0
ia[1]=fix[1];
ia[2]=fix[2];
ia[3]=fix[3];
ia[4]=fix[4];
ia[5]=fix[5];
ia[6]=fix[6];
ia[7]=fix[7];
ia[8]=fix[8];
ia[9]=fix[9];
ia[10]=fix[10];
ia[11]=fix[11];
ia[12]=fix[12];
ia[13]=fix[13];

         printf("Valors: ");
         for(j=1;j<=NumVabs;j++) { printf("%10.2f ",a[j]); } printf(" \n");
alamda = -1;
mrqmin(x,y,sig,NPT,a,ia,NumVabs,covar,alpha,&chisq,fgauss3,&alamda);
k=1;
itst=0;
for (;;) {
printf("\n%s %2d %17s %10.4f %10s %9.2e\n","Iteration #",k,
"chi-squared:",chisq,"alamda:",alamda);
printf("%8s %8s %8s %8s %8s %8s ...\n",
"a[1]","a[2]","a[3]","a[4]","a[5]","a[6]");
for (i=1;i<=NumVabs;i++) printf("%11.3f",a[i]);
```

```
printf("\n");
k++;
ochisq=chisq;
mrqmin(x,y,sig,NPT,a,ia,NumVabs,covar,alpha,&chisq,fgauss4,&alamda);
if (chisq > ochisq)
itst=0;
else if (fabs(ochisq-chisq) < 0.01)
itst++;
if (itst < 8) continue;
alamda=0.0;
mrqmin(x,y,sig,NPT,a,ia,NumVabs,covar,alpha,&chisq,fgauss4,&alamda);
printf("\nUncertainties:\n");
for (i=1;i<=NumVabs;i++) printf("%11.3f",sqrt(covar[i][i]));
printf("\n");
break;
}

/* Guardar els resultats a vabs globals */
pa1[NCALC]=a[1];
xc1[NCALC]=a[2];
pw1[NCALC]=a[3];
    pa2[NCALC]=a[4];
xc2[NCALC]=a[5];
pw2[NCALC]=a[6];
    pa3[NCALC]=a[7];
xc3[NCALC]=a[8];
pw3[NCALC]=a[9];
    pa4[NCALC]=a[10];
xc4[NCALC]=a[11];
pw4[NCALC]=a[12];
yb0[NCALC]=a[13];

/* Per Imprimir més resultats */
// for(i=1;i<=NPT;i++)
//         {
// yres1[i]=0.0;
// for (j=1;j<=MA;j+=3) {
// yres1[i] += a[j]*exp(-SQR((x[i]-a[j+1])/a[j+2]));
// }
//                 printf("RES: %7.2f %8.2f %8.2f \n",x[i],y[i],yres1[i]);
//         }
free_matrix(alpha,1,NumVabs,1,NumVabs);
free_matrix(covar,1,NumVabs,1,NumVabs);
free_vector(sig,1,NPT);
free_vector(y,1,NPT);
free_vector(yres1,1,NPT);
free_ivector(ia,1,NumVabs);
free_vector(x,1,NPT);
return(chisq) ;
}
////////////////////////////7

float fit3gauss(float xcenters[6+1])
{
#define NumVabs 10
long idum=(-911);
int i,*ia,itst,j,k,mfit=NumVabs;
float alamda,chisq,ochisq,*x,*y,*sig,**covar,**alpha;
float *yres1;
```

```
float a[NumVabs+1];
float a1[NumVabs+1];
ia=ivector(1,NumVabs);
x=vector(1,NPT);
y=vector(1,NPT);
yres1=vector(1,NPT);
sig=vector(1,NPT);
covar=matrix(1,NumVabs,1,NumVabs);
alpha=matrix(1,NumVabs,1,NumVabs);
     for(i=1;i<=NPT;i++)
      {
       x[i]=mz[i];
       y[i]=intensity[NCALC][i];
       sig[i]=1.;
      }

//Entrada valors:
a[1]=pa1[NCALC];
a[2]=xcenters[1];
a[3]=xcenters[4];
    a[4]=pa2[NCALC];
a[5]=xcenters[2];
a[6]=xcenters[5];
a[7]=pa3[NCALC];
a[8]=xcenters[3];
a[9]=xcenters[6];
    a[10]=yb0[NCALC];

// FIXAR VALORS: 0
ia[1]=fix[1];
ia[2]=fix[2];
ia[3]=fix[3];
ia[4]=fix[4];
ia[5]=fix[5];
ia[6]=fix[6];
ia[7]=fix[7];
ia[8]=fix[8];
ia[9]=fix[9];
ia[10]=fix[10];

         printf("Valors: ");
         for(j=1;j<=NumVabs;j++) { printf("%10.2f ",a[j]); } printf(" \n");
alamda = -1;
mrqmin(x,y,sig,NPT,a,ia,NumVabs,covar,alpha,&chisq,fgauss3,&alamda);
k=1;
itst=0;
for (;;) {
printf("\n%s %2d %17s %10.4f %10s %9.2e\n","Iteration #",k,
"chi-squared:",chisq,"alamda:",alamda);
printf("%8s %8s %8s %8s %8s %8s ...\n",
"a[1]","a[2]","a[3]","a[4]","a[5]","a[6]");
for (i=1;i<=NumVabs;i++) printf("%11.3f",a[i]);
printf("\n");
k++;
ochisq=chisq;
mrqmin(x,y,sig,NPT,a,ia,NumVabs,covar,alpha,&chisq,fgauss3,&alamda);
if (chisq > ochisq)
itst=0;
else if (fabs(ochisq-chisq) < 0.1)
```

```
itst++;
if (itst < 4) continue;
alamda=0.0;
mrqmin(x,y,sig,NPT,a,ia,NumVabs,covar,alpha,&chisq,fgauss3,&alamda);
printf("\nUncertainties:\n");
for (i=1;i<=NumVabs;i++) printf("%11.3f",sqrt(covar[i][i]));
printf("\n");
break;
}

/* Guardar els resultats a vabs globals */
pa1[NCALC]=a[1];
xc1[NCALC]=a[2];
pw1[NCALC]=a[3];
    pa2[NCALC]=a[4];
xc2[NCALC]=a[5];
pw2[NCALC]=a[6];
        pa3[NCALC]=a[7];
xc3[NCALC]=a[8];
pw3[NCALC]=a[9];
yb0[NCALC]=a[10];

/* Per Imprimir mes resultats */
// for(i=1;i<=NPT;i++)
//         {
// yres1[i]=0.0;
// for (j=1;j<=MA;j+=3) {
// yres1[i] += a[j]*exp(-SQR((x[i]-a[j+1])/a[j+2]));
// }
//                 printf("RES: %7.2f %8.2f %8.2f \n",x[i],y[i],yres1[i]);
//         }
free_matrix(alpha,1,NumVabs,1,NumVabs);
free_matrix(covar,1,NumVabs,1,NumVabs);
free_vector(sig,1,NPT);
free_vector(y,1,NPT);
free_vector(yres1,1,NPT);
free_ivector(ia,1,NumVabs);
free_vector(x,1,NPT);
return(chisq) ;
}
////////////////////////////7
#undef NRANSI
```

4 Evaluation of small molecules

4.1 Results

4.1.1 Selection of molecules described to have an effect on Aβ aggregation

There are many reports with *in vitro* studies in which small molecules are shown to enhance or inhibit Aβ aggregation (for a review see [108, 109]). However, most of them fail to give detailed information on the mechanism of action of these small molecules an thus it is not known the type of Aβ aggregate with which they interact and/or stabilize.

We chose to work with Aβ42 since this variant is most strongly linked to AD etiology than other Aβ forms. We tested the effect of a small library of different compounds on Aβ42 aggregation. The library comprised twenty small molecules (Figure 4.1) with different chemical characteristics (functional groups, flexibility, salts) fulfilling at least one of the following requirements:

- Targeting Aβ aggregation and amyloidogenesis being or having been in clinical trials against AD. These include ammonium tetrathio-molybdate [90], clioquinol [89], epigallocatechin gallate [87, 88], scyllo-inositol [85] and its isomer myo-inositol, tarenflurbil [110] and tramiprosate [81].

- Inhibiting Aβ fibril formation by stabilizing Aβ oligomers *in vitro*. These comprise apigenin [77], chicago sky blue 6B [77], diallyltartardiamide [77], direct red 80 [77], orange G [77], riluzole [83] and tetracycline [82].

- Delaying Aβ fibril formation *in vitro*. These include 2,2'-dihydroxybenzophenone [77], entacapone [79], inrD [93] and salvianolic acid B [80].

- Inhibiting Aβ oligomer formation but not fibrillization *in vitro*. These comprise 2,2'-

dihydroxybenzophenone [77], juglone [77] and methylene blue [77].

4.1.2 First screening of molecules interfering with Aβ aggregation using the filter-retardation assay (FRA)

To carry out a first screening on the effect of the 20 molecules comprising our library on Aβ42 aggregation, we used the FRA (Figure 4.2). This assay is a fast, quantitative method to screen for the effect of compounds against the formation of large, SDS-stable Aβ aggregates. [111, 112]. After different aggregation times (Δt_{agg}), aliquots of the aggregating solution were removed and stored at -20°C. When all the samples were collected, they were diluted, SDS-treated to a final SDS concentration of 2% and heated at 95°C for 5 minutes, to disrupt all non-resistant SDS Aβ aggregates. Those SDS-treated samples were filtered through a cellulose acetate membrane. By using the FRA, high molecular weight, SDS-resistant aggregates are retained in the membrane, while monomeric peptide and small soluble Aβ oligomers pass through the membrane. The amount of SDS-resitant aggregates was quantified by immunodetection using the monoclonal antibody 6E10, which specifically recognizes the N-terminus end of the Aβ peptide.

We followed the aggregation of Aβ42 alone and in the presence of the molecules comprising our library during 12 days. These experiments were carried out by Ricard Illa, an undergraduate student that spent three months working with us. Aβ42 aggregation in the absence of molecules was monitored using both the ThT binding assay and the FRA. Interestingly, we obtained a correspondence between the fluorescence signal of the ThT binding assay and the immunosignal of the FRA (Figure 4.3). Thus, the end of the lag phase assessed by ThT was consistent with the appearance of SDS-resistant aggregates, suggesting that Aβ42 fibrils were the only SDS-resistant aggregates. The ThT binding assay cannot be used to study Aβ42 aggregation in the presence of small molecules, as the small molecule might interfere with the fluorescence excitation or emission needed for ThT and/or the small molecule might inhibit the formation of the complex between ThT and a fibril [113]. Most of the molecules tested accelerated the formation of SDS-resistant aggregates. The degree in which they accelerated the process varied from molecule to molecule. The molecules exhibiting this activity, ordered from higher to lower enhancing ability were: orange G, diallyltartardiamide, ammonium tetrathiomolybdate, chicago sky blue 6B, entacapone, myo-inositol, scyllo-inositol, juglone, clioquinol, tarenflurbil, tramiprosate, apigenin, riluzole and salvianolic acid B. On the other hand, some molecules like methylene blue, 2,2'-dihydroxybenzophenone and tetracycline did not show a clear effect on Aβ42 aggregation, exhibiting a pattern comparable to Aβ42 alone. Finally, epigallocatechin gallate slowed down the formation of SDS-resistant aggregates and the peptide inrD showed the most remarkable inhibitory effect on Aβ42 aggregation.

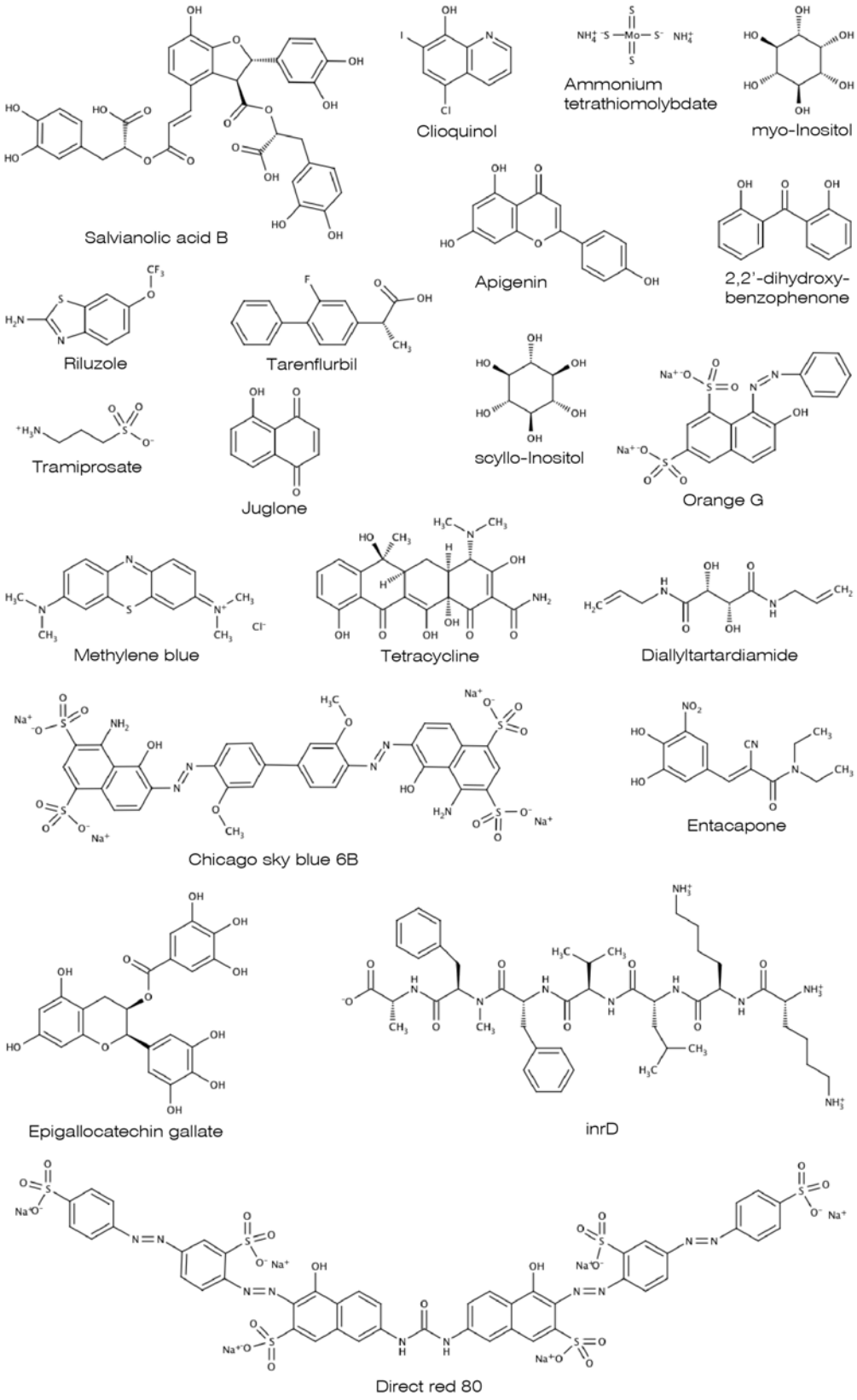

Figure 4.1: The chemical structure of the twenty molecules composing our library and assessed in this study.

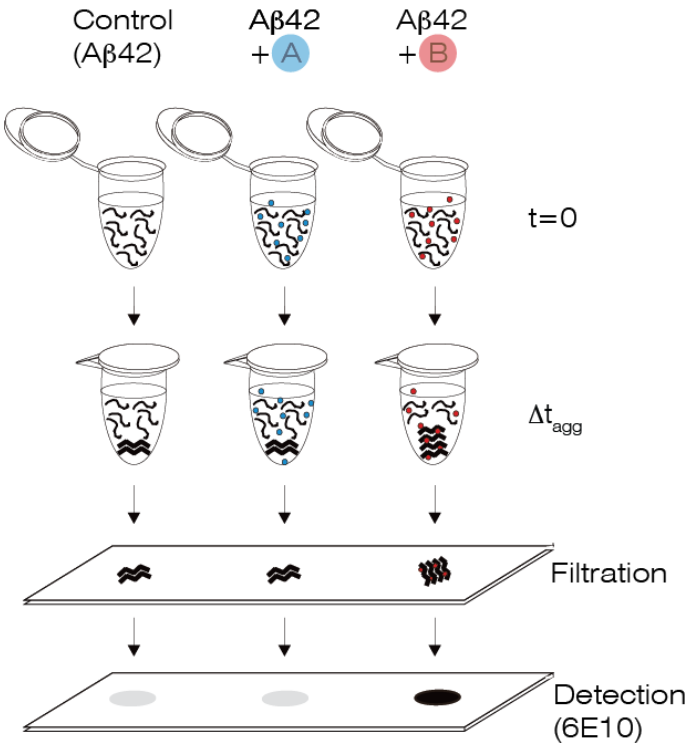

Figure 4.2: Schematic description of the FRA. Three hypothetical samples are depicted: a control of Aβ42, Aβ42 in the presence of small molecule A (in blue) which has no effect on Aβ42 aggregation, and Aβ42 incubated with small molecule B (in red), which enhances Aβ42 fibrillization.

4.1.3 Evaluation of the effect of small molecules and inrD on Aβ42 using the PL-HDX-ESI-MS experiment

Using the PL-HDX-ESI-MS experiment in Chapter 3, we have detected, characterized and quantified three different species during Aβ42 aggregation. This result provided us with an opportunity to study the effect of compounds on the species detected and thus learn about their mechanism of action.

Based on the results obtained with the FRA, we selected a small, representative number of compounds for further studies using the PL-HDX-ESI-MS experiment. We did not choose molecules exhibiting solubility problems as well as salts. We chose diallyltartardiamide (DATD) and entacapone (Ent) as representative compounds of those enhancing Aβ42 aggregation, 2,2'-dihydroxy-benzophenone (DHB) as small molecule not having an effect on Aβ42 aggregation and epigallocatechin gallate (EGCG) and inrD as inhibitors of Aβ42 aggregation.

We performed a new round of aggregation experiments with Aβ42, Aβ42 + Ent, Aβ42 + DATD, Aβ42 + DHB, Aβ42 + inrD and Aβ42 + EGCG, applying the PL-HDX-ESI-MS experiment (Figure 4.5). The MS spectra were adjusted to three species in all cases except for Aβ42 + inrD where two species were necessary, according to the error analysis

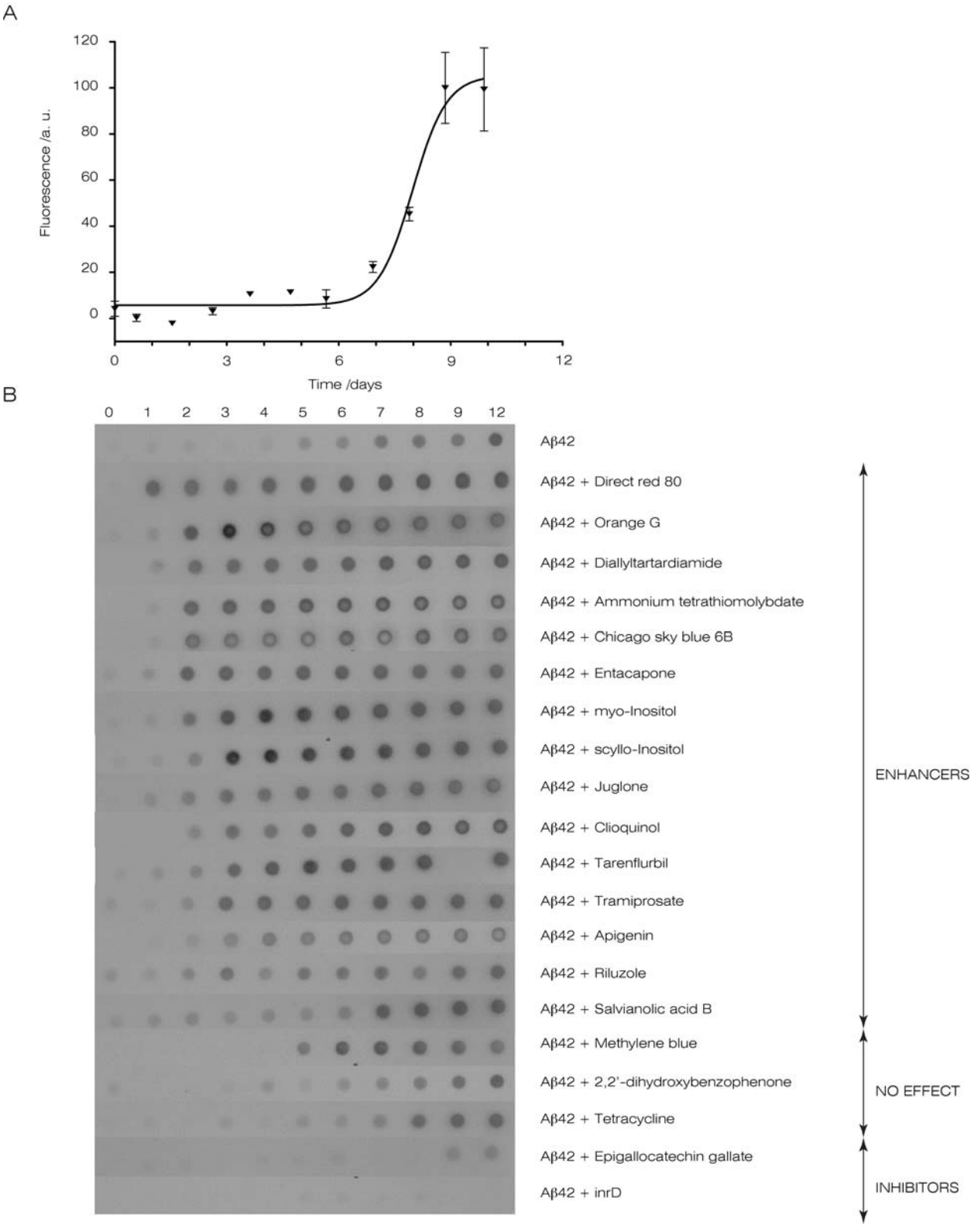

Figure 4.3: Monitoring of Aβ42 aggregation in the presence of the 20 compounds. A) Aβ42 aggregation in the absence of any compound monitored by the ThT binding assay. B) Aβ42 aggregation monitored in the absence (top row) and in the presence (second to twentieth row) of the 20 compounds comprising our library by the FRA. Most of the compounds enhanced Aβ aggregation, while others did not have a clear effect on the process. Epigallocatechin gallate and the peptide inrD exhibited a remarkable inhibitory effect.

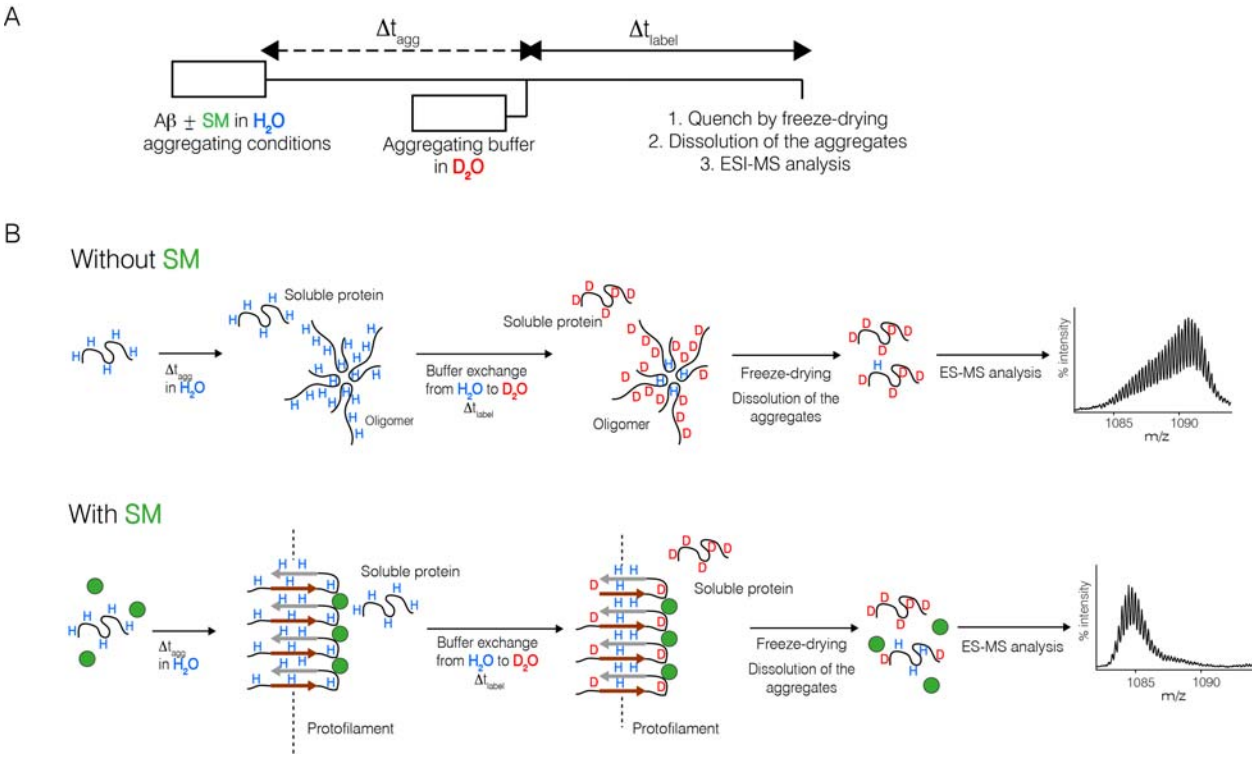

Figure 4.4: The PL-HDX experiment to study Aβ aggregation in the presence of a small molecule: A) Schematic representation of the experiment. B) Hypothetical scenario for a given aggregation time Δt_{agg} in the absence of the small molecule (top) and in the presence of a small molecule enhancing Aβ fibrillization (bottom).

mentioned in the previous chapter (Table 4.1, Materials and Methods). For Aβ42, three different species were detected. The number of exposed amides for each of the detected species were not significantly different from the ones obtained for Aβ42 in the previous chapter (they correspond to a different experiment) (Figure 4.5). Also in agreement with the results obtained for Aβ42 in the previous chapter, $PF_{A\beta42}$ and $EA_{A\beta42}$ were the most heterogeneous species formed during aggregation (Figure 4.7).

Ent and DATD accelerate Aβ42 aggregation

We studied Aβ42 aggregation in the presence of DATD and Ent by means of the PL-HDX-ESI-MS experiment. In both cases, error analysis (Table 4.1, Materials and Methods) involved the adjustment of the spectra to three species (Figure 4.5).

Since no significant differences were observed in the number of exposed amides for the species detected in the absence or in the presence of Ent and DATD (Figure 4.6), we named them as EA, PF and F adding a subscript to indicate the chemical compound under study. For Aβ42 + Ent, $EA_{A\beta42+Ent}$ displays 30 ± 1 while for Aβ42 + DATD the value for $EA_{A\beta42+DATD}$ is 29.8 ± 0.9. $PF_{A\beta42+Ent}$ is 18 ± 1, while $PF_{A\beta42+DATD}$ is 20 ± 2. $F_{A\beta42+Ent}$ is 12.9 ± 0.8, whereas $F_{A\beta42+DATD}$ is 13.7 ± 0.7. Note that these values did not differ significantly from those for

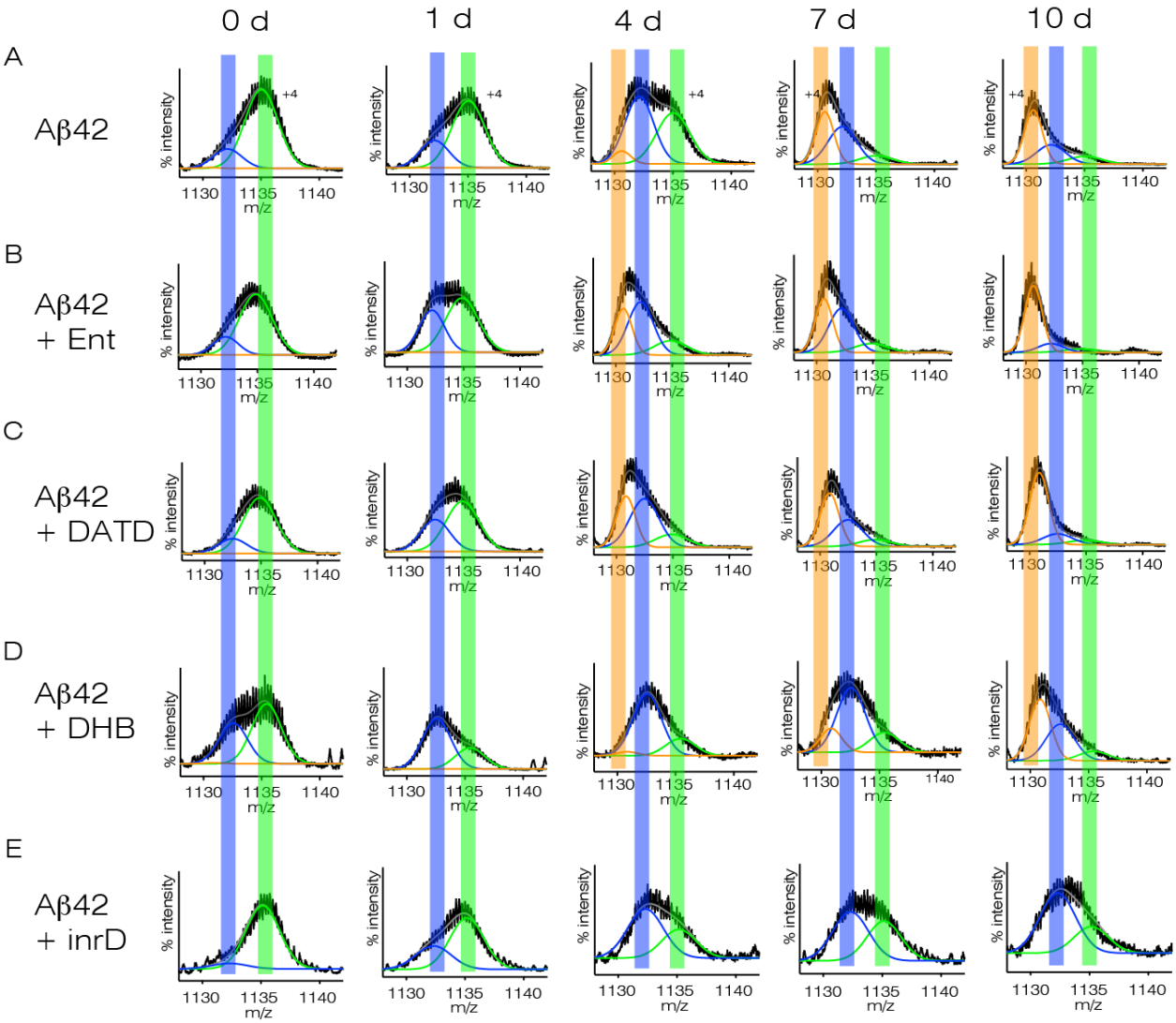

Figure 4.5: PL-HDX-ESI-MS results for Aβ42 in the absence and in the presence of small molecules and a peptide. All the spectra were adjusted to three gaussian curves except for Aβ42 + inrD, in which two gaussians were used. A) Aβ42 in the absence of inhibitors. B) Aβ42 in the presence of entacapone (Ent). C) Aβ42 aggregating with diallyltartardiamide (DATD). D) Aβ42 in the presence of 2,2'-dihydroxybenzophenone (DHB). E) Aβ42 aggregation in the presence of the peptide inrD.

Aβ42 in the absence of small molecule. Similarly to Aβ42 aggregating alone, the presence of Entacapone or Diallyltartardiamide did not influence significantly the heterogeneity of the species formed during the process of aggregation (Figure 4.7).

PL-HDX-ESI-MS experiments allowed us to establish that Ent and DATD affected the relative population of species as a function of time (Figure 4.8). These two small molecules led to a faster decrease of the $EA_{A\beta42+Ent}$ and $EA_{A\beta42+DATD}$ populations with $PF_{A\beta42+Ent}$ and $PF_{A\beta42+DATD}$ being maximal after two days of aggregation and fibrils appearing 2-3 days earlier than in the absence of small molecules. These two small molecules accelerated the kinetics of Aβ42 fibrillization.

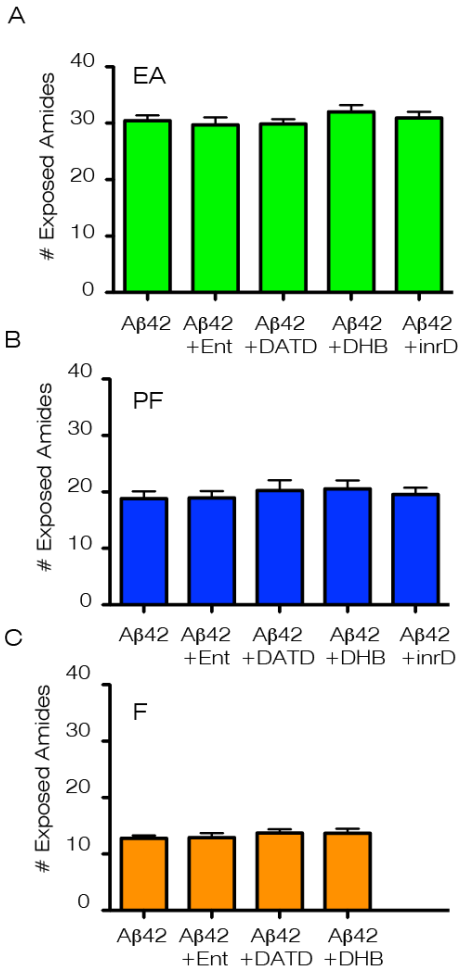

Figure 4.6: Number of exposed amides for each of the species detected during Aβ42 aggregation in the absence and in the presence of the compounds assayed. Number of exposed amides corresponding to the (A) $EA_{A\beta42}$ species, (B) the $PF_{A\beta42}$ species and the (C) $F_{A\beta42}$ species in the absence and in the presence of the compounds assayed.

DHB enhances the formation of high-order aggregates of Aβ42

When we applied the PL-HDX-ESI-MS experiment to Aβ42 aggregating with DHB we found that this small molecule involved the formation of three different species (Figure 4.5; Table 4.1, Materials and Methods). Although the number of exposed amides for each detected species was slightly higher than for $EA_{A\beta42}$, $PF_{A\beta42}$ adn $F_{A\beta42}$, the increase was not significant so we named them as: $EA_{A\beta42+DHB}$ (32 $\pm$ 1 exposed amides), $PF_{A\beta42+DHB}$ (21 $\pm$ 2 exposed amides) and $F_{A\beta42+DHB}$ (13.7 $\pm$ 0.8 exposed amides) (Figure 4.6). Regarding the heterogeneous nature of the species detected, $EA_{A\beta42+DHB}$ was slightly less heterogeneous than that observed for other molecules (Figure 4.7).

The presence of DHB enhanced the formation of $PF_{A\beta42+DHB}$ species, being maximal after 1 day of aggregation. $EA_{A\beta42+DHB}$ population decreased remarkably fast and $F_{A\beta42+DHB}$ species were present from day 3 onwards, although their relative abundance was much lower than that detected in its absence (Figure 4.8). Thus PL-HDX-ESI-MS experiments revealed that the mechanism of action of DHB was stabilizing the formation of $PF_{A\beta42+DHB}$ but not fibrils.

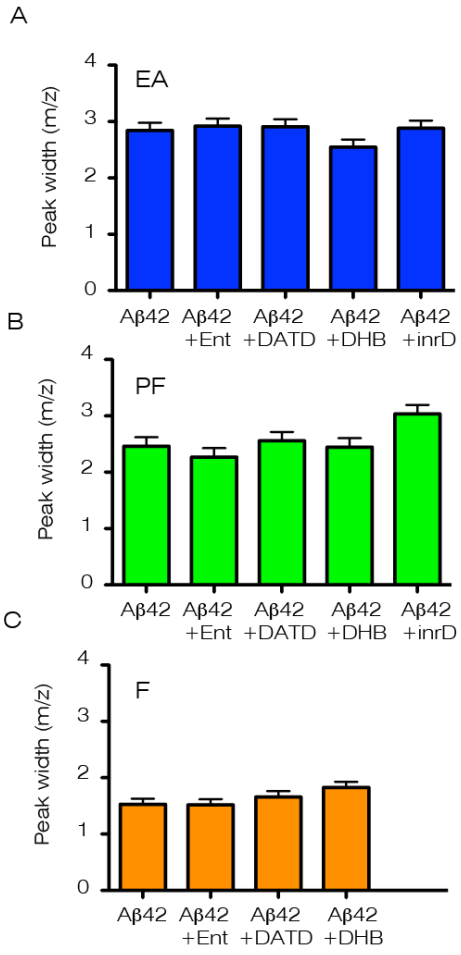

Figure 4.7: Peak widths for each of the species detected during Aβ42 aggregation in the absence and in the presence of the compounds assayed. Peak widths values corresponding to the (A) $EA_{A\beta42}$ species, (B) the $PF_{A\beta42}$ species and the (C) $F_{A\beta42}$ species in the absence and in the presence of the compounds assayed.

inrD inhibits Aβ42 aggregation by oligomer stabilization

Next, we applied the PL-HDX-ESI-MS experiment to study the effect of the peptide inrD in Aβ42 aggregation. In this case, we found that the spectra were fit to just two gaussian curves (Figure 4.5; Table 4.1, Materials and Methods). The number of exposed amides of the two species detected were similar to $EA_{A\beta42}$ and $PF_{A\beta42}$, thus we named them $EA_{A\beta42+inrD}$ (31 $\pm$ 1) and $PF_{A\beta42+inrD}$ (20 $\pm$ 2) (Figure 4.6): It is significant to notice that no F population was present. It is also significant to notice that $PF_{A\beta42+inrD}$ population is as heterogeneous as $EA_{A\beta42+inrD}$ (Figure 4.7). During the timescale of our experiment, inrD inhibited Aβ42 fibrillization by stabilizing an oligomer, $PF_{A\beta42+inrD}$ (Figure 4.8).

EGCG chemically modifies Aβ42

When we applied the PL-HDX-ESI-MS experiment to study Aβ42 aggregation in the presence of EGCG, we obtained complex MS spectra: we observed m/z values higher than what we would expect for fully deuterated Aβ42 (Figure 4.9A). Besides, the signal to noise ratio for the spectra was poorer when increasing Δt_{agg}. To shed light onto this unexpected result, we performed the PL-HDX-ESI-MS experiment on the same samples and aggregation

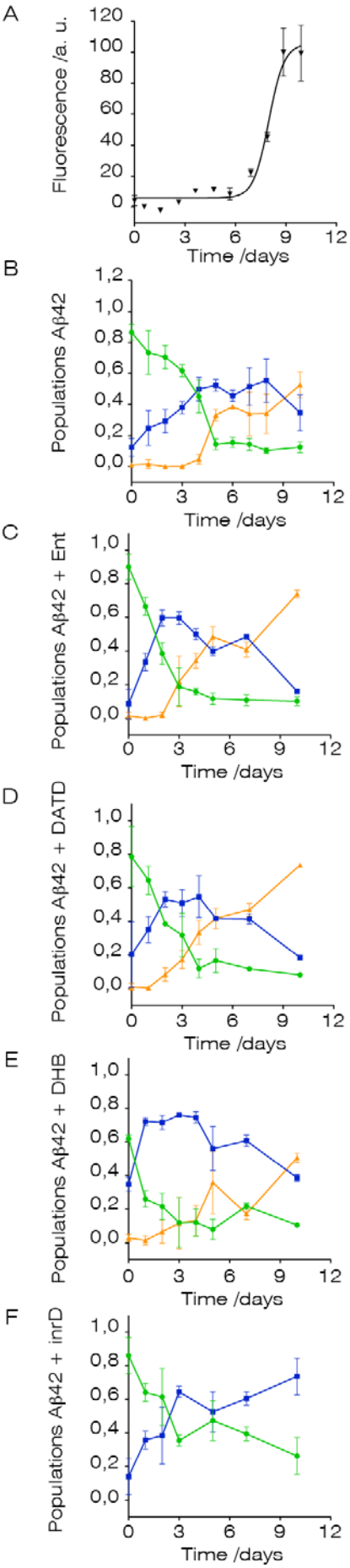

Figure 4.8: Effect of small molecules and a peptide on Aβ42 aggregation. A) ThT binding assay monitoring Aβ42 aggregation in the absence of compounds. Population of the different species detected during (B) Aβ42 aggregation and in the presence of (C) DATD, (D) Ent, (E) DHB and (F) inrD.

time points but without exchanging the protonated buffer tot deuterated one (Figure 4.9B). Under these conditions, all the spectra should show a single peak corresponding to the m/z value of fully protonated Aβ42. However, we observed a second peak corresponding to a mass 16 units higher than fully protonated Aβ42. Moreover, the intensity of this second peak increased at longer aggregation times. Based on the increment in mass, we assigned this second peak to an oxidized form of Aβ42 (the atomic weight of oxygen is approximately 16 uma), and we suspected that the sulfide group of methionine 35 had undergone oxidation.

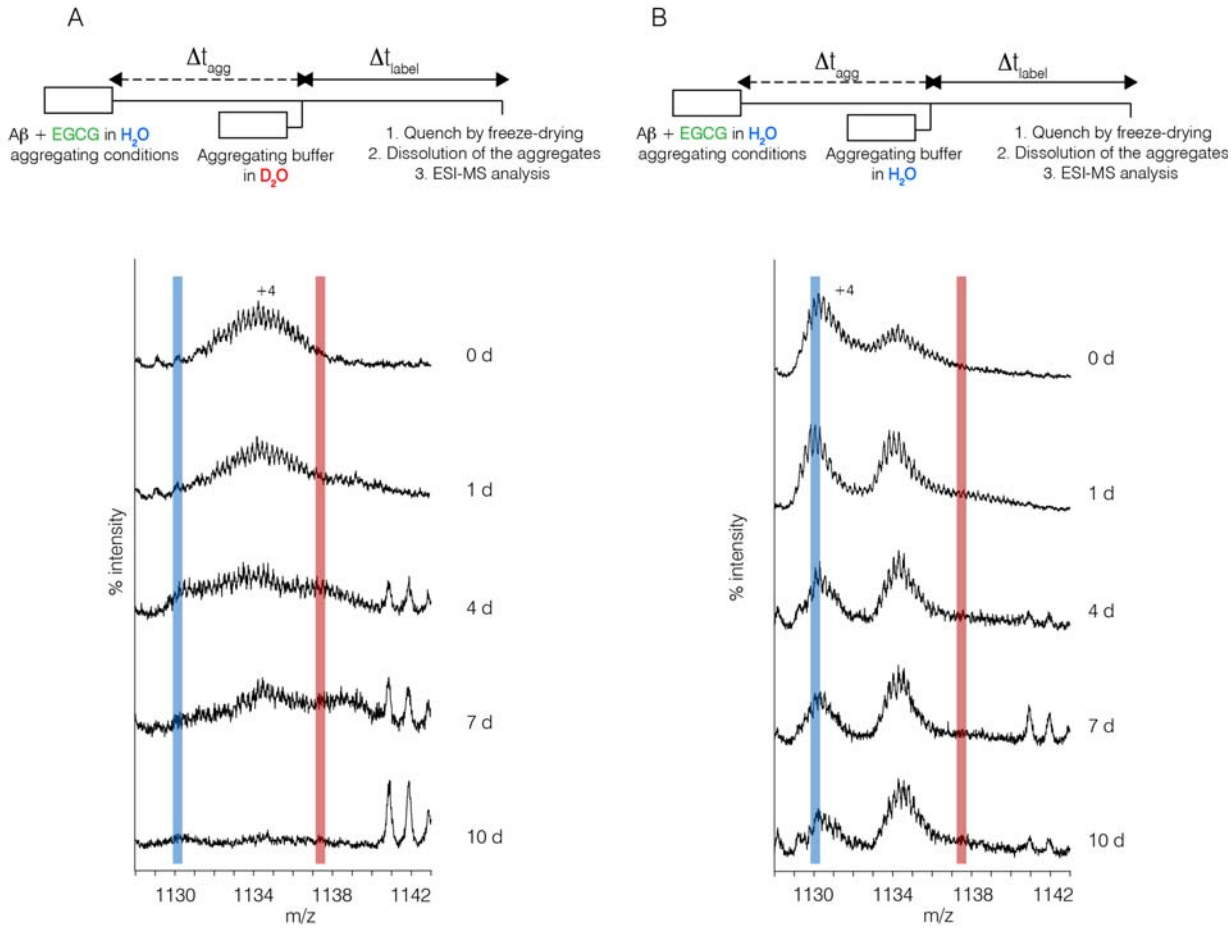

Figure 4.9: EGCG chemically modifies Aβ42. A) PL-HDX-ESI-MS scheme and ESI-MS spectra for Aβ42 aggregation in the presence of EGCG. B) Modified PL-HDX-ESI-MS scheme showing that no buffer exchange to D_2O is performed and corresponding ESI-MS spectra. Red and blue bars indicate, respectively, expected m/z values for fully deuterated and fully protonated Aβ42.

We were able to confirm by NMR studies that in the presence of EGCG, Aβ42 was oxidized in its sulfide group of methionine 35. Since the sulfide and the sulfoxide group involve different chemical environments, the chemical shift of the methyl protons adjacent to these two chemical groups are different and can be quantified by NMR. Using $^{13}C(CH_3)$Met35-Aβ42, that is, Aβ42 where the methyl group in methionine 35 is labeled with ^{13}C, we

recorded a series of 2D $^{1}H-^{13}C$ Heteronuclear Multiple Quantum Correlation (HMQC) NMR spectra at the initial stage of aggregation and after 1.5, 3 and 4 days of aggregation (Figure 4.10). Projection of the 2D $^{1}H-^{13}C$ HMQC spectra on the ^{1}H dimension showed two peaks, corresponding to the methyl protons of non-oxidized (at 2 ppm) and oxidized methionine (at 2.4 ppm). We observed a sharp decrease in the intensity of the non-oxidized methyl of methionine 35 as a function of the aggregation time. This result can be explained by the fact that large aggregates cannot be detected by solution NMR. Since the signal corresponding to the oxidized methyl of methionine 35 showed a similar intensity as aggregation proceeded, we showed further evidence that EGCG covalently modified by oxidation the Aβ42 peptide. Hence, in the presence of EGCG, Aβ42 suffered a chemical modification, the oxidation of its sulfide group in methionine 35.

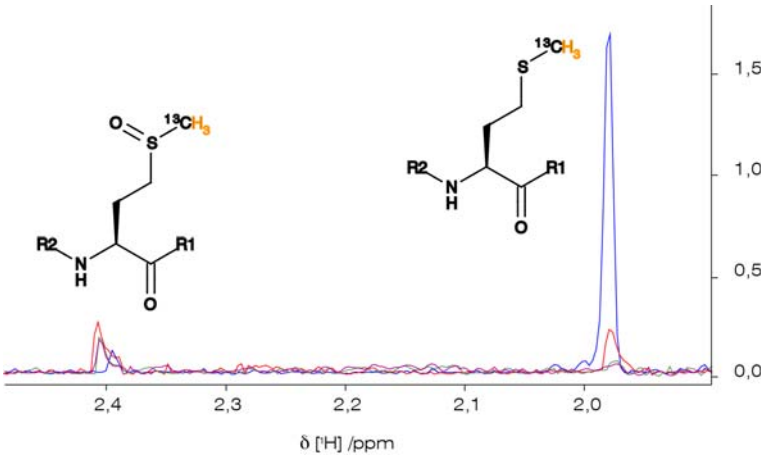

Figure 4.10: Superposition of the ^{1}H projection of the bidimensional $^{1}H-^{13}C$ HMQC NMR spectra obtained during Aβ42 aggregation in the presence of EGCG. The chemical shift of the methyl group of methionine 35 (in orange) appears at 2 ppm and 2.4 ppm, respectively, in the non-oxidized and oxidized form of Aβ42. Aggregation was monitored at 0 days (blue), 1.5 days (red), 3 days (green) and 4 days (violet).

4.2 Discussion

In Chapter 3, we showed that PL-HDX-ESI-MS experiments overcome the heterogeneity of the aggregation process, enabling to detect, characterize and quantify the different species populating during Aβ42 aggregation. We found this methodology to yield very useful and valuable information regarding the mechanism of action five molecules described to modulate Aβ42 aggregation.

The FRA proved to be a good way to screen a library of compounds. Although the information obtained was limited, it enabled to have a first idea of the behavior of several small molecules and a peptide towards Aβ42 aggregation and was a useful tool to select candidates

for a further study. Since the immunoblot intensity clearly correlated with the ThT binding assay, our results indicated that the FRA quantified the amount of Aβ42 fibrils (Figure 4.3).

Both Ent and DATD were shown to accelerate Aβ42 aggregation (Figure 4.5 and 4.8). After applying the PL-HDX-ESI-MS experiment, Ent and DATD were shown to enhance Aβ42 fibrillization: the F population increased faster than in the case when Aβ42 aggregated without any small molecule, and $PF_{A\beta42+Ent}$ and $PF_{A\beta42+DATD}$ were also formed faster. This behavior might be of pharmaceutical relevance. In fact, enhancing fibrillization has also been posed as a possibility to elude soluble oligomer toxicity. In fact, the group of Erich Wanker showed that by enhancing the fibrillization of Aβ42, the small molecule O4 was able to reduce Aβ42 toxicity *in vitro* [112].

The behavior of Ent and DATD, though, was different in our hands from what is reported in the literature. In an article from the Lashuel group [79], Ent, a catechol O-methyltransferase inhibitor, currently marketed as a symptomatic treatment against Parkinson's disease, is shown to protect PC12 cells against amyloid-induced toxicity by inhibiting Aβ42 aggregation. The methodology to assess the effect of Aβ42 aggregation in the presence of Ent was the ThT binding assay and Electron Microscopy. As mentioned, monitoring the ThT binding of an amyloid in the presence of a small molecule is ill-advised, since there are several problems associated: the small molecule might interfere with the fluorescence excitation or emission of ThT and/or the small molecule might inhibit the formation of the complex between ThT and the Aβ fibril [113]. Moreover, not finding a large amount of fibrils in a electron microscopy grid cannot rule out the possibility of having in fact amyloid fibrils in solution that are not as easily deposited for instance as a consequence of the different physicochemical environment the small molecule might confer.

For DATD, the Glabe group reported that it stabilized oligomers and did not form fibrils [77]. However, the evidence came only by positive immunoreactivity of the aggregates formed by DATD and Aβ42 against A11 antibody, a conformation specific antibody detecting only oligomers [75]. Moreover, no experimental data is shown in the case of DATD in the whole paper, making difficult to assess why DATD was classified as having that effect and not another. In our hands, we found DATD enhanced Aβ42 fibrillization. Since $EA_{A\beta42+DATD}$ and $PF_{A\beta42+DATD}$ coexist with $F_{A\beta42+DATD}$, some of them might be positive against A11, which might explain the result obtained by Glabe and co-workers.

The FRA showed that DHB had a negligible effect on Aβ42, since the pattern was very similar for Aβ42 + DHB and Aβ42. With the PL experiment we showed that DHB influenced significantly Aβ42 aggregation by enhancing the formation of the $PF_{A\beta42}$ species, an aggregate that was not large enough or stable enough to be detected by the FRA (Figure 4.3).
DHB was shown to inhibit both oligomerization and fibrillization in a report by the Glabe

group [77]. As stated in the case of DATD, these results were obtained mainly through the use of A11. We found that DHB slightly inhibited the formation of fibrils (Figure 4.8). However, we did not found DHB inhibiting the formation of oligomers, as it enhanced the formation of the oligomer $PF_{A\beta42}$, in apparent contradiction with the activity reported. A possible explanation might be that $PF_{A\beta42}$, the oligomer stabilized by DHB, is not A11-positive.

The inrD peptide was developed in our laboratory and shown to inhibit Aβ42 fibrillization by retarding fibril formation [93]. It also showed a protective effect on SHSY5Y cells. Using PL-HDX-ESI-MS experiment we found that inrD prevented the formation of the F population and it stabilized the oligomer $PF_{A\beta42}$, thus inhibiting Aβ42 aggregation. This information complements the previous work in our laboratory and it sheds light onto the mechanism of action of this peptide. In the previous work [93], by using photo-induced cross-linking of unmodified proteins (PICUP) [114], it was showed that inrD was able to stabilize early-formed oligomers. In our present work we show inrD stabilizing $EA_{A\beta42}$ and $PF_{A\beta42}$ in a time-dependent manner. The peptide inrD, whose design is inspired on the Aβ42 sequence, might be an Aβ42 inhibitor susceptible to further studies in the quest for antiamyloidogenic therapeutic agents.

EGCG was reported to form off-pathway, non-toxic Aβ42 aggregates [87]. Further studies showed that EGCG was able to remodel (disrupt) amyloid fibrils [88] and the reported non-toxic aggregates had a structure amenable to study [115]. Concomitant with our work with this small molecule and Aβ42, a recent study contributed to understanding the mechanism by which EGCG remodeled amyloid fibrils [116]. In this study, the oxidized form of EGCG is shown to covalently interact with Aβ42 through imine bond formation between amino residues and carbonyl groups in oxidized EGCG. In fact, this compound is easily oxidized in the presence of atmospheric oxygen [117].
Taking together our MS and NMR results for Aβ42 + EGCG, we have been able to assess that EGCG is able to covalently modify Aβ42. We have determined that the sulfide group in methionine 35 is oxidized to a sulfone group (Figures 4.9 and 4.10), probably *via* a radical-type reaction in which atmospheric oxygen oxidizes EGCG which oxidizes Aβ42 at its most oxidation-prone place, the sulfide in methionie 35. Moreover, we also found difficulties in ionizing the sample for MS study as the aggregation proceeded. Since our DMSO-based solution has the ability to break even the fibrillar aggregates, we suspect that Aβ42 aggregates are chemically cross-linked when aggregating.
Moreover, several reports have claimed the important role of methionine 35 in Aβ aggregation [118, 119, 120]. With our studies we establish a new link between chemical modifications of Aβ and small molecule inhibition with an overall impact on Aβ aggregation.

To summarize, the PL-HDX-ESI-MS experiment has been shown to be a highly valuable technique to detect, characterize and quantify the species formed in Aβ42 aggregation in the

presence of pharmaceutically and biologically relevant molecules. Moreover, this experiment have been shown to enable the distinction between the effects that small molecules have on Aβ aggregation and a tool to give insights into the mechanism of action of these compounds.

4.3 Materials and Methods

The ThT binding assay, the PL-HDX-ESI-MS experiment and its analysis were carried out as described in Materials and Methods in Chapter 3.

4.3.1 Preparation of Aβ42 in its lowest aggregation state

Aβ42 was prepared using the same protocol and conditions described in Materials and Methods of Chapter 3: Aβ42 in the aggregating solution was obtained after a SEC and the concentration was quantified by HPLC. DMSO was added to the aggregating solution at a 0.5% concentration in order to match the DMSO concentration in Aβ42 aggregating in the presence of our library compounds.

4.3.2 Small molecule and peptide stocks

2,2'-dihydroxybenzophenone, apigenin, diallyltartardiamide, clioquinol, direct red 80, epigallocatechin gallate, juglone, salvianolic acid B, tarenflurbil, tetracycline, entacapone, riluzole and methylene blue were dissolved in DMSO to a final concentration of 60 mM. Chicago sky blue 6B, myo-inositol, orange G, scyllo-inositol and tramiprosate were dissolved in the same aqueous buffer as Aβ42 peptide (50 mM ammonium acetate, 1 mM Tris $\cdot$ HCl, 0.01% sodium azide, pH 7.4) to a final concentration of 60 mM. Ammonium tetrathiomolybdate was dissolved in DMSO to a final concentration of 30 mM and the peptide inrD was dissolved in DMSO to a final concentration of 10 mM.

4.3.3 Aggregation of Aβ42 in the presence of small molecules and peptide inrD

A volume of small molecule stock was added to a freshly prepared Aβ42 solution so that all small molecules were at a 10:1 ratio SM:Aβ42 (300 μM small molecule concentration). Only in the case of the peptide inrD the ratio was kept at 2:1 inrD:Aβ42 (60 μM concentration of inrD). The final DMSO concentration in all the aggregating solutions was 0.5%. Apigenin, clioquinol and juglone weren't soluble enough in those conditions and precipitated immediately when they were diluted from the DMSO stock.

4.3.4 FRA

25 μL triplicate aliquots were collected and frozen at different times of the aggregation process. After collecting aliquots for 12 days, samples were unfrozen and SDS-treated as follows: 225 μL of a 2,22% SDS solution were added to the 25 μL aliquots to obtain a 1/10 dilution and a final SDS concentration of 2%. Then, samples where heated at 95°C for 5 min. SDS-treated samples were analyzed using the FRA, using the Bio-Dot SF Microfiltration Apparatus (Bio-Rad, CA, US). Samples were filtrated through a cellulose acetate membrane with a pore size of 0,2 μm (Schleicher and Schuell, Germany). With this method, high molecular weight aggregates are retained in the membrane, while monomeric peptide and small soluble oligomers are passed through the membrane. The membrane was immunodetected using the monoclonal antibody 6E10 (Invitrogen, CA, US), which specifically recognizes the N-terminus end of the Aβ peptide.

4.3.5 Multigaussian fitting of PL-HDX ESI-MS experiments

The MS spectra for Aβ42 alone and Aβ42 + small molecules/inrD were adjusted to gaussian curves. According to the error analysis, three species were detected in all cases except for Aβ42 + inrD, in which two gaussians were enough to fit the adjustment. The error analysis is depicted in Table 4.1.

4.3.6 NMR spectroscopy

NMR measurements were performed on a Bruker 600 US spectrometer (Bruker, Germany) equipped with four radiofrequency channels and a cryoprobe. $^{1}H-^{13}C$ HMQC experiments were measured at a ^{1}H resonance frequency of 600 MHz. $^{13}C(CH_3)$Met35-Aβ42 was synthesized by James Elliott at Yale University (New Haven, CT, USA) and prepared as described in the "Preparation of Aβ42 in its lowest aggregation state" section. EGCG dissolved in DMSO$-d_6$ was added to a freshly prepared Aβ42 sample at a final 300 μM concentration (10:1 EGCG:Aβ42 ratio). DMSO$-d_6$ was used to reference spectra.

Aβ42

# gaussian	error	relative error
1	9,52E+10	
2	1,42E+10	85,1
3	8,15E+09	42,4
4	6,98E+09	14,3

Aβ42 + Ent

# gaussian	error	relative error
1	3,18E+10	
2	9,41E+09	70,4
3	4,72E+09	49,8
4	4,01E+09	15,1

Aβ42 + DATD

# gaussian	error	relative error
1	5,12E+10	
2	8,30E+09	83,8
3	4,73E+09	43,0
4	4,35E+09	8,0

Aβ42 + DHB

# gaussian	error	relative error
1	8,47E+09	
2	3,83E+09	54,8
3	1,99E+09	48,1
4	1,76E+09	11,5

Aβ42 + inrD

# gaussian	error	relative error
1	6,85E+09	
2	2,34E+09	65,8
3	2,10E+09	10,5
4	1,98E+09	5,7

Table 4.1: Error analysis for Aβ42 in the presence or absence of different small molecules and inrD.

5 Conclusions

The conclusions of the present thesis are the following:

1. Using Pulse-labeling Hydrogen/Deuterium Exchange (PL-HDX) experiments, we have been able to detect, quantify and characterize different aggregates formed during Aβ aggregation.

2. The fact that the aggregates detected showed distinct degree of protection against HDX indicates that during Aβ aggregation structural rearrangements take place.

3. E22Δ-Aβ42 immediately forms fibrils upon dissolution, and Aβ42 aggregates faster than Aβ40.

4. By carrying parallel PL-HDX and neurotoxicity experiments, protofibrillar species, defined as short and curvilinear protofilaments observed by TEM together with the most abundant species detected by MS at intermediate aggregation stages, have been established as the most toxic aggregate to primary neural cultures.

5. The lyophilization step in PL-HDX experiments must be carried out under controlled conditions.

6. The FRA has proven an efficient method to perform a first screening of molecules modulating Aβ aggregation.

7. Using the PL-HDX experiment we have been able to characterize the mechanism by which different molecules interfere with Aβ aggregation:

   Entacapone and Diallyltartardiamide enhance Aβ42 fibrillization by accelerating the kinetics of fibril formation.

   2,2'-dihydroxybenzophenone inhibits Aβ42 aggregation by enhancing the formation of a defined oligomeric species, $PF_{A\beta42+DHB}$.

The peptide inrD completely inhibits fibrillization in the timescale studied by stabilizing the eariler aggregates $EA_{A\beta 42+inrD}$and the protofibrillar species $PF_{A\beta 42+inrD}$.

Epigallocatechin gallate chemically modifies Aβ42 aggregates.

6 Resum

6.1 Introducció

La malalatia d'Alzheimer (MA) és una malalatia neurodegenerativa, la forma més comú de demència i implica una pèrdua gradual de capacitats cognitives, com la memòria. El principal factor de risc és l'edat, i la incidència de la MA es duplica cada 5 anys a partir dels 65. La MA pren el seu nom del Dr. Alois Alzheimer, el psiquiatra alemany que va identificar el primer cas l'any 1901. La malaltia es caracteritza pels següents signes: mort neuronal, i dipòsit de plaques amiloides i de cabdells neurofibril·lars.

Als anys 80 es va descobrir que els cabdells neurofibril·lars estaven formats principalment d'agregats de la proteïna tau en forma hiperfosforilada, mentres que la proteïna beta-amiloide (βA) era el component principal de les plaques amiloides. Malgrat les dues proteïnes són necessàries perquè tingui lloc la pèrdua neuronal en la MA, l'agent causatiu principal s'atribueix a la proteïna βA.

La proteïna βA es produeix pel processament de la proteïna precursora amiloide (PPA). La PPA és una proteïna transmembrana i per a formar βA, dues secretases actuen en ella: la β- i la γ-secretasa. Com que la γ-secretasa no actua en un lloc específic, la proteïna βA es forma en diferents longituds, des de 38 a 43 aminoàcids. La βA de 40 aminoàcids (βA40) és la forma més abundant, mentres que la formada per 42 aminoàcids (βA42) és la forma més implicada en els dèficits cognitius associats a la MA. La proteïna βA agrega amb sí mateixa, formant espècies oligomèriques de baix pes molecular, que evolucionen en protofibril·les i posteriorment aquestes reverteixen en la formació de fibril·les amiloides, els components principals de les plaques.

En un primer moment, la comunitat científica assignà les fibril·les amiloides com l'entitat responsable de la neurotoxicitat en la MA. Tanmateix, diversos estudis demostraren la manca de correlació entre quantitat de plaques amiloides i severitat de la MA, però la bona correlació entre severitat de la MA i la quantitat de βA soluble. Per aquesta raó, la hipòtesi actual

treballa amb l'assumpció que les espècies intermèdies en l'agregació de βA (oligòmers i protofibril·les) són les responsables dels dèficits cognitius i de la mort neuronal que s'observa en la MA.

6.2 Agregació de βA

6.2.1 Caracterització biofísica

L'estudi dels agregats de βA presenta dificultats importants, degut al fet que les espècies intermèdies són dinàmiques i metaestables. És per això que els científics han tractar d'estudiar els oligòmers de βA estabilitzant-los en determinades condicions. La manca d'informació estructural i de caracterització dels diferents estadis de l'agregació de βA van fer-nos decidir a estudiar aquest procés utilitzant la tècnica de bescanvi protó/deuteri per marcatge per pols (PL-HDX, de l'anglès *pulse-labeling hydrogen/deuterium exchange*). Aquesta tècnica consisteix en dissoldre βA en una solució tampó protonada i, a diferents temps d'agregació, Δt_{agg}, bescanviar el tampó per aigua deuterada en un interval curt (un pols) de temps, Δt_{label} (temps de marcatge, *label* en anglès). Δt_{label} s'agafa de manera que els protons amides exposats de βA es bescanvien, mentre que aquells que no són accessibles al dissolvent, perquè formen part d'una estructura més compacta no són bescanviats. El bescanvi s'atura congelant la mostra amb nitrogen líquid i liofilitzant. Aquestes mostres posteriorment es dissolen en una dissolució de DMSO, que manté el contingut de deuteri, i s'analitzen per espectrometria de masses (EM) d'ionització per *electrospray*. L'EM de la capacitat de detectar i caracteritzar poblacions de molècules amb diferents graus de bescanvi, de manera que detecta les diverses espècies presents en un estadi d'agregació determinat. Aquesta metodologia permet la detecció i caracterització de les espècies dinàmiques i metaestables presents en l'agregació de βA.

A l'hora d'estudiar l'agregació de βA, vam decidir caracteritzar els processos d'agregació de βA40, βA42 i també de E22Δ-βA42. Aquesta darrera variant és una mutació de la proteïna βA42 on falta l'àcid glutàmic a la posició 22, trobada en pedigrís japonesos i caracteritzada, en primera instància, per formar oligòmers però no fibril·les amiloides. Estudis posteriors, tanmateix, van demostrar que E22Δ-βA42 també formava fibril·les amiloides.

En primer lloc vam estudiar l'agregació d'aquestes tres proteïnes amb diversos mètodes tradicionals. L'assaig de Tioflavina T (ThT) mesura la quantitat de fibril·les amiloides presents en solució. La proteïna βA40 es troba en forma fibril·lar després de 19 dies d'agregació, mentre que la proteïna βA42 forma fibril·les després de 9 dies d'agregació. També vam caracteritzar l'agregació de les variants de βA mitjançant microscopia de transmissió electrònica (MTE), una tècnica que permet estudiar la morfologia dels diferents agregats de βA. Vam observar

que la proteïna βA40 necessitava 17 dies per a formar fibril·les ben definides, mentre βA42 en necessitava 9. És important fer notar que tant en l'agregació de βA40 com en la de βA42 vam detectar intermedis protofibril·lars (filaments petits, curts i curvilinis d'uns 200 nm). En la proteïna E22Δ-βA42 vam observar protofibril·les i fibril·les des dels primers instants d'agregació. Després de 2 dies, la majoria de proteïna es trobava en forma fibril·lar.

Les fibril·les formades pels variants de βA van ser caracteritzades utilitzant difracció de raigs X. Malgrat no vam ser capaços d'alinear les fibril·les, vam poder obtenir patrons de difracció que ens permeteren quantificar les distàncies intramoleculars i intermoleculars entre les diferents *strands* de les fibril·les. En el cas de βA40 i de βA42 vam obtenir valors idèntics: 10.4 i 4.7 Å, mentre que per E22Δ-βA42 la distància intramolecular va resultar ser lleugerament més curta: 10.1 Å.

Malgrat obtenir informació important mitjançant les tres tècniques comentades anteriorment, cap d'elles ens permeten obtenir informació estructural dels intermedis d'agregació de la proteïna βA. Per això vam estudiar els tres variants de βA amb la tècnica introduïda anteriorment: el PL-HDX acoblat a l'EM.

Per tal de poder treballar amb aquesta metodologia del PL-HDX vam haver de desenvolupar un sistema experimental que ens permetés desalar les mostres i que alhora fos resistent al DMSO. Ho vam aconseguir utilitzant cablejat, unions i vàlvules de Tefló i mantentint els dissolvents i el sistema de vàlvules a baixa temperatura amb gel. El valor òptim de voltage capil·lar per a evitar adductes en els pics dels espectres de masses va resultar ésser de 4 kV.

També fou molt rellevant de cara a la realització experimental de la tesi la descoberta del bescanvi protó-deuteri entre diferents mostres en el procés de liofilització. Per tal d'assegurarnos una correcta liofilització i per mantenir la informació del bescanvi, resultà clau dur a terme les liofilitzacions en un liofilitzador propi, sense cap altra mostra processant-se fora de la d'interès.

Amb les condicions d'EM optimitzades, vam dur a terme els experiments de PL-HDX acoblat a l'EM per a les tres variants de βA. En tots tres casos els espectres de masses segueixen un patró similar: en els estadis inicials, la proteïna βA té una massa més gran que al final de l'agregació. Això és degut al fet que βA es troba primer en una forma molt poc agregada, i per tant té molt poques amides exposades que puguin bescanviar, mentre que després de diversos dies d'agregació, βA forma estructures més compactes on el bescanvi HD és més petit.

Per tal d'obtenir més informació de l'experiment de PL-HDX, vam ajustar globalment els espectres per les diferents proteïnes a una combinació de corbes gaussianes. Cada corba gaussiana representa una espècie diferent present en l'agregació de βA. Per cada proteïna, tots els espectres de massa corresponents foren ajustats a un nombre de gaussianes definit:

3 en el cas de βA40 i βA42, i 2 en el cas d'E22Δ-βA42.

En el cas de βA40, la primera espècie detectada es corresponia en massa amb la proteïna amb totes les amides exposades, indicant que aquesta espècie inclou monòmer i/o agregats sense protecció contra HDX. La població relativa d'aquesta primera espècie decreix gradualment des de 0 a 17 dies. Les protofibril·les de βA40 foren les segones espècies detectades, corresponent a masses de 25.1 $\pm$ 1.0 amides exposades. Basant-nos en l'amplada de banda associada a les protofibril·les de βA40, aquesta va resultar ser l'espècie més heterogènia formada durant l'agregació, essent la seva presència constant però màxima als 13 dies d'agregació. La darrera espècie detectada corresponia a masses de 13.5 $\pm$ 0.6 amides exposades. La seva població es correlacionava amb la senyal de ThT i l'observació de fibril·les ben definides per MTE; aquesta espècie la vam assignar a fibril·les.

L'agregació de βA42 també fou estudiada amb l'estratègia de PL-HDX. Malgrat el nombre d'espècies trobades per βA40 i βA42 fou el mateix, els nostres experiments varen demostrar que la naturalesa dels agregats primerencs és diferent per les dues proteïnes. Els corresponents a βA42 mostraren un grau de protecció més elevat que en βA40: 32.8 $\pm$ 0.8 (de 41) vs 37.4 $\pm$ 0.5 (de 39) per βA40. Aquests resultats són consistents amb la tendència superior a agregar per part de βA42. La tercera població detectada la vam assignar, com en el cas de βA40, a fibril·les amiloides, mentre que l'espècie intermèdia, amb 23.6 $\pm$ 1.8 amides exposades, resultà ser l'espècie detectada més heterogènia. Quan aquesta espècie és màxima en l'agregació, les imatges de MTE mostren clarament protofibril·les abundants, pel que vam assignar aquesta segona població de βA42 a protofibril·les.

Finalment, l'experiment de PL-HDX també el vam aplicar a l'estudi d'E22Δ-βA42. Vam detectar dues espècies: protofibril·les, que mostraren un nombre d'amides exposades superior al monòmer d'E22Δ-βA42 (30.8 $\pm$ 0.3 de 41) i fibril·les. La quantitat de protofibril·les en el cas d'E22Δ-βA42 decreix ràpidament en els estadis inicials i la població de fibril·les incrementa. Aquests experiments també mostren una evidència més de l'alta tendència a agregar d'aquesta proteïna.

6.2.2 Estudis de toxicitat

L'experiment de PL-HDX ens va permetre caracteritzar, detectar i quantificar les diferents espècies conformant l'agregació de βA. Aquesta descoberta obre la possibilitat de mesurar la contribució de cada espècie a una variable determinada. Com que βA està relacionada amb la neurotoxicitat en la MA, vam estudiar la influència dels agregats de βA en cultius primaris de neurones d'hipocamp de ratolins.

Per posar a punt els experiments de neurotoxicitat vam utilitzar l'assaig de bromur de 3-(4,5-dimetilthiazol-2-il)-2,5-dipheniltetrazole (MTT) i vam treballar amb els oligòmers sintètics

de βA42 coneguts com a ADDLs. Vam trobar que les condicions òptimes per a determinar la toxicitat d'Aβ en cultius primaris neuronals eren treballar a una concentració de 5 μM de βA i incubar les mostres en els cultius durant 24 hores. En aquests assaigs previs també vam determinar que el nostre tampó d'agregació presentava certa toxicitat però no impedia fer les mesures que nosaltres volíem dur a terme.

També fou rellevant per a l'estudi de toxicitat determinar mitjançant l'experiment de PL-HDX acoblat a EM el fet que els agregats de βA conservaven l'estructura després d'haver estat congelats a -20°C i descongelats. Aquesta observació fou important ja que vam fer els assaigs de toxicitat en paral·lel el mateix dia, utilitzant els mateixos cultius primaris.

En aquests experiments de neurotoxicitat vam utilitzar un conjunt de mostres idèntiques a les usades pels experiments de PL-HDX i vam mesurar la supervivència dels cultius primaris mitjançant l'assaig d'MTT. En el cas de βA40, la supervivència neuronal va decréixer des d'un 90% a una toxicitat màxima de 65% als 17 dies. La viabilitat s'incrementà fins a un 80% al cap de 24 dies. Per a un Δt_{agg} donat, vam combinar les poblacions obtingudes per EM amb els resultats d'MTT i vam usar una regressió multilineal per a obtenir la toxicitat de les diferents espècies: 101 $\pm$ 12 pels agregats primerencs, 56 $\pm$ 13 per les protofibril·les de βA40 i 78 $\pm$ 7 per les fibril·les.

Quan els mateixos experiments es dugueren a terme amb preparacions de βA42, vam observar un patró similar que en el cas de βA40, malgrat la relació entre protofibril·les de βA42 i neurotoxicitat resultà ser molt més significativa. Els temps inicials d'agregació en βA42 mostraren una toxicitat superior que en βA40 (començant per un 80% de viabilitat a dia 0) i la viabilitat decreixé gradualment fins a un màxim de 38% als 7 dies d'agregació. La viabilitat tornava a pujar fins arribar al mateix valor que al principi, 80%, al cap d'11 dies. Combinant aquestes dades amb les obtingudes en l'experiment de PL-HDX vam obtenir els següents valors de toxicitat per les diferents espècies de βA42: 74 $\pm$ 7 pels estadis d'agregació primerencs, 17 $\pm$ 10 per les protofibril·les i 106 $\pm$ 12 per les fibril·les. Malgrat les quantitats relatives de protofibril·les en βA40 i βA42 són similars, les protofibril·les de βA42 mostraren una neurotoxicitat superior i una correlació més gran amb la toxicitat global mesurada.

En el cas d'E22Δ-βA42 no vam observar toxicitat en les preparacions i, per tant, no vam poder determinar la toxicitat corresponent a les espècies conformant el procés d'agregació d'E22Δ-βA42.

6.2.3 Discussió

Amb l'experiment de PL-HDX hem estat capaços d'identificar les diferents espècies presents en el procés d'agregació de tres variants de la proteïna βA: βA40, βA42 i E22Δ-βA42. Malgrat vam detectar el mateix nombre d'espècies per βA40 i βA42, les dades obtingudes

demostren que hi ha diferències estructurals entre ells. El nombre diferent d'amides exposades en els agregats primerencs de les dues proteïnes és consistent amb la tendència més gran a agregar de βA42. A més, malgrat les protofibril·les per βA40 i βA42 mostraren també un nombre similar d'amides exposades, les protofibril·les de βA42 mostraren ser molt més tòxiques que per βA40, consistent amb la major toxicitat de la proteïna βA42. Aquestes diferències poden ser explicades pel fet que els dos aminoàcids extra en βA42 confereixen una hidrofobicitat superior que implica una major tendència a l'agregació i una interacció més forta amb membranes cel·luars que porta a una major toxicitat. També cal tenir en compte que el comportament de la proteïna E22Δ-βA42 que hem observat està d'acord amb treballs anteriors, en què es mostrava que aquesta proteïna agregava molt ràpidament.

El fet de detectar tres espècies amb estructures diferents, així com la seva evolució en funció del temps, està d'acord amb el mecanisme de formació amiloide anomenat conversión conformacional nucleada. Aquest mecanisme proposa que les monòmers o els agregates primerencs poc estructurats progressen vers estructures protofibril·lars, que són capaces encara d'evolucionar en estructures fibril·lars més rígides.

En definitiva, hem detectat diferents agregats presents durant l'agregació de βA utilitzant l'experiment de PL-HDX acoblat a EM. Mitjançant estudis paral·lels de neurotoxicitat hem estat capaços de determinar que les protofibril·les, provinents d'un reordenament estrucutral, són les espècies més tòxiques per les neurones. Així doncs, el nostre treball apunta vers l'establiment de determinants estructurals de la neurotoxicitat de les protofibril·les de βA a més de ser un punt de partida pel desenvolupament d'estratègies terapèutiques contra la MA.

6.3 Avaluació de petites molècules

6.3.1 Assaig d'una biblioteca de molècules interferint l'agregació de βA

S'han dut a terme molts estudis en els quals diversos composts mostren la capacitat d'incrementar o inhibir l'agregació de βA. Tanmateix, la majoria d'aquests no dóna informació detallada en el mecanisme d'acció d'aquestes molècules i, per tant, es desconeix el tipus d'agregat amb que aquestes molècules interactuen o estabilitzen.

Per tal d'aportar informació en aquest camp, vam provar l'efecte d'una petita biblioteca de compostos en l'agregació de la proteïna βA42, ja que és aquesta la que està més associada amb l'etiologia de la MA. Aquesta biblioteca consistia de 20 molècules amb diferents característiques químiques i els compostos que la formaven complien almenys un de les següents

premises: 1) estar o haver estat en fases clíniques contra la MA, 2) inhibir la fibril·lació de βA estabilitzant oligòmers de βA *in vitro*, 3) retardar la formació de fibril·les de βA, i 4) inhibir la formació d'oligòmers però no de fibril·les de βA.

Per tal de dur a terme un primer procés de selecció, vam utilitzar un procediment anomenat assaig de retenció en filtre (ARF). Aquest experiment proporciona una manera de determinar l'efecte de compostos en la formació d'agregats de βA estables en dodecilsulfat de sodi (SDS, de l'anglès *sodium dodecyl sulfate*). Utilitzant l'ARF, els agregats d'alt pes molecular, resistents a l'SDS queden retinguts en una membrana, mentre que la proteïna monomèrica i els agregats petits i solubles passen a través d'ella. La quantitat d'agregats resistents a SDS es poden quantificar per immunodetecció amb l'anticòs monoclonal 6E10, que reconeix específicament la part N-terminal de βA.

Vam seguir l'agregació de βA42 en absència i en presència de les molècules de la nostra biblioteca per l'ARF. L'agregació de βA42 en absència de composts també la vam mesurar amb l'assaig de ThT. Això ens va permetre identificar els agregats resistents a SDS amb les fibril·les de βA42. La majoria de les molècules (15 de 20) que vam provar acceleraren la formació d'agregats resistents a SDS. Tres molècules mostraren no tenir un efecte clar en l'agregació de βA42, mentre que dues molècules inhibiren la formació d'agregats resistents a SDS.

Basant-nos en aquests resultats obtinguts per l'ARF, vam seleccionar un nombre petit però representatiu de composts per a ésser estudiats pel mètode del PL-HDX acoblat a EM. Les molècules que vam triar foren l'entacapona (Ent) i la diamida de dialliltartrat (DATD, de l'anglès) com a compostos representatius accelerant l'agregació de βA42, la 2,2'-dihidroxibenzofenona (DHB) com a molècula sense efecte en l'agregació de βA42, i també el gal·lat d'epigal·locatequina (EGCG, de l'anglès) i el pèptide inrD com a compostos inhibint l'agregació de βA42.

6.3.2 Estudi per PL-HDX de l'efecte de 5 molècules en l'agregació de βA

Així doncs, vam dur a terme experiments d'agregació de βA42 en absència i presència de les 5 molècules anteriorment mencionades durant 12 dies, i vam aplicar l'experiment de PL-HDX acoblat a EM.

Quan βA42 agregava en presència de l'Ent o de la DATD vam detectar tres espècies. Aquestes no mostraven diferències significatives en quant a amides exposades o heterogeneïtat amb βA42 control, però la formació de l'espècie fibril·lar es formava molt més ràpidament, mentre que els agregats primerencs deixaven d'estar presents en solució als 2 dies d'agregació. Així doncs, aquestes dues molècules acceleraven la cinètica de formació de fibril·les de βA42.

Quan vam aplicar l'experiment de PL-HDX a βA42 + DHB, vam descobrir que aquesta molècula involucrava la formació de tres espècies diferents. Com en els casos anteriors, les característiques de protecció i homogeneïtat no diferien significativament de βA42 control, però la DHB tenia una influència siginificativa en l'espècie protofibril·lar. Malgrat els agregats primerencs desapareixien ràpidament durant l'agregació, era la població de protofibril·les la que augmentava significativament, i no les fibril·les. La DHB promovia la formació i estabilització de protofibril·les, però no fibril·les de βA42.

En el cas de l'agregació de βA42 en presència del pèptid inrD, els experiments de PL-HDX van demostrar que només dues espècies es formaven. En determinar el nombre d'amides exposades i la heterogeneïtat de les dues espècies formades, vam poder concloure que en el temps que durava l'experiment, el pèptid inrD inhibia la formació de fibril·les, estabilitzant l'espècie oligomèrica protofibril·lar.

Quan vam aplicar l'experiment de PL-HDX per estudiar l'agregació de βA42 en presència d'EGCG, vam obtenir uns espectres de masses complexos: vam observar valors d'm/z més grans que els que esperaríem per βA42 totalment deuterada (bescanviada). A més, la relació senyal soroll per l'espectra era pitjor en incrementar Δt_{agg}. Aquests resultats inesperats van fer que duguéssim a terme l'experiment de PL-HDX en les mateixes mostres i temps d'agregació però sense canviar la solució protonada a aigua deuterada. Així, tots els espectres obtinguts haurien de mostrar un únic pic corresponent a βA42 totalment protonada. Tanmateix, vam observar un segon pic corresponent a una massa superior a βA42 en 16 uma. A més, la intensitat d'aquest segon pic incrementava a temps d'agregació més llargs. Basantnos en aquest increment en massa i l'anàlisi d'aquestes mostres per ressonància magnètica nuclear (RMN), vam assignar aquest segon pic a una forma oxidada de βA42 en la qual el grup sulfur de la metionina 35 era oxidat a grup sulfòxid. Així doncs, en presència d'EGCG, la proteïna βA42 sofria una modificació química.

6.3.3 Discussió

Aplicar la metodologia de PL-HDX ha resultat ser molt útil per tal d'obtenir informació rellevant sobre el mecanisme d'acció de 5 molècules en l'agregació de βA42. Aquestes compostos van ser escollides gràcies al mètode d'ARF, molt útil per a seleccionar candidats per a un posterior estudi més detallat.

Tant l'Ent com la DATD van resultar ser molècules accelerant l'agregació de βA42. Aquest comportament és diferent del descrit prèviament per aquestes molècules. En treball del grup del Dr. Lashuel, l'Ent inhibeix l'agregació de βA42. Aquest comportament és derivat d'un estudi de βA42 + Ent amb l'assaig de ThT i per MTE. L'assaig de ThT no està recomanat per a estudiar l'agregació en presència de molècules, ja que la molècula pot interaccionar

amb la fluorescència de ThT i, per tant, donar resultats erronis. A més, no trobar fibril·les amiloides en un reixeta de MTE no elimina la possibilitat que de fet les fibril·les amiloides estiguin presents en solució però no s'hagin dipositat bé en la reixeta per la interacció de la molècula.
En el cas de la DATD, el grup del Dr. Glabe va establir que formava oligòmers de βA42 però no fibril·les. Tanmateix, l'evidència només prové d'estudis d'immunoreactivitat dels agregats formats per la DATD i βA42 contra l'anticòs A11, un anticòs que reconeix específicament oligòmers. A més, l'article en qüestió no mostra en cap moment dades experimentals en el cas de la DATD, fent difícil l'assignació d'una funció específica a la DATD. Nosaltres vam trobar que la DATD accelerava la fibril·lació de βA42. Ja que els agregats primerencs i les protofibril·les coexisteixen amb les fibril·les, aquestes mostres podrien ser positives davant l'A11, explicant el resultats del Dr. Glabe i col·laboradors.

L'ARF va mostrar que la DHB tenia un efecte negligible en βA42. Amb la tècnica del PL-HDX vam demostrar que la DHB influïa significativament en l'agregació de βA42 promovent la formació d'espècies protofibril·lars, un agregat no detectable per l'ARF. El grup del Dr. Glabe va estblir que DHB inhibia l'oligomerització i la fibril·lació de βA42. Com en el cas de la DATD, aquest resultats s'obtingueren amb l'ús de l'anticòs A11. Nosaltres vam establir que la DHB inhibia la formació de fibril·les però no vam trobar que inhibís la formació d'oligòmers, sinó més aviat al contrari. Aquests resultats són fàcilment explicables si l'oligòmer estabilitzat per la DHB no és positiu contra l'A11.

El pèptid inrD, desenvolupat en el nostre laboratori, inhibia la fibril·lació de βA42 retardant la formació de fibril·les. Amb l'experiment de PL-HDX vam demostrar que l'inrD prevenia la formació de la població fibril·lar i estabilitzava l'oligòmer protofibril·lar, inhibint l'agregació de βA42. Aquesta informació complementa el que ja està descrit i en proporciona de nova sobre el mecanisme d'acció d'aquest pèptid: l'inrD estabilitza els agregats primerencs i les protofibril·les en funció del temps. Aquest inhibidor podria ser un candidat a estudis posteriors en la cerca d'agents terapèutics antiamiloidogènics.

En treballs previs es va descriure com l'EGCG formava agregats de βA42 que no eren tòxics. També es descrigué la capacitat d'aquesta molècula per a disgregar fibril·les amiloides. Un estudi recent donà nova informació en el mecanisme de disgregació de fibril·les amiloides per l'EGCG: la forma oxidada de l'EGCG interaccionava covalentment amb els grups amino de les proteïnes. A més, diversos estudis han determinat el rol important que té la metionina 35 en l'agregació de βA.
Amb els nostres estudis establim una nova connexió entre modificacions químiques de βA i la inhibició per molècules petites amb un efecte global en l'agregació de βA. Amb els nostres resultats d'EM i de RMN, hem pogut determinar que l'EGCG modifica covalentment la proteïna βA42. El grup sulfur en la metionina 35 és oxidat a sulfona, probablement com a conseqüència de la presència d'EGCG oxidada que alhora oxida βA42 en el lloc més

susceptible de ser-ho, en la metionina 35. En trobar dificultats en ionitzar la mostra per l'estudi d'EM a temps llargs d'agregació, vam suposar que aquests agregats de βA42 són units covalentment quan l'agregació té lloc, ja que la dissolució de DMSO que utilitzem per EM és capaç de trencar també els agregats fibril·lars. Aquesta reacció covalent podria tenir lloc com s'ha descrit, per mitjà dels grups amino de les proteïnes. Combinant els nostres resultats amb els obtinguts prèviament per d'altres, vam ser capaços d'explicar l'oxidació de βA42, la seva agregació i la seva unió covalent amb l'EGCG.

Com a conclusió, l'experiment de PL-HDX ha resultat ésser una tècnica potent per a detectar, caracteritzar i quantificar les espècies formades en l'agregació de βA42 modulada per molècules, una manera de distingir entre els efectes diferents que tenen diversos compostos, i una eina per a aprofundir en el mecanisme d'acció de molècules interaccionant amb βA42.

Bibliography

[1] Roland Jakob-Roetne and Helmut Jacobsen. Alzheimer's Disease: From Pathology to Therapeutic Approaches. *Angewandte Chemie International Edition*, 48(17):3030–3059, 2009.

[2] Rudolph E Tanzi. The genetics of Alzheimer disease. *Cold Spring Harbor Perspectives in Medicine*, 2(10), 2012.

[3] Anders Wimo and Martin Prince. World Alzheimer Report 2010. Technical report, 2010.

[4] David H Small and Roberto Cappai. Alois Alzheimer and Alzheimer's disease: a centennial perspective. *Journal of Neurochemistry*, 99(3):708–710, 2006.

[5] George G Glenner and Caine W Wong. Alzheimer's disease: Initial report of the purification and characterization of a novel cerebrovascular amyloid protein. *Biochemical and Biophysical Research Communications*, 120(3):885 – 890, 1984.

[6] Inge Grundke-Iqbal, Khalid Iqbal, Yunn-Chyn Tung, Maureen Quinlan, Henryk M Wisniewski, and Lester I Binder. Abnormal phosphorylation of the microtubule-associated protein tau in Alzheimer cytoskeletal pathology. *Proceedings of the National Academy of Sciences*, 83(13):4913–4917, 1986.

[7] John Hardy and Gerald A Higgins. Alzheimer's disease: the amyloid cascade hypothesis. *Science*, 256(5054):184–185, 1992.

[8] Eva-Marie Mandelkow and Eckhard Mandelkow. Tau as a marker for Alzheimer's disease. *Trends in Biochemical Sciences*, 18(12):480 – 483, 1993.

[9] Erik D Roberson, K Scearce-Levie, Jorge J Palop, F Yan, I H Cheng, T Wu, H Gerstein, G Q Yu, and Lennart Mucke. Reducing Endogenous Tau Ameliorates Amyloid -

Induced Deficits in an Alzheimer's Disease Mouse Model. *Science*, 316(5825):750–754, 2007.

[10] Lars M Ittner, Yazi D Ke, Fabien Delerue, Mian Bi, Amadeus Gladbach, Janet van Eersel, Heidrun Wölfing, Billy C Chieng, MacDonald J Christie, Ian A Napier, Anne Eckert, Matthias Staufenbiel, Edna Hardeman, and Jürgen Götz. Dendritic function of tau mediates amyloid-beta toxicity in Alzheimer's disease mouse models. *Cell*, 142(3):387–397, 2010.

[11] Keith A Vossel, Kai Zhang, Jens Brodbeck, Aaron C Daub, Punita Sharma, Steven Finkbeiner, Bianxiao Cui, and Lennart Mucke. Tau reduction prevents Aβ-induced defects in axonal transport. *Science*, 330(6001):198–198, 2010.

[12] Megan L Kerr and David H Small. Cytoplasmic domain of the β-amyloid protein precursor of Alzheimer's disease: Function, regulation of proteolysis, and implications for drug development. *Journal of Neuroscience Research*, 80(2):151–159, 2005.

[13] James A Duce, Andrew Tsatsanis, Michael A Cater, Simon A James, Elysia Robb, Krutika Wikhe, Su Ling Leong, Keyla Perez, Timothy J Johanssen, Mark A Greenough, Hyun-Hee Cho, Denise Galatis, Robert D Moir, Colin L Masters, Catriona A McLean, Rudolph E Tanzi, Roberto Cappai, Kevin J Barnham, Giuseppe D Ciccotosto, Jack T Rogers, and Ashley I Bush. Iron-export ferroxidase activity of β-amyloid precursor protein is inhibited by zinc in Alzheimer's disease. *Cell*, 142(6):857–867, 2010.

[14] Kourosh Honarmand Ebrahimi, Peter-Leon Hagedoorn, and Wilfred R Hagen. A Synthetic Peptide with the Putative Iron Binding Motif of Amyloid Precursor Protein (APP) Does Not Catalytically Oxidize Iron. *PLoS ONE*, 7(8):e40287, 2012.

[15] Karie N Dahlgren, Arlene M Manelli, W Blaine Stine, Lorinda K Baker, Grant A Krafft, and Mary Jo LaDu. Oligomeric and fibrillar species of amyloid-beta peptides differentially affect neuronal viability. *Journal of Biological Chemistry*, 277(35):32046–32053, 2002.

[16] Eileen McGowan, Fiona Pickford, Jungsu Kim, Luisa Onstead, Jason Eriksen, Cindy Yu, Lisa Skipper, M Paul Murphy, Jenny Beard, Pritam Das, Karen Jansen, Michael DeLucia, Wen-Lang Lin, Georgia Dolios, Rong Wang, Christopher B Eckman, Dennis W Dickson, Mike Hutton, John Hardy, and Todd E Golde. Aβ42 Is Essential for Parenchymal and Vascular Amyloid Deposition in Mice. *Neuron*, 47(2):191–199, 2005.

[17] Kaj Blennow. Biomarkers in Alzheimer's disease drug development. *Nature Medicine*, 16(11):1218–1222, 2010.

[18] Alex E Roher, Jonathan D Lowenson, Steven Clarke, Amina S Woods, Robert J Cotter, Eric Gowing, and Melvyn J Ball. beta-Amyloid-(1-42) is a major component of cerebrovascular amyloid deposits: implications for the pathology of Alzheimer disease. *Proceedings of the National Academy of Sciences*, 90(22):10836–10840, 1993.

[19] M Fändrich. On the structural definition of amyloid fibrils and other polypeptide aggregates. *Cellular and Molecular Life Sciences*, 64(16):2066–2078, 2007.

[20] Jean D Sipe and Alan S Cohen. Review: History of the Amyloid Fibril. *Journal of Structural Biology*, 130(2-3):88–98, 2000.

[21] Takami Tomiyama, Tetsu Nagata, Hiroyuki Shimada, Rie Teraoka, Akiko Fukushima, Hyoue Kanemitsu, Hiroshi Takuma, Ryozo Kuwano, Masaki Imagawa, Suzuka Ataka, Yasuhiro Wada, Eito Yoshioka, Tomoyuki Nishizaki, Yasuyoshi Watanabe, and Hiroshi Mori. A new amyloid β variant favoring oligomerization in Alzheimer's-type dementia. *Annals of Neurology*, 63(3):377–387, 2008.

[22] Adam L Cloe, Joseph P R O Orgel, Joseph R Sachleben, Robert Tycko, and Stephen C Meredith. The Japanese mutant Aβ (ΔE22-Aβ(1-39)) forms fibrils instantaneously, with low-thioflavin T fluorescence: seeding of wild-type Aβ(1-40) into atypical fibrils by ΔE22-Aβ(1-39). *Biochemistry*, 50(12):2026–2039, 2011.

[23] Oxana Yu Ovchinnikova, Verena H Finder, Ivana Vodopivec, Roger M Nitsch, and Rudi Glockshuber. The Osaka FAD Mutation E22Δ Leads to the Formation of a Previously Unknown Type of Amyloid β Fibrils and Modulates Aβ Neurotoxicity. *Journal of Molecular Biology*, 408(4):780–791, 2011.

[24] Mohammed Inayathullah and David B Teplow. Structural dynamics of the ΔE22 (Osaka) familial Alzheimer's disease-linked amyloid β-protein. *Amyloid*, 18(3):98–107, 2011.

[25] Dennis J Selkoe. The molecular pathology of Alzheimer's disease. *Neuron*, 6(4):487–498, 1991.

[26] Catriona A McLean, Robert A Cherny, F W Fraser, S J Fuller, M J Smith, Konrad Beyreuther, Ashley I Bush, and Colin L Masters. Soluble pool of Abeta amyloid as a determinant of severity of neurodegeneration in Alzheimer's disease. *Annals of Neurology*, 46(6):860–866, 1999.

[27] Lih-Fen Lue, Yu-Min Kuo, Alex E Roher, Libuse Brachova, Yong Shen, Lucia Sue, Thomas G Beach, Janice H Kurth, Russel E Rydel, and Joseph Rogers. Soluble amyloid β peptide concentration as a predictor of synaptic change in Alzheimer's disease. *American Journal of Pathology*, 155(3):853–862, 1999.

[28] John Hardy and Dennis J Selkoe. The amyloid hypothesis of Alzheimer's disease: progress and problems on the road to therapeutics. *Science*, 297(5580):353–356, 2002.

[29] Dominic M Walsh and Dennis J Selkoe. Abeta oligomers - a decade of discovery. *Journal of Neurochemistry*, 101(5):1172–1184, 2007.

[30] Dominic M Walsh, Igor Klyubin, Julia V Fadeeva, William K Cullen, Roger Anwyl, Michael S Wolfe, Michael J Rowan, and Dennis J Selkoe. Naturally secreted oligomers of amyloid beta protein potently inhibit hippocampal long-term potentiation in vivo. *Nature*, 416(6880):535–539, 2002.

[31] Sylvain E Lesné, Ming Teng Koh, Linda Kotilinek, Rakez Kayed, Charles G Glabe, Austin Yang, Michela Gallagher, and Karen H Ashe. A specific amyloid-β protein assembly in the brain impairs memory. *Nature*, 440(7082):352–357, 2006.

[32] Ganesh M Shankar, Shaomin Li, Tapan H Mehta, Amaya Garcia-Munoz, Nina E Shepardson, Imelda M Smith, Francesca M Brett, Michael A Farrell, Michael J Rowan, Cynthia A Lemere, Ciaran M Regan, Dominic M Walsh, Bernardo L Sabatini, and Dennis J Selkoe. Amyloid-β protein dimers isolated directly from Alzheimer's brains impair synaptic plasticity and memory. *Nature Medicine*, 14(8):837–842, 2008.

[33] Gal Bitan, Erica A Fradinger, Sean M Spring, and David B Teplow. Neurotoxic protein oligomers – what you see is not always what you get. *Amyloid*, 12(2):88–95, 2005.

[34] Ryan Naylor, Andrew Francis Hill, and Kevin J Barnham. Neurotoxicity in Alzheimer's disease: is covalently crosslinked Aβ responsible? *European Biophysics Journal*, 37(3):265–268, 2007.

[35] Andrew D Watt, Keyla A Perez, Alan Rembach, Nicki A Sherrat, Lin Wai Hung, Timothy J Johanssen, Catriona A McLean, Woan Mei Kok, Craig A Hutton, Michelle Fodero-Tavoletti, Colin L Masters, Victor L Villemagne, and Kevin J Barnham. Oligomers, fact or artefact? SDS-PAGE induces dimerization of β-amyloid in human brain samples. *Acta Neuropathologica*, 125(4):549–564, 2013.

[36] Mark Wogulis, Sarah Wright, Damian Cunningham, Tamie Chilcote, Kyle Powell, and Russell E Rydel. Nucleation-Dependent Polymerization Is an Essential Component of Amyloid-Mediated Neuronal Cell Death. *Journal of Neuroscience*, 25(5):1071–1080, 2005.

[37] Asad Jan, Oskar Adolfsson, Igor Allaman, Anna-Lucia Buccarello, Pierre J Magistretti, Andrea Pfeifer, Andreas Muhs, and Hilal A Lashuel. Aβ42 neurotoxicity is mediated by ongoing nucleated polymerization process rather than by discrete Aβ42 species. *Journal of Biological Chemistry*, 286(10):8585–8596, 2011.

[38] Dominic M Walsh. Amyloid beta -Protein Fibrillogenesis. Structure and biological activity of protofibrillar intermediates. *Journal of Biological Chemistry*, 274(36):25945–25952, 1999.

[39] Mary P Lambert, A K Barlow, Brett A Chromy, C Edwards, R Freed, M Liosatos, T E Morgan, I Rozovsky, B Trommer, Kirsten L Viola, P Wals, C Zhang, Caleb E Finch, Grant A Krafft, and William L Klein. Diffusible, nonfibrillar ligands derived from Abeta1-42 are potent central nervous system neurotoxins. *Proceedings of the National Academy of Sciences*, 95(11):6448–6453, 1998.

[40] Stefan Barghorn, Volker Nimmrich, Andreas Striebinger, Carsten Krantz, Patrick Keller, Bodo Janson, Michael Bahr, Martin Schmidt, Robert S Bitner, John E Harlan, Eve Barlow, Ulrich Ebert, and Heinz Hillen. Globular amyloid beta-peptide oligomer - a homogenous and stable neuropathological protein in Alzheimer's disease. *Journal of Neurochemistry*, 95(3):834–847, 2005.

[41] Liping Yu, Rohinton Edalji, John E Harlan, Thomas F Holzman, Ana Pereda Lopez, Boris Labkovsky, Heinz Hillen, Stefan Barghorn, Ulrich Ebert, Paul L Richardson, Laura Miesbauer, Larry Solomon, Diane Bartley, Karl Walter, Robert W Johnson, Philip J Hajduk, and Edward T Olejniczak. Structural Characterization of a Soluble Amyloid β-Peptide Oligomer. *Biochemistry*, 48(9):1870–1877, 2009.

[42] H LeVine. Thioflavine T interaction with synthetic Alzheimer's disease beta-amyloid peptides: detection of amyloid aggregation in solution. *Protein Science*, 2(3):404–410, 1993.

[43] Cristina Rodríguez-Rodríguez, Albert Rimola, Luis Rodríguez-Santiago, Piero Ugliengo, Ángel Álvarez-Larena, Hugo Gutiérrez-de Terán, Mariona Sodupe, and Pilar González-Duarte. Crystal structure of thioflavin-T and its binding to amyloid fibrils: insights at the molecular level. *Chemical Communications*, 46(7):1156, 2010.

[44] Keith A Johnson, Nick C Fox, Reisa A Sperling, and William E Klunk. Brain imaging in Alzheimer disease. *Cold Spring Harbor Perspectives in Medicine*, 2(4):a006213, 2012.

[45] Kyle L Morris and Louise C Serpell. X-ray fibre diffraction studies of amyloid fibrils. *Methods in Molecular Biology*, 849:121–135, 2012.

[46] Ivano Bertini, Leonardo Gonnelli, Claudio Luchinat, Jiafei Mao, and Antonella Nesi. A new structural model of Aβ40 fibrils. *Journal of the American Chemical Society*, 133(40):16013–16022, 2011.

[47] Anant K Paravastu, Richard D Leapman, Wai-Ming Yau, and Robert Tycko. Molecular structural basis for polymorphism in Alzheimer's β-amyloid fibrils. *Proceedings of the National Academy of Sciences*, 105(47):18349–18354, 2008.

[48] Jun-Xia Lu, Wei Qiang, Wai-Ming Yau, Charles D Schwieters, Stephen C Meredith, and Robert Tycko. Molecular Structure of beta-Amyloid Fibrils in Alzheimer's Disease Brain Tissue. *Cell*, 154(6):1257–1268, 2013.

[49] Indu Kheterpal, Shaolian Zhou, Kelsey D Cook, and Ronald Wetzel. Abeta amyloid fibrils possess a core structure highly resistant to hydrogen exchange. *Proceedings of the National Academy of Sciences*, 97(25):13597–13601, 2000.

[50] Indu Kheterpal, Hilal A Lashuel, Dean M Hartley, Thomas Walz, Peter T Lansbury, Jr, and Ronald Wetzel. Abeta protofibrils possess a stable core structure resistant to hydrogen exchange. *Biochemistry*, 42(48):14092–14098, 2003.

[51] Indu Kheterpal, Maolian Chen, Kelsey D Cook, and Ronald Wetzel. Structural Differences in Aβ Amyloid Protofibrils and Fibrils Mapped by Hydrogen Exchange – Mass Spectrometry with On-line Proteolytic Fragmentation. *Journal of Molecular Biology*, 361(4):785–795, 2006.

[52] Thorsten Lührs, Christiane Ritter, Marc Adrian, Dominique Riek-Loher, Bernd Bohrmann, Heinz Döbeli, David Schubert, and Roland Riek. 3D structure of Alzheimer's amyloid-β (1–42) fibrils. *Proceedings of the National Academy of Sciences*, 102(48):17342–17347, 2005.

[53] Iris A Mastrangelo, Mahiuddin Ahmed, Takeshi Sato, Wei Liu, Chengpu Wang, Paul Hough, and Steven O Smith. High-resolution Atomic Force Microscopy of Soluble Aβ42 Oligomers. *Journal of Molecular Biology*, 358(1):106–119, 2006.

[54] Arthur Laganowsky, Cong Liu, Michael R Sawaya, Julian P Whitelegge, Jiyong Park, Minglei Zhao, Anna Pensalfini, Angela B Soriaga, Meytal Landau, Poh K Teng, Duilio Cascio, Charles G Glabe, and David Eisenberg. Atomic view of a toxic amyloid small oligomer. *Science*, 335(6073):1228–1231, 2012.

[55] Sandra Chimon, Medhat A Shaibat, Christopher R Jones, Diana C Calero, Buzulagu Aizezi, and Yoshitaka Ishii. Evidence of fibril-like β-sheet structures in a neurotoxic amyloid intermediate of Alzheimer's β-amyloid. *Nature Structural & Molecular Biology*, 14(12):1157–1164, 2007.

[56] Nicolas L Fawzi, Jinfa Ying, Dennis A Torchia, and G Marius Clore. Kinetics of Amyloid β Monomer-to-Oligomer Exchange by NMR Relaxation. *Journal of the American Chemical Society*, 132(29):9948–9951, 2010.

[57] Nicolas L Fawzi, Jinfa Ying, Rodolfo Ghirlando, Dennis A Torchia, and G Marius Clore. Atomic-resolution dynamics on the surface of amyloid-β protofibrils probed by solution NMR. *Nature*, 480(7376):268–272, 2011.

[58] Aleksey Lomakin and David B Teplow. Quasielastic light scattering study of amyloid β-protein fibrillogenesis. *Methods in Molecular Biology*, 849:69–83, 2012.

[59] Michal Sharon and Carol V Robinson. The Role of Mass Spectrometry in Structure Elucidation of Dynamic Protein Complexes. *Annual Review of Biochemistry*, 76(1):167–193, 2007.

[60] Summer L Bernstein, Nicholas F Dupuis, Noel D Lazo, Thomas Wyttenbach, Margaret M Condron, Gal Bitan, David B Teplow, Joan-Emma Shea, Brandon T Ruotolo, Carol V Robinson, and Michael T Bowers. Amyloid-β protein oligomerization and the importance of tetramers and dodecamers in the aetiology of Alzheimer's disease. *Nature Chemistry*, 1(4):326–331, 2009.

[61] Megan M Murray, Summer L Bernstein, Vy Nyugen, Margaret M Condron, David B Teplow, and Michael T Bowers. Amyloid β Protein: Aβ40 Inhibits Aβ42 Oligomerization. *Journal of the American Chemical Society*, 131(18):6316–6317, 2009.

[62] Priyanka Narayan, Angel Orte, Richard W Clarke, Benedetta Bolognesi, Sharon Hook, Kristina A Ganzinger, Sarah Meehan, Mark R Wilson, Christopher M Dobson, and David Klenerman. The extracellular chaperone clusterin sequesters oligomeric forms of the amyloid-β(1-40) peptide. *Nature Structural & Molecular Biology*, 19(1):79–83, 2011.

[63] Zoltan Szabo, E Klement, K Jost, M Zarandi, Katalin Soós, and Botond Penke. An FT-IR study of the β-amyloid conformation: Standardization of aggregation grade. *Biochemical and Biophysical Research Communications*, 265(2):297–300, 1999.

[64] Emilie Cerf, Rabia Sarroukh, Shiori Tamamizu Kato, Leonid Breydo, Sylvie Derclaye, Yves F Dufrêne, Vasanthy Narayanaswami, Erik Goormaghtigh, Jean Marie Ruysschaert, and Vincent Raussens. Antiparallel β-sheet: a signature structure of the oligomeric amyloid β-peptide. *Biochemical Journal*, 421(3):415–423, 2009.

[65] Natàlia Carulla, Min Zhou, Muriel Arimon, Margarida Gairí, Ernest Giralt, Carol V Robinson, and Christopher M Dobson. Experimental characterization of disordered and ordered aggregates populated during the process of amyloid fibril formation. *Proceedings of the National Academy of Sciences*, 106(19):7828–7833, 2009.

[66] Krista L Lanctôt, Nathan Herrmann, Kenneth K Yau, Lyla R Khan, Barbara A Liu, Maysoon M LouLou, and Thomas R Einarson. Efficacy and safety of cholinesterase inhibitors in Alzheimer's disease: a meta-analysis. *Canadian Medical Association Journal*, 169(6):557–564, 2003.

[67] Barry Reisberg, Rachelle Doody, Albrecht Stöffler, Frederick Schmitt, Steven Ferris, and Hans Jörg Möbius. Memantine in moderate-to-severe Alzheimer's disease. *New*

England Journal of Medicine, 348(14):1333–1341, 2003.

[68] Martin Citron. Alzheimer's disease: strategies for disease modification. *Nature Reviews Drug Discovery*, 9(5):387–398, 2010.

[69] Bruno P. Imbimbo, Luciana Giardino, Sandra Sivilia, Alessandro Giuliani, Marco Gusciglio, Vladimiro Pietrini, Elda Del Giudice, Antonello D'Arrigo, Alberta Leon, Gino Villetti, and Laura Calzá. CHF5074, a Novel γ-Secretase Modulator, Restores Hippocampal Neurogenesis Potential and Reverses Contextual Memory Deficit in a Transgenic Mouse Model of Alzheimer's Disease. *Journal of Alzheimer's Disease*, 20(1):159 – 173, 2010.

[70] Dennis J Selkoe. Resolving controversies on the path to Alzheimer's therapeutics. *Nature Medicine*, 17(9):1060–1065, 2011.

[71] A Kutzelnigg, A Schneeberger, D Meshkat, M Schmitz, S Kasper, F Mattner, and W Schmidt. Affitopes of amyloid-beta as active vaccines in the treatment of Alzheimer's disease: Results of a phase I study with Affitope AD02. In *27th World Congress of the International College of NeuroPsychopharmacology (CINP)*.

[72] A D Snow, J A Cummings, T P Lake, and L A Esposito. Exebryl-1: A novel small-molecule drug that markedly reduces amyloid plaque load and improves memory, enters human clinical trials. In *12th International Conference of Alzheimer's Disease and Related Disorders (ICAD)*.

[73] Paul A Adlard, Amelia Sedjahtera, Lydia Gunawan, Lisa Bray, Dominic Hare, Jessica Lear, Philip Doble, Ashley I Bush, David I Finkelstein, and Robert A Cherny. A novel approach to rapidly prevent age-related cognitive decline. *Aging Cell*, 13(2):351–359, 2013.

[74] Francesca Mangialasche, Alina Solomon, Bengt Winblad, Patrizia Mecocci, and Miia Kivipelto. Alzheimer's disease: clinical trials and drug development. *Lancet Neurology*, 9(7):702–716, 2010.

[75] Rakez Kayed, Elizabeth Head, Jennifer L Thompson, Theresa M McIntire, Saskia C Milton, Carl W Cotman, and Charles G Glabe. Common structure of soluble amyloid oligomers implies common mechanism of pathogenesis. *Science*, 300(5618):486–489, 2003.

[76] Rakez Kayed, Elizabeth Head, Floyd Sarsoza, Tommy Saing, Carl W Cotman, Mihaela Necula, Lawrence Margol, Jessica W Wu, Leonid Breydo, Jennifer L Thompson, Suhail Rasool, Tatyana Gurlo, Peter Butler, and Charles G Glabe. Fibril specific, conformation dependent antibodies recognize a generic epitope common to amyloid fibrils and

fibrillar oligomers that is absent in prefibrillar oligomers. *Molecular Neurodegeneration*, 2(1):18, 2007.

[77] Mihaela Necula, Rakez Kayed, Saskia C Milton, and Charles G Glabe. Small molecule inhibitors of aggregation indicate that amyloid beta oligomerization and fibrillization pathways are independent and distinct. *Journal of Biological Chemistry*, 282(14):10311–10324, 2007.

[78] Mihaela Necula, Leonid Breydo, Saskia C Milton, Rakez Kayed, Wytze E van der Veer, Paul Tone, and Charles G Glabe. Methylene blue inhibits amyloid Abeta oligomerization by promoting fibrillization. *Biochemistry*, 46(30):8850–8860, 2007.

[79] Saviana Di Giovanni, Simona Eleuteri, K E Paleologou, Guowei Yin, Markus Zweckstetter, Pierre-Alain Carrupt, and Hilal A Lashuel. Entacapone and tolcapone, two catechol O-methyltransferase inhibitors, block fibril formation of alpha-synuclein and beta-amyloid and protect against amyloid-induced toxicity. *Journal of Biological Chemistry*, 285(20):14941–14954, 2010.

[80] Siva Sundara Kumar Durairajan, Qiuju Yuan, Lixia Xie, Wing-Sai Chan, Wan-Fung Kum, Irene Koo, Chenli Liu, Youqiang Song, Jian-Dong Huang, William L Klein, and Min Li. Salvianolic acid B inhibits Aβ fibril formation and disaggregates preformed fibrils and protects against Aβ-induced cytotoxicty. *Neurochemistry International*, 52(4-5):741–750, 2008.

[81] Francine Gervais, Julie Paquette, Céline Morissette, Pascale Krzywkowski, Mathilde Yu, Mounia Azzi, Diane Lacombe, Xianqi Kong, Ahmed Aman, Julie Laurin, Walter A Szarek, and Patrick Tremblay. Targeting soluble Aβ peptide with Tramiprosate for the treatment of brain amyloidosis. *Neurobiology of Aging*, 28(4):537–547, 2007.

[82] Cristina Airoldi, Laura Colombo, Claudia Manzoni, Erika Sironi, Antonino Natalello, Silvia Maria Doglia, Gianluigi Forloni, Fabrizio Tagliavini, Elena Del Favero, Laura Cantù, Francesco Nicotra, and Mario Salmona. Tetracycline prevents Aβ oligomer toxicity through an atypical supramolecular interaction. *Organic & Biomolecular Chemistry*, 9(2):463–472, 2011.

[83] Ali Reza A Ladiwala, Jonathan S Dordick, and Peter M Tessier. Aromatic small molecules remodel toxic soluble oligomers of amyloid β through three independent pathways. *Journal of Biological Chemistry*, 286(5):3209–3218, 2011.

[84] JoAnne McLaurin, R Golomb, A Jurewicz, J P Antel, and Paul E Fraser. Inositol stereoisomers stabilize an oligomeric aggregate of Alzheimer amyloid beta peptide and inhibit abeta -induced toxicity. *Journal of Biological Chemistry*, 275(24):18495–18502, 2000.

[85] JoAnne McLaurin, Meredith E Kierstead, Mary E Brown, Cheryl A Hawkes, Mark H L Lambermon, Amie L Phinney, Audrey A Darabie, Julian E Cousins, Janet E French, Melissa F Lan, Fusheng Chen, Sydney S N Wong, Howard T J Mount, Paul E Fraser, David Westaway, and Peter St George-Hyslop. Cyclohexanehexol inhibitors of Aβ aggregation prevent and reverse Alzheimer phenotype in a mouse model. *Nature Medicine*, 12(7):801–808, 2006.

[86] Daniela Fenili, Mary E Brown, Rebecca Rappaport, and JoAnne McLaurin. Properties of scyllo–inositol as a therapeutic treatment of AD-like pathology. *Journal of Molecular Medicine*, 85(6):603–611, 2007.

[87] Dagmar E Ehrnhoefer, Jan Bieschke, Annett Boeddrich, Martin Herbst, Laura Masino, Rudi Lurz, Sabine Engemann, A Pastore, and Erich E Wanker. EGCG redirects amyloidogenic polypeptides into unstructured, off-pathway oligomers. *Nature Structural & Molecular Biology*, 15(6):558–566, 2008.

[88] Jan Bieschke, J Russ, Ralf P Friedrich, Dagmar E Ehrnhoefer, H Wobst, K Neugebauer, and Erich E Wanker. EGCG remodels mature -synuclein and amyloid- fibrils and reduces cellular toxicity. *Proceedings of the National Academy of Sciences*, 107(17):7710–7715, 2010.

[89] Robert A Cherny, Craig S Atwood, M E Xilinas, D N Gray, Walton D Jones, Catriona A McLean, Kevin J Barnham, Irene Volitakis, F W Fraser, Y Kim, X Huang, Lee E Goldstein, Robert D Moir, J T Lim, Konrad Beyreuther, H Zheng, R E Tanzi, Colin L Masters, and Ashley I Bush. Treatment with a copper-zinc chelator markedly and rapidly inhibits beta-amyloid accumulation in Alzheimer's disease transgenic mice. *Neuron*, 30(3):665–676, 2001.

[90] H M Alvarez, Y Xue, C D Robinson, M A Canalizo-Hernandez, R G Marvin, R A Kelly, A Mondragon, J E Penner-Hahn, and T V O'Halloran. Tetrathiomolybdate Inhibits Copper Trafficking Proteins Through Metal Cluster Formation. *Science*, 327(5963):331–334, 2010.

[91] Celine Adessi and Claudio Soto. Converting a Peptide into a Drug: Strategies to Improve Stability and Bioavailability. *Current Medicinal Chemistry*, 9(9):963 – 978, 2002.

[92] Erica A Fradinger, Bernhard H Monien, B Urbanc, Aleksey Lomakin, Miao Tan, Huiyuan Li, Sean M Spring, Margaret M Condron, Luis Cruz, Cui-Wei Xie, George B Benedek, and Gal Bitan. C-terminal peptides coassemble into Abeta42 oligomers and protect neurons against Abeta42-induced neurotoxicity. *Proceedings of the National Academy of Sciences*, 105(37):14175–14180, 2008.

[93] Dolors Grillo-Bosch, Natàlia Carulla, Montse Cruz, Laia Sánchez, Rosa Pujol-Pina, Sergio Madurga, Francesc Rabanal, and Ernest Giralt. Retro-Enantio N-Methylated Peptides as β-Amyloid Aggregation Inhibitors. *ChemMedChem*, 4(9):1488–1494, 2009.

[94] Yu-Zhu Zhang, Yvonne Paterson, and Heinrich Roder. Rapid amide proton exchange rates in peptides and proteins measured by solvent quenching and two-dimensional NMR. *Protein Science*, 4(4):804–814, 1995.

[95] Laia Sánchez, Sergio Madurga, Tara Pukala, Marta Vilaseca, Carmen López-Iglesias, Carol V Robinson, Ernest Giralt, and Natàlia Carulla. Aβ40 and Aβ42 Amyloid Fibrils Exhibit Distinct Molecular Recycling Properties. *Journal of the American Chemical Society*, 133(17):6505–6508, 2011.

[96] Natàlia Carulla, Gemma L Caddy, Damien R Hall, Jesús Zurdo, Margarida Gairí, Miguel Feliz, Ernest Giralt, Carol V Robinson, and Christopher M Dobson. Molecular recycling within amyloid fibrils. *Nature*, 436(7050):554–558, 2005.

[97] Paul W Sylvester. Optimization of the tetrazolium dye (MTT) colorimetric assay for cellular growth and viability. *Methods in Molecular Biology*, 716:157–168, 2011.

[98] Hans Zempel, Edda Thies, Eckhard Mandelkow, and Eva-Maria Mandelkow. Aβ oligomers cause localized Ca2+ elevation, missorting of endogenous Tau into dendrites, Tau phosphorylation, and destruction of microtubules and spines. *Journal of Neuroscience*, 30(36):11938–11950, 2010.

[99] Gal Bitan, Marina D Kirkitadze, Aleksey Lomakin, Sabrina S Vollers, George B Benedek, and David B Teplow. Amyloid β-protein (Aβ) assembly: Aβ40 and Aβ42 oligomerize through distinct pathways. *Proceedings of the National Academy of Sciences*, 100(1):330–335, 2003.

[100] Sara M Butterfield and Hilal A Lashuel. Amyloidogenic Protein-Membrane Interactions: Mechanistic Insight from Model Systems. *Angewandte Chemie International Edition*, 49(33):5628–5654, 2010.

[101] Christian Haass and Dennis J Selkoe. Soluble protein oligomers in neurodegeneration: lessons from the Alzheimer's amyloid beta-peptide. *Nature Reviews Molecular Cell Biology*, 8(2):101–112, 2007.

[102] Tricia R Serio, Anil G Cashikar, Anthony S Kowal, George J Sawicki, Jahan J Moslehi, Louise C Serpell, Morton F Arnsdorf, and Susan L Lindquist. Nucleated Conformational Conversion and the Replication of Conformational Information by a Prion Determinant. *Science*, 289(5483):1317–1321, 2000.

[103] Nunilo Cremades, Samuel I A Cohen, Emma Deas, Andrey Y Abramov, Allen Y Chen, Angel Orte, Massimo Sandal, Richard W Clarke, Paul Dunne, Francesco A

Aprile, Carlos W Bertoncini, Nicholas W Wood, Tuomas P J Knowles, Christopher M Dobson, and David Klenerman. Direct Observation of the Interconversion of Normal and Toxic Forms of alpha-Synuclein. *Cell*, 149(5):1048–1059, 2012.

[104] Natàlia Carulla, Min Zhou, Ernest Giralt, Carol V Robinson, and Christopher M Dobson. Structure and Intermolecular Dynamics of Aggregates Populated during Amyloid Fibril Formation Studied by Hydrogen/Deuterium Exchange. *Accounts of Chemical Research*, 43(8):1072–1079, 2010.

[105] William T Vetterling William H Press, Samuel A Teukolsky and Brian P Flannery. *Numerical Recipes in C: The Art of Scientific Computing*. Cambrdige University Press, 2nd edition, 1992.

[106] Indu Kheterpal, Ronald Wetzel, and Kelsey D Cook. Enhanced correction methods for hydrogen exchange-mass spectrometric studies of amyloid fibrils. *Protein Science*, 12(3):635–643, 2003.

[107] Mary P Lambert, Kirsten L Viola, Brett A Chromy, Lei L Chang, T E Morgan, Jiaxin Yu, Duane L Venton, Grant A Krafft, Caleb E Finch, and William L Klein. Vaccination with soluble Aβ oligomers generates toxicity-neutralizing antibodies. *Journal of Neurochemistry*, 79(3):595–605, 2001.

[108] Tingyu Liu and Gal Bitan. Modulating Self-Assembly of Amyloidogenic Proteins as a Therapeutic Approach for Neurodegenerative Diseases: Strategies and Mechanisms. *ChemMedChem*, 7(3):359–374, 2012.

[109] Cheryl A Hawkes, Vivian Ng, and JoAnne McLaurin. Small molecule inhibitors of Aβ-aggregation and neurotoxicity. *Drug Development Research*, 70(2):111–124, 2009.

[110] Robert C Green, Lon S Schneider, David A Amato, Andrew P Beelen, Gordon Wilcock, Edward A Swabb, Kenton H Zavitz, and Tarenflurbil Phase 3 Study Group. Effect of tarenflurbil on cognitive decline and activities of daily living in patients with mild Alzheimer disease: a randomized controlled trial. *JAMA: the Journal of the American Medical Association*, 302(23):2557–2564, 2009.

[111] Volker Heiser, Sabine Engemann, Wolfgang Bröcker, Ilona Dunkel, Annett Boeddrich, Stephanie Waelter, Eddi Nordhoff, Rudi Lurz, Nancy Schugardt, and Susanne Rautenberg. Identification of benzothiazoles as potential polyglutamine aggregation inhibitors of Huntington's disease by using an automated filter retardation assay. *Proceedings of the National Academy of Sciences*, 99(suppl 4):16400–16406, 2002.

[112] Jan Bieschke, Martin Herbst, Thomas Wiglenda, Ralf P Friedrich, Annett Boeddrich, Franziska Schiele, Daniela Kleckers, Juan Miguel Lopez del Amo, Björn A Grüning,

and Qinwen Wang. Small-molecule conversion of toxic oligomers to nontoxic β-sheet–rich amyloid fibrils. *Nature Chemical Biology*, 8(1):93–101, 2011.

[113] Sean A Hudson, Heath Ecroyd, Tak W Kee, and John A Carver. The thioflavin T fluorescence assay for amyloid fibril detection can be biased by the presence of exogenous compounds. *FEBS Journal*, 276(20):5960–5972, 2009.

[114] Gal Bitan and David B Teplow. Rapid photochemical cross-linking–a new tool for studies of metastable, amyloidogenic protein assemblies. *Accounts of Chemical Research*, 37(6):357–364, 2004.

[115] Juan Miguel Lopez del Amo, Uwe Fink, Muralidhar Dasari, Gerlinde Grelle, Erich E Wanker, Jan Bieschke, and Bernd Reif. Structural Properties of EGCG-Induced, Non-toxic Alzheimer's Disease Aβ Oligomers. *Journal of Molecular Biology*, 421(4-5):517–524, 2012.

[116] Fernando L Palhano, Jiyong Lee, Neil P Grimster, and Jeffery W Kelly. Toward the Molecular Mechanism(s) by Which EGCG Treatment Remodels Mature Amyloid Fibrils. *Journal of the American Chemical Society*, 135(20):7503–7510, 2013.

[117] Shengmin Sang, Mao-Jung Lee, Zhe Hou, Chi-Tang Ho, and Chung S Yang. Stability of tea polyphenol (-)-epigallocatechin-3-gallate and formation of dimers and epimers under common experimental conditions. *Journal of Agricultural and Food Chemistry*, 53(24):9478–9484, 2005.

[118] Gal Bitan, Bogdan Tarus, Sabrina S Vollers, Hilal A Lashuel, Margaret M Condron, John E Straub, and David B Teplow. A molecular switch in amyloid assembly: Met35 and amyloid beta-protein oligomerization. *Journal of the American Chemical Society*, 125(50):15359–15365, 2003.

[119] Panchanan Maiti, Roberto Piacentini, Cristian Ripoli, Claudio Grassi, and Gal Bitan. Surprising toxicity and assembly behaviour of amyloid β-protein oxidized to sulfone. *Biochemical Journal*, 433(2):323–332, 2010.

[120] Panchanan Maiti, Aleksey Lomakin, George B Benedek, and Gal Bitan. Despite its role in assembly, methionine 35 is not necessary for amyloid beta-protein toxicity. *Journal of Neurochemistry*, 113(5):1252–1262, 2010.

List of Figures